MCRJ Volume 3 | No. 2 | 2008

ISSN 1985-3807

Malaysian Construction Research Journal

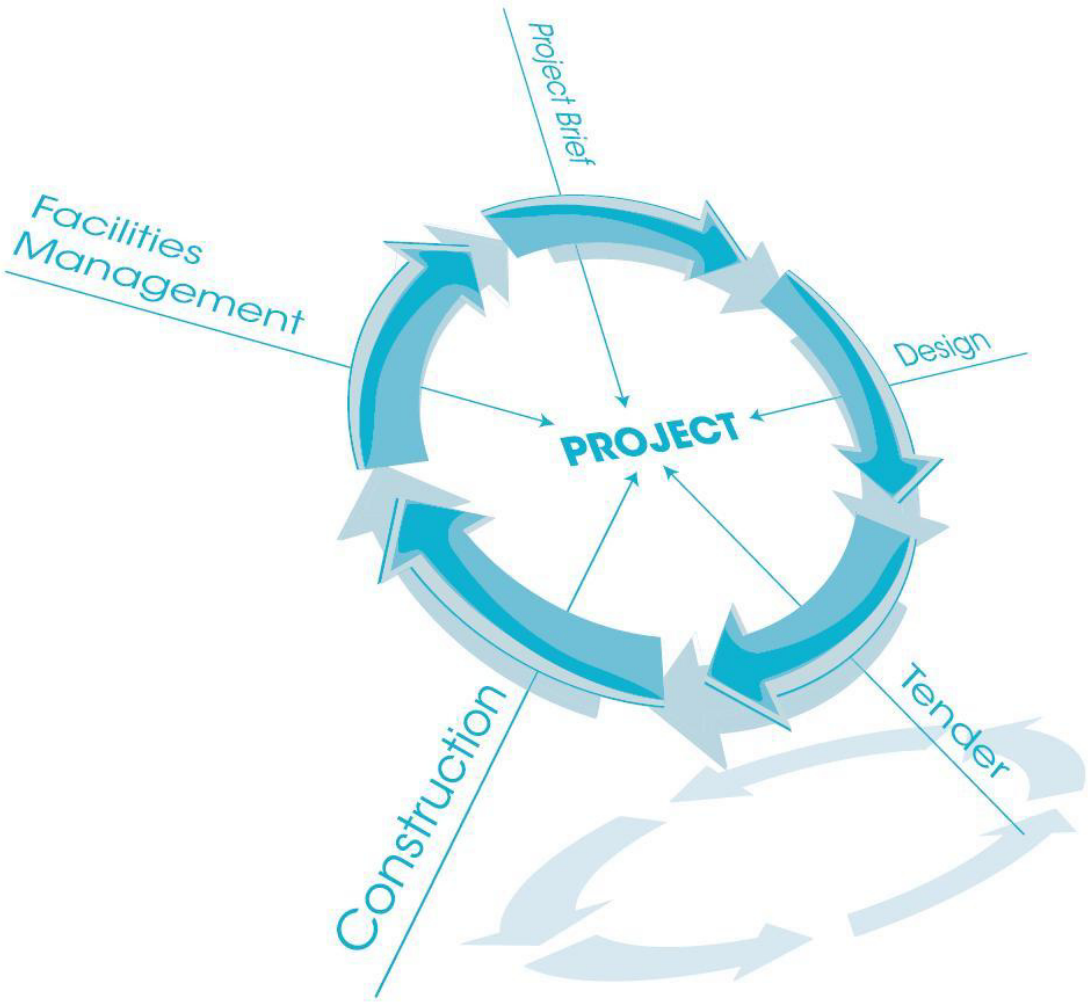

CREAM
CONSTRUCTION RESEARCH INSTITUTE OF MALAYSIA

CIDB MALAYSIA

Contents

Editorial Advisory Board

Editorial

Welcome from the Editors

The Editorial welcomes all readers to this third issue of Malaysian Construction Research Journal (MCRJ). Special thanks to all contributing authors for their technical papers. The Editorial would also like to express their acknowledgement to all reviewers for their invaluable comment and suggestion. This issue highlights five titles which focus on topics related to Construction Materials and one title on soil stability.

In this issue, ***Rangan*** presents extensive studies conducted on fly ash-based geopolymer concrete. Test data are used to identify the effects of salient factors that influence the properties of the geopolymer concrete in the fresh and hardened states. These results are utilised to propose a simple method for the design of geopolymer concrete mixtures. The last part of the paper describes the results of the geopolymer concrete members and illustrates the application of the geopolymer concrete in the construction industry.

Hashim et al discuss on the utilisation of calcined kaolin as a pozzolanic mineral admixture for high-performance mortar and concrete. This paper presents the findings of an on-going investigation on to the effects of laboratory produces metakaolin, in enhancing the strength and durability characteristics of concrete. Metakoalin was found to enhance the overall strength and elastic properties of concrete and also greatly reduced the water absorption of concrete.

Cheng et al evaluate five full-scale inverted-tee girders with circular web openings. The experiments revealed that concrete fractured from tension zones around an opening, with crack developed vertically towards the beam flanges. An analytical solution for the load-deflection calculation of prestressed beam with web openings at any load stage was also developed. The solution assumes a trilinear deflection response characterised by the flexural cracking initiation, steel yielding, and ultimate capacity.

Badorul et al investigate the effect of unit water absorption on the strength of brickwork. An empirical model was developed to predict the compressive strength of brickwork based on the unit water absorption, unit strength and mortar strength obtained from laboratory tests.

Bujang et al describe a study on the performance of shell footings using a non-linear finite element analysis with a finite element code, PLAXIS. The shell footing is found to have a better load carrying capacity compared with the conventional slab (flat) footing of similar cross sectional area.

In his second paper, ***Bujang et al*** present results of a field study on the effect of surface cover on the water infiltration rate into a cut slope of unsaturated residual soil and a parametric study to examine the effect of surface cover on the factor of safety of soil slope using the Seep/W and Slope/W programs.

Editorial Committee

STUDIES ON FLY ASH-BASED GEOPOLYMER CONCRETE

B. Vijaya Rangan
Emeritus Professor of Civil Engineering, Past Dean, Faculty of Engineering and Computing, Curtin University of Technology, Perth, WA 6845, Australia

Abstract
A comprehensive summary from extensive studies conducted on fly ash-based geopolymer concrete is presented. Test data are used to identify the effects of salient factors that influence the properties of the geopolymer concrete in the fresh and hardened states. These results are utilised to propose a simple method for the design of geopolymer concrete mixtures. Test data of various short-term and long-term properties of the geopolymer concrete are then presented. The last part of the paper describes the results of the tests conducted on large-scale reinforced geopolymer concrete members and illustrates the application of the geopolymer concrete in the construction industry. The economic merits of the geopolymer concrete are also mentioned.

Keywords: *Design, Fly ash, Geopolymer concrete, Long-term properties, Products, Short-term properties, Structural members*

INTRODUCTION

The global use of concrete is second only to water. As the demand for concrete as a construction material increases, so also the demand for Portland cement. It is estimated that the production of cement will increase from about from 1.5 billion tons in 1995 to 2.2 billion tons in 2010 (Malhotra, 1999).

On the other hand, the climate change due to global warming has become a major concern. The global warming is caused by the emission of greenhouse gases, such as carbon dioxide (CO_2), to the atmosphere by human activities. Among the greenhouse gases, CO_2 contributes about 65% of global warming (McCaffery, 2002). The cement industry is held responsible for some of the CO_2 emissions, because the production of one ton of Portland cement emits approximately one ton of CO_2 into the atmosphere (Davidovits, 1994; McCaffery, 2002).

Several efforts are in progress to supplement the use of Portland cement in concrete in order to address the global warming issues. These include the utilisation of supplementary cementing materials such as fly ash, silica fume, granulated blast furnace slag, rice-husk ash and metakaolin, and the development of alternative binders to Portland cement.

In this respect, the geopolymer technology shows considerable promise for application in concrete industry as an alternative binder to the Portland cement (Duxson et al, 2007). In terms of global warming, the geopolymer technology could significantly reduce the CO_2 emission to the atmosphere caused by the cement industries as shown by the detailed analyses of Gartner (2004).

GEOPOLYMERS

Davidovits (1988; 1994) proposed that an alkaline liquid could be used to react with the silicon (Si) and the aluminum (Al) in a source material of geological origin or in by-product materials such as fly ash and rice husk ash to produce binders. Because the chemical

reaction that takes place in this case is a polymerisation process, he coined the term 'Geopolymer' to represent these binders.

Geopolymers are members of the family of inorganic polymers. The chemical composition of the geopolymer material is similar to natural zeolitic materials, but the microstructure is amorphous. The polymerization process involves a substantially fast chemical reaction under alkaline condition on Si-Al minerals, that results in a three-dimensional polymeric chain and ring structure consisting of Si-O-Al-O bonds (Davidovits, 1994).

The schematic formation of geopolymer material could be described by Equations (1) and (2) (Davidovits, 1994; van Jaarsveld et al., 1997):

$$\underset{\text{(Si-Al materials)}}{n(Si_2O_5,Al_2O_2)+2nSiO_2+4nH_2O+NaOH \text{ or } KOH} \rightarrow Na^+,K^+ + n(OH)_3\text{-Si-O-}Al^-\text{-O-Si-}\underset{\displaystyle|\;|}{(OH)_2} \quad \underset{\text{(Geopolymer precursor)}}{} \quad (1)$$

$$n(OH)_3\text{-Si-O-}\underset{\displaystyle|}{Al^-}\text{-O-Si-}\underset{\displaystyle|}{(OH)_2} + NaOH \text{ or } KOH \rightarrow (Na+,K+)\text{-}(\text{-Si-O-}\underset{\displaystyle|}{Al^-}\text{-O-Si-}\underset{\displaystyle|}{O}\text{-}) + 4nH_2O \quad \underset{\text{(Geopolymer backbone)}}{} \quad (2)$$

To date, the exact mechanism of setting and hardening of the geopolymer material is not clear, as well.

The last term in Equation 2 reveals that water is released during the chemical reaction that occurs in the formation of geopolymers. This water, expelled from the geopolymer matrix during the curing and further drying periods, leaves behind discontinuous nano-pores in the matrix, which provide benefits to the performance of geopolymers.

The last term in Equation 2 reveals that water is released during the chemical reaction that occurs in the formation of geopolymers. This water, expelled from the geopolymer matrix during the curing and further drying periods, leaves behind discontinuous nano-pores in the matrix, which provide benefits to the performance of geopolymers. The water in a geopolymer mixture, therefore, plays no role in the chemical reaction that takes place; it merely provides the workability to the mixture during handling. This is in contrast to the chemical reaction of water in a Portland cement concrete mixture during the hydration process.

There are two main constituents of geopolymers, namely the source materials and the alkaline liquids. The source materials for geopolymers based on alumina-silicate should be rich in silicon (Si) and aluminium (Al). These could be natural minerals such as kaolinite, clays, etc. Alternatively, by-product materials such as fly ash, silica fume, slag, rice-husk

ash, red mud, etc could be used as source materials. The choice of the source materials for making geopolymers depends on factors such as availability, cost, type of application, and specific demand of the end users.

The alkaline liquids are from soluble alkali metals that are usually Sodium or Potassium based. The most common alkaline liquid used in geopolymerisation is a combination of sodium hydroxide (NaOH) or potassium hydroxide (KOH) and sodium silicate or potassium silicate.

According to Davidovits (1994), geopolymeric materials have a wide range of applications in various industries such as in the automobile and aerospace, non-ferrous foundries and metallurgy, civil engineering and plastic industries. The type of application of geopolymeric materials is determined by the chemical structure in terms of the atomic ratio Si: Al in the polysialate.

This paper is devoted to heat-cured low-calcium fly ash-based geopolymer concrete. Low-calcium (ASTM Class F) fly ash is preferred as a source material than high-calcium (ASTM Class C) fly ash. The presence of calcium in high amounts may interfere with the polymerisation process and alter the microstructure (Gourley, 2003; Gourley and Johnson, 2005).

CONSTITUENTS OF GEOPOLYMER CONCRETE

Geopolymer concrete can be manufactured by using the low-calcium (ASTM Class F) fly ash obtained from coal-burning power stations. Most of the fly ash available globally is low-calcium fly ash formed as a by-product of burning anthracite or bituminous coal. Although coal burning power plants are considered to be environmentally unfriendly, the extent of power generated by these plants is on the increase due to the huge reserves of good quality coal available worldwide and the low cost of power produced from these sources. Therefore, huge quantities of fly ash will be available for many years in the future (Malhotra, 2006). The chemical composition and the particle size distribution of the fly ash must be established prior to use. An X-Ray Fluorescence (XRF) analysis may be used to determine the chemical composition of the fly ash.

Low-calcium fly ash has been successfully used to manufacture geopolymer concrete when the silicon and aluminum oxides constituted about 80% by mass, with the Si-to-Al ratio of about 2. The content of the iron oxide usually ranged from 10 to 20% by mass, whereas the calcium oxide content was less than 5% by mass. The carbon content of the fly ash, as indicated by the loss on ignition by mass, was as low as less than 2%. The particle size distribution tests revealed that 80% of the fly ash particles were smaller than 50 μm (Gourley, 2003; Gourley and Johnson, 2005; Hardjito and Rangan, 2005; Wallah and Rangan, 2006; Sumajouw and Rangan, 2006; Fernandez-Jimenez et al, 2006a; Sofi et al, 2006a; Siddiqui, 2007). The reactivity of low-calcium fly ash in geopolymer matrix has been studied by Fernandez-Jimenez, et al (2006b).

Coarse and fine aggregates used by the concrete industry are suitable to manufacture geopolymer concrete. The aggregate grading curves currently used in concrete practice are applicable in the case of geopolymer concrete (Hardjito and Rangan, 2005; Wallah and Rangan, 2006; Sumajouw and Rangan, 2006; Gourey, 2003; Gourley and Johnson, 2005; Siddiqui, 2007).

A combination of sodium silicate solution and sodium hydroxide (NaOH) solution can be used as the alkaline liquid. It is recommended that the alkaline liquid is prepared by mixing both the solutions together at least 24 hours prior to use.

The sodium silicate solution is commercially available in different grades. The sodium silicate solution (A53) with SiO_2-to-Na_2O ratio by mass of approximately 2, i.e., SiO_2 = 29.4%, Na_2O = 14.7%, and water = 55.9% by mass, is recommended.

The sodium hydroxide with 97-98% purity, in flake or pellet form, is commercially available. The solids must be dissolved in water to make a solution with the required concentration. The concentration of sodium hydroxide solution can vary in the range between 8 Molar and 16 Molar. The mass of NaOH solids in a solution varies depending on the concentration of the solution. For instance, NaOH solution with a concentration of 8 Molar consists of 8x40 = 320 grams of NaOH solids per litre of the solution, where 40 is the molecular weight of NaOH. The mass of NaOH solids was measured as 262 grams per kg of NaOH solution with a concentration of 8 Molar. Similarly, the mass of NaOH solids per kg of the solution for other concentrations was measured as 10 Molar: 314 grams, 12 Molar: 361 grams, 14 Molar: 404 grams, and 16 Molar: 444 grams (Hardjito and Rangan, 2005). Note that the mass of water is the major component in both the alkaline solutions.

In order to improve the workability, a high range water reducer and extra water may be added to the mixture.

MIXTURE PROPORTIONS OF GEOPOLMER CONCRETE

The primary difference between geopolymer concrete and Portland cement concrete is the binder. The silicon and aluminum oxides in the low-calcium fly ash reacts with the alkaline liquid to form the geopolymer paste that binds the loose coarse aggregates, fine aggregates, and other un-reacted materials together to form the geopolymer concrete.

As in the case of Portland cement concrete, the coarse and fine aggregates occupy about 75 to 80% of the mass of geopolymer concrete. This component of geopolymer concrete mixtures can be designed using the tools currently available for Portland cement concrete.

The compressive strength and the workability of geopolymer concrete are influenced by the proportions and properties of the constituent materials that make the geopolymer paste. Experimental results (Hardjito and Rangan, 2005) have shown the following:

- Higher concentration (in terms of molar) of sodium hydroxide solution results in higher compressive strength of geopolymer concrete.
- Higher ratio of sodium silicate solution-to-sodium hydroxide solution by mass lead to higher compressive strength of geopolymer concrete.
- The addition of naphthalene sulphonate-based super plasticiser, up to approximately 4% of fly ash by mass, improves the workability of the fresh geopolymer concrete; however, there is a slight degradation in the compressive strength of hardened concrete when the super plasticiser dosage is greater than 2%.
- The slump value of the fresh geopolymer concrete increases when the water content of the mixture increases.
- As the H_2O-to-Na_2O molar ratio increases, the compressive strength of geopolymer concrete decreases.

As can be seen from the above, the interaction of various parameters on the compressive strength and the workability of geopolymer concrete is complex. In order to assist the design of low-calcium fly ash-based geopolymer concrete mixtures, a single parameter called '*water-to-geopolymer solids ratio'* by mass was devised. In this parameter, the total mass of water is the sum of the mass of water contained in the sodium silicate solution, the mass of water used in the preparation of the sodium hydroxide solution, and the mass of extra water, if any, present in the mixture. The mass of geopolymer solids is the sum of the

mass of fly ash, the mass of sodium hydroxide solids used to make the sodium hydroxide solution, and the mass of solids in the sodium silicate solution (i.e. the mass of Na_2O and SiO_2).

Tests were performed to establish the effect of water-to-geopolymer solids ratio by mass on the compressive strength and the workability of geopolymer concrete. The test specimens were 100x200 mm cylinders, heat-cured in an oven at various temperatures for 24 hours. The results of these tests, plotted in Figure 1, show that the compressive strength of geopolymer concrete decreases as the water-to-geopolymer solids ratio by mass increases (Hardjito and Rangan, 2005). This observed trend is analogous to the well-known effect of water-to-cement ratio on the compressive strength of Portland cement concrete. Obviously, as the water-to-geopolymer solids ratio increased, the workability increased as the mixtures contained more water.

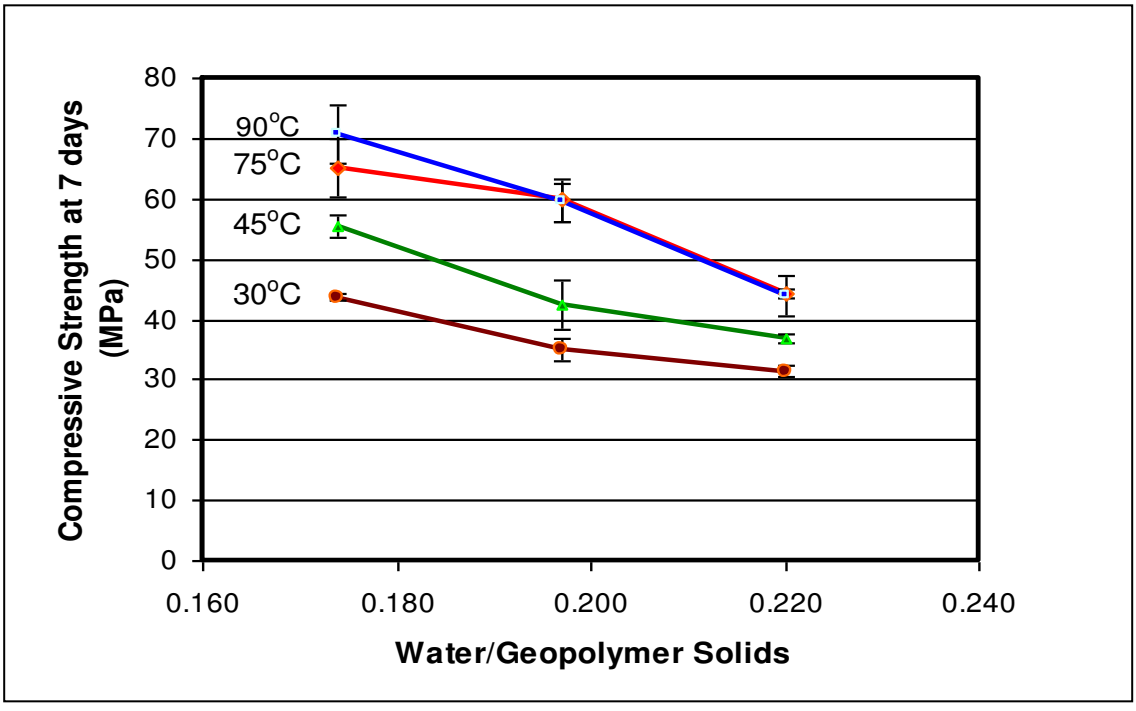

Figure 1. Effect of Water-to-Geopolymer Solids Ratio by Mass on Compressive Strength of Geopolymer Concrete (Hardjito and Rangan, 2005)

Similar trend shown in Figure 1 is also observed by Siddiqui (2007) in the studies conducted on steam-cured reinforced geopolymer concrete culverts.

The proportions of the two different geopolymer concrete mixtures used in laboratory studies are given in Table 1 (Wallah and Rangan, 2006). The details of numerous other mixtures are reported elsewhere (Hardjito and Rangan, 2005; Sumajouw and Rangan, 2006; Siddiqui, 2007).

Table 1. Geopolymer Concrete Mixture Proportions (Wallah and Rangan, 2006)

Materials		Mass (kg/m^3)	
		Mixture-1	Mixture-2
Coarse aggregates:	20 mm	277	277
	14 mm	370	370
	7 mm	647	647
Fine sand		554	554
Fly ash (low-calcium ASTM Class F)		408	408
Sodium silicate solution(SiO_2/Na_2O=2)		103	103
Sodium hydroxide solution		41 (8 Molar)	41 (14 Molar)
Super Plasticizer		6	6
Extra water		None	22.5

MIXING, CASTING, AND COMPACTION OF GEOPOLYMER CONCRETE

Geopolymer concrete can be manufactured by adopting the conventional techniques used in the manufacture of Portland cement concrete. In the laboratory, the fly ash and the aggregates were first mixed together in dry state in 80-litre capacity pan mixer for about three minutes. The aggregates were prepared in saturated-surface-dry (SSD) condition.

The alkaline liquid was mixed with the super plasticiser and the extra water, if any. The liquid component of the mixture was then added to the dry materials and the mixing continued usually for another four minutes. The fresh concrete could be handled up to 120 minutes without any sign of setting and without any degradation in the compressive strength. The fresh concrete was cast and compacted by the usual methods used in the case of Portland cement concrete (Hardjito and Rangan, 2005; Wallah and Rangan, 2006; Sumajouw and Rangan, 2006). Fresh fly ash-based geopolymer concrete was usually cohesive. The workability of the fresh concrete was measured by means of the conventional slump test.

The compressive strength of geopolymer concrete is influenced by the wet-mixing time. Test results show that the compressive strength increased as the wet-mixing time increased (Hardjito and Rangan, 2005).

CURING OF GEOPOLYMER CONCRETE

Heat-curing of low-calcium fly ash-based geopolymer concrete is generally recommended. Heat-curing substantially assists the chemical reaction that occurs in the geopolymer paste.

Both curing time and curing temperature influence the compressive strength of geopolymer concrete. The effect of curing time is illustrated in Figure 2 (Hardjito and Rangan, 2005). The test specimens were 100x200 mm cylinders heat-cured at 60^{o}C in an oven. The curing time varied from 4 hours to 96 hours (4 days). Longer curing time improved the polymerisation process resulting in higher compressive strength. The rate of increase in strength was rapid up to 24 hours of curing time; beyond 24 hours, the gain in strength is only moderate. Therefore, heat-curing time need not be more than 24 hours in practical applications.

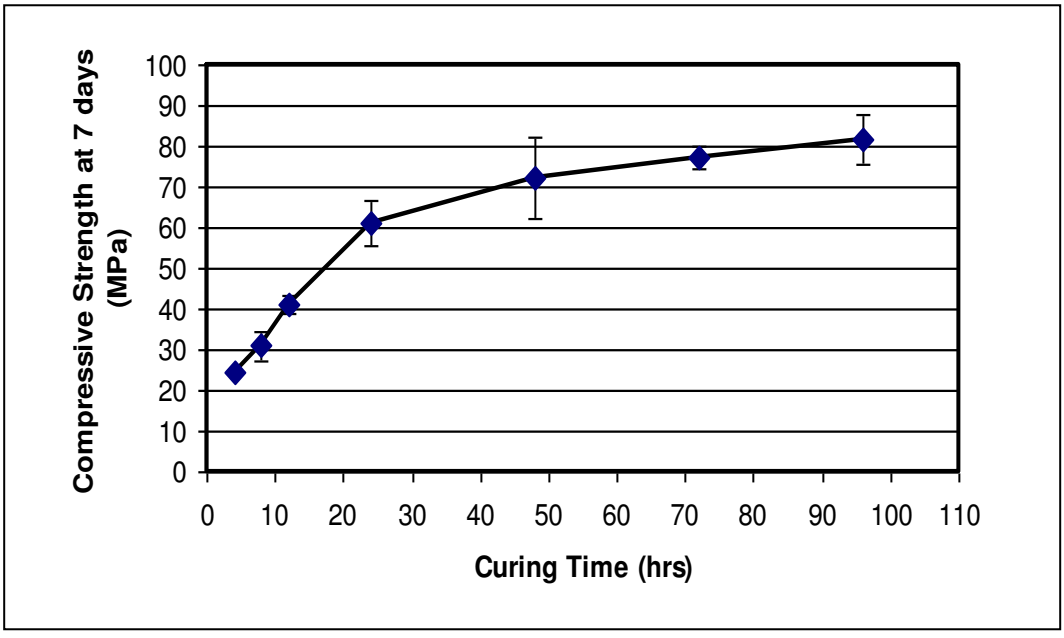

Figure 2. Effect of Curing Time on Compressive Strength of Geopolymer Concrete (Hardjito and Rangan, 2005)

Figure 1 shows the effect of curing temperature on the compressive strength of geopolymer concrete (Hardjito and Rangan, 2005). Higher curing temperature resulted in larger compressive strength.

Heat-curing can be achieved by either steam-curing or dry-curing. Test data show that the compressive strength of dry-cured geopolymer concrete is approximately 15% larger than that of steam-cured geopolymer concrete (Hardjito and Rangan, 2005). The temperature required for heat-curing can be as low as 30 degrees C (Figure 1). In tropical climates, this range of temperature can be provided by the ambient conditions.

The required heat-curing regime can be manipulated to fit the needs of practical applications. In laboratory trials (Hardjito and Rangan, 2005), precast products were manufactured using geopolymer concrete; the design specifications required steam-curing at 60^{o}C for 24 hours. In order to optimise the usage of formwork, the products were cast and steam-cured initially for about 4 hours. The steam-curing was then stopped for some time to allow the release of the products from the formwork. The steam-curing of the products then continued for another 21 hours. This two-stage steam-curing regime did not produce any degradation in the strength of the products.

A two-stage steam-curing regime was also used by Siddiqui (2007) in the manufacture of prototype reinforced geopolymer concrete box culverts. It was found that steam curing at 80 ˚C for a period of 4 hours provided enough strength for de-moulding of the culverts; this was then followed by further steam curing for another 20 hours at 80 ˚C to attain the required design compressive strength.

Also, the start of heat-curing of geopolymer concrete can be delayed for several days. Tests have shown that a delay in the start of heat-curing up to five days did not produce any degradation in the compressive strength. In fact, such a delay in the start of heat-curing substantially increased the compressive strength of geopolymer concrete (Hardjito and Rangan, 2005). This may be due to the geopolymerisation that occurs prior to the start of heat-curing.

The above flexibilities in the heat-curing regime of geopolymer concrete can be exploited in practical applications and prototype products can be manufactured so that they are ready for use within 24 hours after casting.

DESIGN OF GEOPOLYMER CONCRETE MIXTURES

Concrete mixture design process is vast and generally based on performance criteria. Based on the information given above, some simple guidelines for the design of heat-cured low-calcium fly ash-based geopolymer concrete are proposed (Rangan, 2008).

The role and the influence of aggregates are considered to be the same as in the case of Portland cement concrete. The mass of combined aggregates may be taken to be between 75% and 80% of the mass of geopolymer concrete.

The performance criteria of a geopolymer concrete mixture depend on the application. For simplicity, the compressive strength of hardened concrete and the workability of fresh concrete are selected as the performance criteria. In order to meet these performance criteria, the alkaline liquid-to-fly ash ratio by mass, *water-to-geopolymer solids ratio* (*see 'Mixture Proportions of Geopolymer Concrete' for definition*) by mass, the wet-mixing time, the heat-curing temperature, and the heat-curing time are selected as parameters.

With regard to alkaline liquid-to-fly ash ratio by mass, values in the range of 0.30 and 0.45 are recommended. Based on the results obtained from numerous mixtures made in the laboratory over a period of four years, the data given in Table 2 are proposed for the design of low-calcium fly ash-based geopolymer concrete. Note that wet-mixing time of 4 minutes, and steam-curing at 60^{o}C for 24 hours after casting are proposed. The data given in Figures 1 and 2 may be used as guides to choose other curing temperature, and curing time.

Sodium silicate solution is cheaper than sodium hydroxide solids. Commercially available sodium silicate solution (A53) with SiO_2-to-Na_2O ratio by mass of approximately 2, i.e., Na_2O = 14.7%, SiO_2 = 29.4%, and water = 55.9% by mass, and sodium hydroxide solids (NaOH) with 97-98% purity are recommended. Laboratory experience suggests that the ratio of sodium silicate solution-to-sodium hydroxide solution by mass may be taken approximately as 2.5 (Hardjito and Rangan, 2005).

The design data given in Table 2 assumes that the aggregates are in saturated-surface-dry (SSD) condition. In other words, the coarse and fine aggregates in a geopolymer concrete mixture must neither be too dry to absorb water from the mixture nor too wet to add water to the mixture. In practical applications, aggregates may contain water over and above the SSD condition. Therefore, the extra water in the aggregates above the SSD condition must be estimated and included in the calculation of water-to-geopolymer solids ratio given in Table 2.

Table 2: Data for Design of Low-Calcium Fly Ash-Based Geopolymer Concrete Mixtures (Rangan, 2008, 2009)

Water-to-geopolymer solids ratio, by mass	Workability	Design compressive strength (wet-mixing time of 4 minutes, steam curing at 60°C for 24 hours after casting), MPa
0.16	Very Stiff	60
0.18	Stiff	50
0.20	Moderate	40
0.22	High	35
0.24	High	30

Notes:

- The fineness modulus of combined aggregates is taken to be in the range of 4.5 and 5.0.
- When cured in dry-heat, the compressive strength may be about 15% larger than the above given values.
- When the wet-mixing time is increased from 4 minutes to 16 minutes, the above compressive strength values may increase by about 30%.
- Standard deviation of compressive strength is about 10% of the above given values.

SHORT-TERM PROPERTIES OF GEOPOLYMER CONCRETE

Behavior in Compression

The behavior and failure mode of fly ash-based geopolymer concrete in compression is similar to that of Portland cement concrete. Test data show that the strain at peak stress is in the range of 0.0024 to 0.0026 (Hardjito and Rangan, 2005). Collins et al (1993) have proposed that the stress-strain relation of Portland cement concrete in compression can be predicted using the following expression:

$$\sigma_c = f_{cm} \frac{\varepsilon_c}{\varepsilon_{cm}} \frac{n}{n - 1 + (\varepsilon_c / \varepsilon_{cm})^{nk}} \qquad (3)$$

where f_{cm} = peak stress, ε_{cm} = strain at peak stress, $n = 0.8 + (f_{cm}/17)$, and $k = 0.67 + (f_{cm}/62)$ when $\varepsilon_c/\varepsilon_{cm} > 1$ or equal to 1.0 when $\varepsilon_c/\varepsilon_{cm} \leq 1$. Test data show that the measured stress-strain curve correlated well with that calculated using Equation 3.

As expected, the modulus of elasticity increased as the compressive strength of geopolymer concrete increased (Hardjito and Rangan, 2005).

For Portland cement concrete, the draft Australian Standard AS3600 (2005) recommends the following expression to calculate the value of the modulus of elasticity within an error of plus or minus 20 %:

$$E_c = \rho^{1.5} (0.024 \sqrt{f_{cm}} + 0.12) \qquad \text{(MPa)} \qquad (4)$$

where ρ is the unit-weight of concrete in kg/m^3, and f_{cm} is the mean compressive strength in MPa.

American Concrete Institute (ACI) Committee 363 (1992) has recommended the following expression to calculate the modulus of elasticity:

$$E_c = 3320 \sqrt{f_{cm}} + 6900 \qquad \text{(MPa)} \qquad (5)$$

Test data showed that the measured values of modulus elasticity were consistently lower than the values calculated using Equation 4 and Equation 5. This is due to the type of coarse aggregates used in the manufacture of the geopolymer concrete (Rangan, 2008).

Sofi et al (2007a) used low-calcium fly ash from three different sources to manufacture geopolymer mortar and concrete specimens. The measured values of modulus of elasticity reported in that study showed a trend similar to that observed in the results given by Hardjito and Rangan (2005).

Experimental studies have shown that the aggregate-binder interfaces are stronger in geopolymers than in the case of Portland cement (Lee and van Deventer, 2004). This may lead to superior mechanical properties and long-term durability of geopolymer concretes (Provis et al, 2007).

The Poisson's ratio of fly ash-based geopolymer concrete with compressive strength in the range of 40 to 90 MPa falls between 0.12 and 0.16. These values are similar to those of Portland cement concrete.

Indirect Tensile Strength

The tensile strength of fly ash-based geopolymer concrete was measured by performing the cylinder splitting test on 150x300 mm concrete cylinders. These test results showed that the tensile splitting strength of geopolymer concrete is only a fraction of the compressive strength, as in the case of Portland cement concrete (Hardjito and Rangan, 2005).

The draft Australian Standards for Concrete Structures AS3600 (2005) recommends the following design expression to determine the characteristic principal tensile strength (f_{ct}) of Portland cement concrete:

$$f_{ct} = 0.4 \sqrt{f_{cm}} \qquad \text{(MPa)} \qquad (6)$$

Neville (2000) recommended that the relation between the tensile splitting strength and the compressive strength of Portland cement concrete may be expressed as:

$$f_{ct} = 0.3 (f_{cm})^{2/3} \qquad \text{(MPa)} \qquad (7)$$

The calculated values of f_{ct} using Equations 6 and 7 showed that the measured indirect tensile strength of fly ash-based geopolymer concrete is larger than the values recommends by the draft Australian Standard AS3600 (2005) and Neville (2000) for Portland cement concrete.

Sofi et al (2007a) also performed indirect tensile tests on geopolymer mortar and concrete specimens made using three different sources of low-calcium fly ash. The trend of the test results observed in that study is similar to that observed in the results given by Hardjito and Rangan (2005).

Unit-weight

The unit-weight of concrete primarily depends on the unit mass of aggregates used in the mixture. Tests show that the unit-weight of the low-calcium fly ash-based geopolymer concrete is similar to that of Portland cement concrete. When granite-type coarse aggregates were used, the unit-weight varied between 2330 and 2430 kg/m^3 (Hardjito and Rangan, 2005).

LONG-TERM PROPERTIES OF GEOPOLYMER CONCRETE

Compressive Strength

Two geopolymer concrete mixture proportions used in laboratory studies are given in Table 1 (Wallah and Rangan, 2006). Numerous batches of these mixtures were manufactured during a period of four years. For each batch of geopolymer concrete made, 100x200 mm cylinders specimens were prepared. At least three of these cylinders were tested for compressive strength at an age of seven days after casting. The unit-weight of specimens was also determined at the same time. For these numerous specimens made from Mixture-1 and Mixture-2 and heat-cured at 60^{o}C for 24 hours after casting, the average results are presented in Table 3 (Wallah and Rangan, 2006).

Table 3. Mean Compressive Strength and Unit-weight of Geopolymer Concrete (Wallah and Rangan, 2006)

Mixture	Curing type	7th Day compressive strength (heat-curing at 60^{o}C for 24 hours), MPa		Unit-weight, kg/m^3	
		Mean	Standard deviation	Mean	Standard deviation
Mixture-1	Dry curing (oven)	58	6	2379	17
	Steam curing	56	3	2388	15
Mixture-2	Dry curing (oven)	45	7	2302	52
	Steam curing	36	8	2302	49

In order to observe the effect of age on compressive strength of heat-cured geopolymer concrete, 100x200 mm cylinders were made from several batches of Mixture-1 given in Table 1. The specimens were heat-cured in an oven for 24 hours at 60°C. Test data showed that the compressive strength increased with age in the order of 10 to 20 percent when compared to the 7th day compressive strength (Wallah and Rangan 2006).

The above test data demonstrate the consistent quality, reproducibility, and long-term stability of low-calcium fly ash-based geopolymer concrete.

Creep and Drying Shrinkage

The creep and drying shrinkage behavior of heat-cured low-calcium fly ash-based geopolymer concrete was studied for a period of one year (Wallah and Rangan, 2006). The geopolymer concrete mixture proportions used in that study were Mixture-1 and Mixture-2, as given in Table 1. The test specimens were 150x300 mm cylinders, heat-cured at 60oC for 24 hours. The creep tests commenced on the 7th day after casting the test specimens and the sustained stress was 40% of the compressive strength on that day. The test results obtained for specimens made using Mixture-1 and heat-cured in an oven are shown in Figure 3 (Wallah and Rangan, 2006). The test trends were similar for both Mixture-1 and Mixture-2, heat-cured either in an oven or steam-cured.

Test results (Figure 3) show that heat-cured fly ash-based geopolymer concrete undergoes very little drying shrinkage in the order of about 100 micro strains after one year. This value is significantly smaller than the range of values of 500 to 800 micro strains experienced by Portland cement concrete.

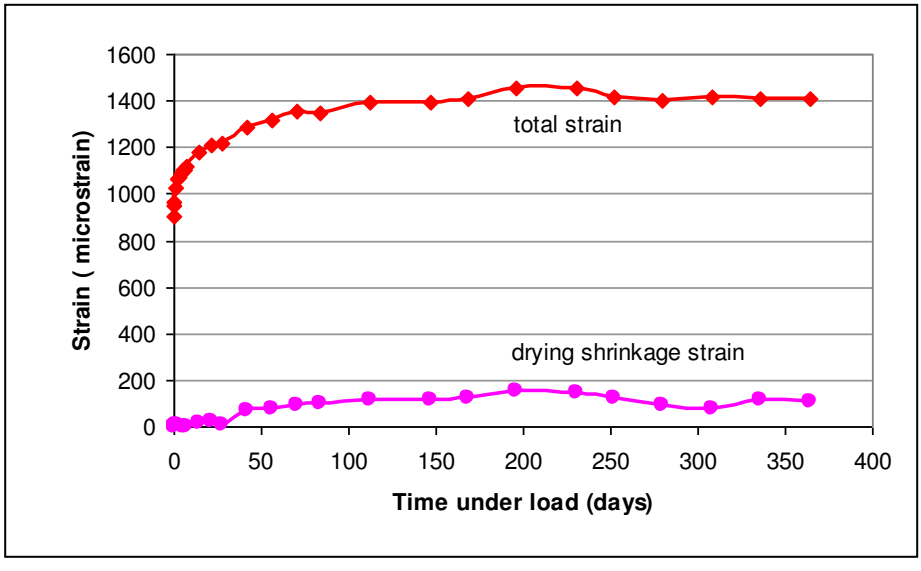

Figure 3. Total Strain and Drying Shrinkage Strain of Heat-Cured Geopolymer Concrete (Wallah and Rangan, 2006)

The creep coefficient, defined as the ratio of creep strain-to-elastic strain, after one year of loading for heat-cured geopolymer concrete with compressive strength of 40, 47 and 57 MPa is between 0.6 and 0.7, while for geopolymer concrete with compressive strength of 67 MPa this value is between 0.4 and 0.5. The specific creep, defined as the creep strain per

unit of sustained stress, data are shown in Figure 4 (Wallah and Rangan, 2006). These values are about 50% of the values recommended by the draft Australian Standard AS3600 for Portland cement concrete.

The low drying shrinkage and the low creep of heat-cured geopolymer concrete offer benefits to the long-term performance of geopolymer concrete members.

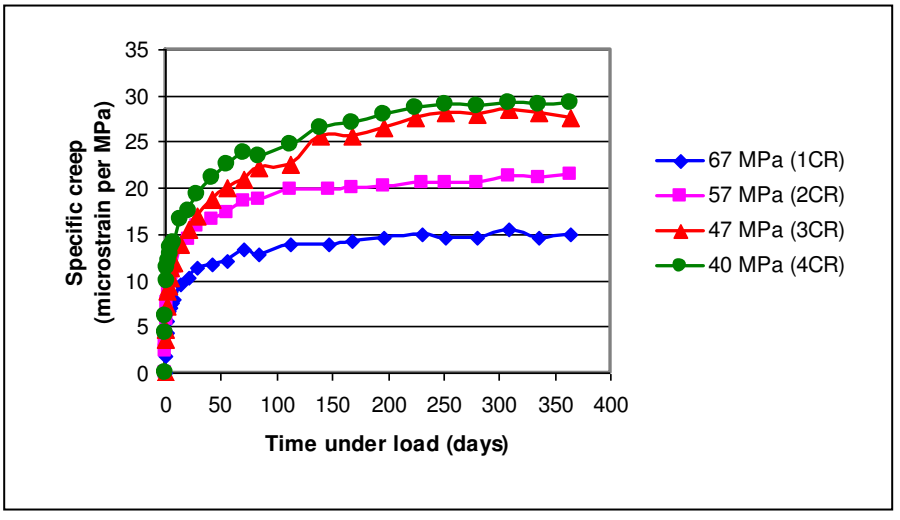

Figure 4. Effect of Compressive Strength on Creep of Heat-Cured Geopolymer Concrete (Wallah and Rangan, 2006)

The drying shrinkage strains of geopolymer concrete cured in ambient conditions are many folds larger than those experienced by the heat-cured specimens (Figure 5). As indicated by Equation 2, water is released during the chemical reaction process of geopolymers. In the specimens cured in ambient conditions, this water may evaporate over a period of time causing significantly large drying shrinkage strains especially in first two weeks as can be seen in Figure 5 (Wallah and Rangan, 2006)

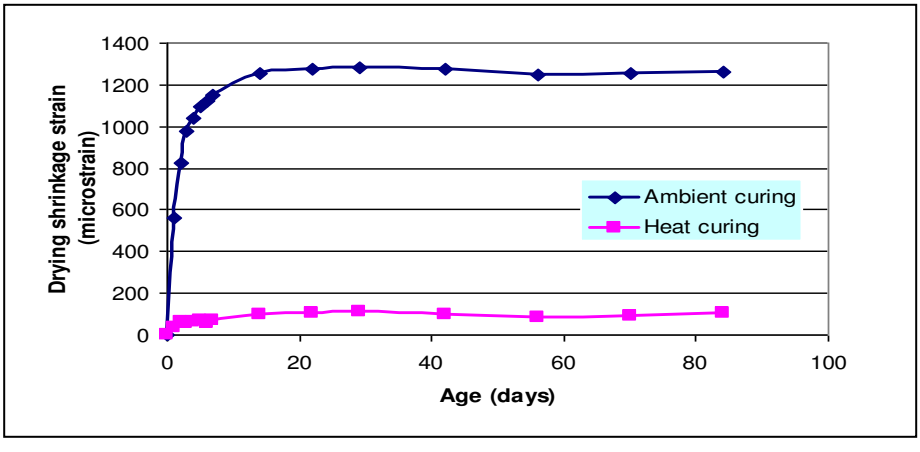

Figure 5: Drying Shrinkage of Heat-cured and Ambient-cured Geopolymer Concrete (Wallah and Rangan, 2006)

Sulfate Resistance

Tests were performed to study the sulfate resistance of heat-cured low-calcium fly ash-based geopolymer concrete. The test specimens were made using Mixture-1 (Table 1) and heat-cured at 60oC for 24 hours after casting; they were immersed in 5% sodium sulfate solution for various periods of exposure up to one year. The sulfate resistance was evaluated based on the change in mass, change in length, and change in compressive strength of the specimens after sulfate exposure. The test specimens were 100x200 mm cylinders for change in mass and change in compressive strength tests and 75x75x285 mm prisms for change in length test (Wallah and Rangan, 2006).

Test results showed that heat-cured low-calcium fly ash-based geopolymer concrete has an excellent resistance to sulfate attack. There was no damage to the surface of test specimens after exposure to sodium sulfate solution up to one year. There were no significant changes in the mass and the compressive strength of test specimens after various periods of exposure up to one year. The change in length was extremely small and less than 0.015% (Wallah and Rangan, 2006).

The deterioration of Portland cement concrete due to sulfate attack is attributed to the formation of expansive gypsum and ettringite which causes expansion, cracking, and spalling in the concrete. Low-calcium fly ash-based geopolymer concrete undergoes a different mechanism to that of Portland cement concrete and the geopolymerisation products are also different from hydration products. The main product of geopolymerisation, as given by Equation 2, is not susceptible to sulfate attack like the hydration products. Because there is generally no gypsum or ettringite formation in the main products of geopolymerisation, there is no mechanism of sulfate attack in heat-cured low-calcium fly ash-based geopolymer concrete. However, the presence of high calcium either in the fly ash or in the aggregates could cause the formation of gypsum and ettringite in geopolymer concrete.

Sulfuric Acid Resistance

Tests were performed to study the sulfuric acid resistance of heat-cured low-calcium fly ash-based geopolymer concrete. The concentration of sulfuric acid solution was 2%, 1% and 0.5%. The sulfuric acid resistance of geopolymer concrete was evaluated based on the mass loss and the residual compressive strength of the test specimens after acid exposure up to one year. The test specimens, 100x200 mm cylinders, were made using Mixture-1 (Table 1) and heat-cured at 60oC for 24 hours after casting (Wallah and Rangan, 2006).

The visual appearance of specimens after exposure to sulfuric acid solution showed that acid attack slightly damaged the surface of the specimens.

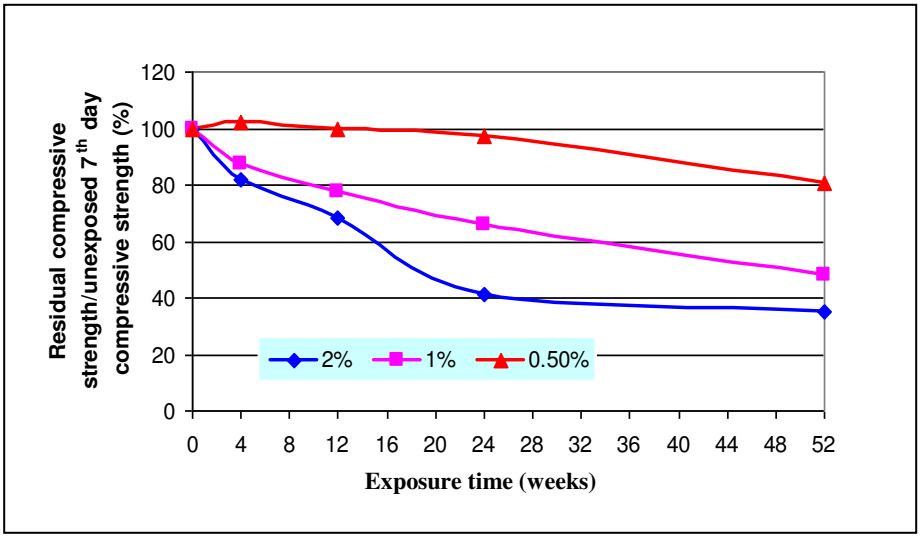

Figure 6. Acid Resistance of Heat-cured Geopolymer Concrete (Wallah and Rangan, 2006)

The maximum mass loss of test specimens of about 3% after one year of exposure is relatively small compared to that for Portland cement concrete as reported in other studies. As shown in Figure 6, exposure to sulfuric acid caused degradation in the compressive strength; the extent of degradation depended on the concentration of the acid solution and the period of exposure (Wallah and Rangan, 2006).

The acid resistance of geopolymer concrete must be considered in relation to the performance of Portland cement concrete in a similar environment. Past research data have shown that geopolymeric materials performed significantly better in acid resistance compared to Portland cement (Davidovits, 1994; Gourley and Johnson, 2005). The superior performance of geopolymeric materials in acidic environment is attributed to the lower calcium content of the source material.

REINFORCED GEOPOLYMER CONCRETE COLUMNS AND BEAMS

In order to demonstrate the application of heat-cured low-calcium fly ash-based geopolymer concrete, twelve reinforced columns and twelve reinforced beams were manufactured and tested (Sumajouw and Rangan, 2006).

In the column test program, the primary parameters were longitudinal reinforcement ratio, load eccentricity, and compressive strength of geopolymer concrete. The longitudinal reinforcement ratio was 1.47% and 2.95%. The column cross-section was 175 mm square. The average yield strength of longitudinal steel was 519 MPa. Closed ties made of 6mm diameter hard-drawn wires at 100 mm spacing were used as lateral reinforcement. The concrete cover was 15 mm. The columns were subjected to eccentric compression and bent in single curvature bending. The columns were pin-ended with an effective length of 1684 mm.

The mixture proportions of geopolymer concrete used in the manufacture of column specimens are given in Table 4. The average slump of fresh concrete varied between 210 mm and 240 mm. The nominal compressive strength of geopolymer concrete was 40 MPa for GCI and GCII series and, 60 MPa for GCIII and GCIV series. These target compressive

strengths were achieved by using the mixtures given in Table 8 and by exploiting the flexibilities of heat-curing regime of geopolymer concrete. Accordingly, in the case of GC-I and GC-II column series, the test specimens were steam-cured at a temperature of 60oC for 24 hours after casting; on the other hand, the specimens of GC-III and GC-IV series were kept in laboratory ambient conditions for three days and then steam-cured at a temperature of 60oC for 24 hours.

The mixture proportions of geopolymer concrete used in the manufacture of beam specimens are also given in Table 4. The average slump of the fresh concrete varied from 175 mm for GBIII series to 255 mm for GBI series. The target compressive strength of geopolymer concrete was 40 MPa for GBI series, 50 MPa for GBII series, and 70 MPa for GBIII series. The specimens were kept in laboratory ambient conditions for three days after casting, and then steam-cured at 60^{o}C for 24 hours to achieve the target strengths.

The beam cross-section was 200mm wide by 300mm deep, and 3300mm in length. The test parameters were concrete compressive strength and longitudinal tensile reinforcement ratio. All beams contained two 12mm diameter deformed bars as compression reinforcement, and two-legged vertical stirrups made of 12 mm diameter deformed bars at 150 mm spacing as shear reinforcement. The longitudinal tensile reinforcement ratios were 0.64, 1.18, 1.84, and 2.69%. The average yield strength of tensile steel bars varied between 550 and 560 MPa. The concrete cover was 25 mm. The beams were simply supported over a span of 3000mm, and subjected to two concentrated loads placed symmetrically on the span. The distance between the loads was 1000mm.

Table 4. Geopolymer Concrete Mixture Proportions for Reinforced Columns and Beams (Sumajouw and Rangan, 2006)

Materials	Columns		Beams
	Mass (kg/m^3)		
10mm aggregates	555	550	550
7mm aggregates	647	640	640
Fine sand	647	640	640
Fly ash	408	404	404
Sodium hydroxide solution	41 (16Molar)	41 (14Molar)	41 (14 Molar)
Sodium silicate solution	103	102	102
Super plasticizer	6	6	6
Extra added water	26 (GCI and GCII)	16.5 (GCIII and GCIV)	25.5 (GBI) 17.0 (GBII) 13.5(GBIII)

The behavior and failure modes of reinforced geopolymer concrete columns were similar to those observed in the case of reinforced Portland cement concrete columns (Sumajouw and Rangan, 2006). As expected, the load capacity of columns was influenced by the load-eccentricity, the concrete compressive strength, and the longitudinal reinforcement ratio. When the load eccentricity decreased, the load capacity of columns increased. The load

capacity also increased when the compressive strength of concrete and the longitudinal reinforcement ratio increased.

The load-carrying capacity of reinforced geopolymer concrete columns was calculated using both a simplified stability analysis proposed by Rangan (1990) and the moment-magnifier method incorporated in the daft Australian Standard for Concrete Structures AS 3600 (2005) and the American Concrete Institute Building Code ACI 318-02 (2002). The calculated failure loads correlate well with the test values (Sumajouw and Rangan, 2006). These results demonstrate that the methods of calculations used in the case of reinforced Portland cement concrete columns are applicable for reinforced geopolymer concrete columns.

The behaviour and failure mode of reinforced geopolymer concrete beams were similar to those observed in the case of reinforced Portland cement concrete beams. The flexural capacity of beams was influenced by the concrete compressive strength and the tensile reinforcement ratio. The flexural strength of reinforced geopolymer concrete beams was calculated using the conventional flexural strength theory of reinforced concrete beams as described in standards and building codes such as the draft Australian Standard, AS 3600 (2005) and the ACI Building Code, ACI 318-02 (2002). The results showed that for beams with tensile reinforcement ratio of 1.18%, 1.84%, and 2.69%, the test and calculated values agreed well. In the case of beams with tensile steel ratio of 0.64%, as expected, the calculated values were conservative due to the neglect of the effect of strain hardening of tensile steel bars on the ultimate bending moment (Sumajouw and Rangan, 2006).

Mid-span deflection at service load of reinforced geopolymer concrete beams was calculated using the elastic bending theory and the serviceability design provisions given in the draft Australian Standard, AS 3600 (2005). According to AS3600, the calculation of short-term deflection of reinforced concrete beams should include the effects of cracking, tension stiffening, and shrinkage properties of the concrete. In these calculations, the service load was taken as the test failure load divided by 1.5; measured values of modulus of elasticity and drying shrinkage strain of geopolymer concrete were used. Good correlation of test and calculated deflections at service load was observed (Sumajouw and Rangan, 2006).

In all, the above results demonstrate that reinforced low-calcium (ASTM Class F) fly ash-based geopolymer concrete structural members can be designed using the design provisions currently used in the case of reinforced Portland cement concrete members. The studies carried out by Chang, et al (2007), Sarker, et al (2007a, 2007b), and Sofi, et al (2007b) also demonstrate the application of fly ash-based geopolymer concrete.

GEOPOLYMER PRECAST CONCRETE PRODUCTS

Gourley and Johnson (2005) have reported the details of geopolymer precast concrete products on a commercial scale. The products included sewer pipes, railway sleepers, and wall panels. Reinforced geopolymer concrete sewer pipes with diameters in the range from 375 mm to 1800 mm have been manufactured using the facilities currently available to make similar pipes using Portland cement concrete. Tests performed in a simulated aggressive sewer environment have shown that geopolymer concrete sewer pipes outperformed comparable Portland cement concrete pipes by many folds. Gourley and Johnson (2005) also reported the good performance of reinforced geopolymer concrete railway sleepers in mainline tracks and excellent resistance of geopolymer mortar wall panels to fire.

Siddiqui (2007) demonstrated the manufacture of reinforced geopolymer concrete culverts on a commercial scale. Tests have shown that the culverts performed well and met the specification requirements of such products.

ECONOMIC BENEFITS OF GEOPOLYMER CONCRETE

Heat-cured low-calcium fly ash-based geopolymer concrete offers several economic benefits over Portland cement concrete. The price of one ton of fly ash is only a small fraction of the price of one ton of Portland cement. Therefore, after allowing for the price of alkaline liquids needed to the make the geopolymer concrete, the price of fly ash-based geopolymer concrete is estimated to be about 10 to 30 percent cheaper than that of Portland cement concrete.

In addition, the appropriate usage of one ton of fly ash earns approximately one carbon-credit that has a redemption value of about 10 to 20 Euros. Based on the information given in this paper, one ton low-calcium fly ash can be utilized to manufacture approximately three cubic meters of high quality fly ash-based geopolymer concrete, and hence earn monetary benefits through carbon-credit trade.

Furthermore, the very little drying shrinkage, the low creep, the excellent resistance to sulfate attack, and good acid resistance offered by the heat-cured low-calcium fly ash-based geopolymer concrete may yield additional economic benefits when it is utilized in infrastructure applications.

CONCLUDING REMARKS

The paper presented information on heat-cured fly ash-based geopolymer concrete. Low-calcium fly ash (ASTM Class F) is used as the source material, instead of the Portland cement, to make concrete.

Low-calcium fly ash-based geopolymer concrete has excellent compressive strength and is suitable for structural applications. The salient factors that influence the properties of the fresh concrete and the hardened concrete have been identified. Data for the design of mixture proportions are included.

The elastic properties of hardened geopolymer concrete and the behavior and strength of reinforced geopolymer concrete structural members are similar to those observed in the case of Portland cement concrete. Therefore, the design provisions contained in the current standards and codes can be used to design reinforced low-calcium fly ash-based geopolymer concrete structural members.

Heat-cured low-calcium fly ash-based geopolymer concrete also shows excellent resistance to sulfate attack, good acid resistance, undergoes low creep, and suffers very little drying shrinkage. The paper has identified several economic benefits of using geopolymer concrete.

REFERENCES

ACI Committee 318 (2002) *Building Code Requirements for Structural Concrete*, American Concrete Institute, Farmington Hills, MI.

ACI Committee 363 (1992) *State of the Art Report on High-Strength Concrete*, American Concrete Institute, Detroit, USA.

Chang, E. H. , Sarker, P., Lloyd, N. and Rangan, B.V. (2007) "Shear behaviour of reinforced fly ash-based geopolymer concrete beams", *Proceedings of the23rd Biennial Conference of the Concrete Institute of Australia*, Adelaide, Australia, pp 679 – 688.

Collins, M. P., Mitchell, D. and MacGregor, J.G (1993) "Structural Design Considerations for High Strength Concrete", *ACI Concrete International* 15(5): 27-34.

Committee BD-002 Standards Australia (2005) *Concrete Structures: Draft Australian Standard AS3600-200x,* Standards Australia.

Davidovits, J. (1988) "Soft Mineralogy and Geopolymers", *Proceedings of the of Geopolymer 88 International Conference*, the Université de Technologie, Compiègne, France.

Davidovits, J. (1994) "High-Alkali Cements for 21st Century Concretes. in Concrete Technology, Past, Present and Future", *Proceedings of V. Mohan Malhotra Symposium*, Editor: P. Kumar Metha, ACI SP- 144, 383-397.

Duxson, P., Provis, J. L., Lukey, G. C. and van Deventer, J. S. J. (2007) "The Role of Inorganic Polymer Technology in the Development of Green Concrete", *Cement and Concrete Research*, 37(12), 1590-1597.

Fernández-Jiménez, A. M., Palomo, A., and López-Hombrados, C. (2006a) "Engineering Properties of Alkali-activated Fly Ash Concrete", *ACI Materials Journal*, 103(2), 106-112.

Fernández-Jiménez, A. M., de la Torre, A. G., Palomo, A., López-Olmo, G., Alonso, M. M. and Aranda, M. A. G. (2006b) "Quantitative Determination of Phases in the Alkali Activation of Fly Ash, Part I, Potential Ash Reactivity", *Fuel*, 85(5-6), 625-634.

Gartner, E. (2004) "Industrially Interesting Approaches to 'Low-CO_2' Cements", *Cement and Concrete Research,* 34(9), 1489-1498.

Gourley, J. T. (2003) "Geopolymers; Opportunities for Environmentally Friendly Construction Materials", Paper presented at the *Materials 2003 Conference: Adaptive Materials for a Modern Society,* Sydney.

Gourley, J. T., & Johnson, G. B. (2005) "Developments in Geopolymer Precast Concrete", Paper presented at the *International Workshop on Geopolymers and Geopolymer Concrete*, Perth, Australia.

Hardjito, D. and Rangan, B. V. (2005) *Development and Properties of Low-Calcium Fly Ash-based Geopolymer Concrete,* Research Report GC1, Faculty of Engineering, Curtin University of Technology, Perth, available at *espace@curtin*.

Lee, W. K. W. and van Deventer, J. S. J. (2004) "The Interface between Natural Siliceous Aggregates and Geopolymers", *Cement and Concrete Research*, 34(2) 195-206.

Malhotra, V. M. (1999) "Making concrete 'greener' with fly ash", *ACI Concrete International*, 21, 61-66.

Malhotra, V.M. (2006) "Reducing CO2 Emissions", *ACI Concrete International*, 28, 42-45.

McCaffrey, R. (2002) "Climate Change and the Cement Industry", *Global Cement and Lime Magazine (Environmental Special Issue)*, 15-19.

Neville, A. M. (2000) *Properties of Concrete*, Prentice Hall.

Provis, J. L., Muntingh, Y., Lloyd, R. R., Xu, H., Keyte, L. M., Lorenzen, L., Krivenko, P. V. and van Deventer J. S. J. (2007) "Will Geopolymers Stand the Test of Time?", *Ceramic Engineering and Science Proceedings*, 28(9), 235-248.

Rangan, B.V. (1990) "Strength of Reinforced Concrete Slender Columns", *ACI Structural* Journal, 87(1) 32-38.

Rangan, B.V. (2008) "*Low-Calcium Fly Ash-based Geopolymer Concrete"*, Chapter 26 in Concrete Construction Engineering Handbook, Editor-in Chief: E.G. Nawy, Second Edition, CRC Press, New York.

Rangan, B.V. (2009) "Engineering Properties of Geopolymer Concrete", Chapter 13 in Geopolymers: Structures, Processing, Properties, and Applications, Editors: J.Provis and J. van Deventer, Woodhead Publishing Limited, London.

Sarker, P.K., Grigg A. and Chang, E.H. (2007a) "Bond Strength of Geopolymer Concrete with Reinforcing Steel", Proceedings of *Recent Developments in Structural Engineering, Mechanics and Computation*, CD ROM, Editor: A. Zingoni, Millpress, the Netherlands, 1315-1320.

Sarker, P.K., and deMeillon, T. (2007b) "Residual Strength of Geopolymer Concrete After Exposure to High Temperature", Proceedings of *Recent Developments in Structural Engineering, Mechanics and Computation,* CD ROM, Editor: A. Zingoni, Millpress, the Netherlands, 1566-1571.

Siddiqui, K.S. (2007) "Strength and Durability of Low-Calcium Fly Ash-based Geopolymer Concrete", *Final Year Honours Dissertation*, The University of Western Australia, Perth.

Sofi, M., van Deventer, J. S. J., Mendis, P. A. and Lukey, G. C. (2007a) "Engineering Properties of Inorganic Polymer Concretes (IPCs)", *Cement and Concrete Research*, 37(2), 251- 257.

Sofi, M., van Deventer, J. S. J., Mendis, P. A. and Lukey, G. C. (2007b) "Bond Performance of Reinforcing Bars in Inorganic Polymer Concrete (IPC)", *Journal of Materials Science*, 42(9), 3007-3016.

Sumajouw, M.D.J. and Rangan, B.V. (2006) *Low-Calcium Fly Ash-Based Geopolymer Concrete: Reinforced Beams and Columns,* Research Report GC3, Faculty of Engineering, Curtin University of Technology, Perth, available at *espace@curtin* or *www.geopolymer.org*.

Wallah, S.E. and Rangan, B.V. (2006) *Low-Calcium Fly Ash-Based Geopolymer Concrete: Long-Term Properties*, Research Report GC2, Faculty of Engineering, Curtin University of Technology, Perth, available at *espace@curtin* or *www.geopolymer.org*.

Van Jaarsveld, J. G. S., van Deventer, J. S. J. and Lorenzen L. (1997) "The Potential Use of Geopolymeric Materials to Immobilise Toxic Metals: Part I. Theory and Applications", *Minerals Engineering* 10(7), 659-669.

THE POTENTIAL OF CALCINED MALAYSIAN KAOLIN AS A POZZOLANIC ADMIXTURE FOR CONCRETE

Hashim Abdul Razak[1], Wong Hong Seong[2] and Chai Hwa Kian[3]

[1]Department of Civil Engineering, University of Malaya, Malaysia
[2]Department of Civil Engineering, Imperial College of Science and Technology, UK
[3]Department of Civil Engineering, Osaka University, Japan

Abstract

The utilisation of calcined kaolin as a pozzolanic mineral admixture for high-performance mortar and concrete has received much interests in recent years. Commercial application of metakaolin in the concrete industry has already commenced in industrialised countries, particularly in the Unites States and Japan. Despite being a major producer of refined kaolin, Malaysia has yet to realise the full potential of its local clay, since only a limited research has been conducted on the material so far. This paper presents the findings of an on-going investigation on to the effects of laboratory produced metakaolin, in enhancing the strength and durability characteristics of concrete. Metakaolin mixtures of up to 15% replacement were designed and tested for compressive strength, flexural, tensile splitting, modulus of elasticity, initial surface absorption, water absorption and sorptivity. It was found that the mixtures with metakaolin did not adversely affect the workability of concrete. In fact, improvement in the areas of bleeding and finishability was noted. Metakaolin was found to enhance the overall strength and elastic properties of concrete. The inclusion of metakaolin also greatly reduced the water absorption of concrete.

Keywords: Compressive strength, durability, high-performance concrete, kaolin, metakaolin, modulus of elasticity, tensile strength

INTRODUCTION

Natural pozzolans in the form of calcined earths blended with lime have been used to produce cementitious materials for thousands of years. Fired clay pottery fragments which were ground to powder form and mixed with lime, created the first man-made hydraulic cement and its uses dates back some 3600 years ago (Cook, 1986). Today, the role of calcined earths has remained as a traditional construction material in India and Egypt. Despite the fact that the pozzolanicity of clay soils has been recognised a long time ago, calcined soil pozzolanas faced considerable competition from industrial waste materials or by-products such as fly ash, granulated blastfurnace slag and silica fume, which are generally cheaper. However, these materials are not easily available in many regions, and thus calcined clay may present a better alternative for supplementary cementitious materials, economically and technically.

Metakaolin ($Al_2Si_2O_7$) is a white, ultrafine powdered form of anhydrous aluminosilicate derived from the calcination of raw kaolin. Calcination is a term referring to the controlled process of burning at a specific temperature range, to obtain a quasi-amorphous material. Heating first removes the absorbed water on the kaolinite particle surface, and as the temperature is increased to 600-900^{o}C, the interlayer and hydrate water is expelled, causing the crystalline structure to collapse. This process of thermal activation (Sayanam, 1989 and Ambroise, 1986) or dehydroxylation, leads to the breakdown or partial breakdown of the crystal lattice structure, forming a transition phase which is highly disordered, amorphous and possesses pozzolanicity. However, prolonged exposure to temperatures above the

dehydroxylation temperature promotes recrystallisation to form mullite and hence loss in pozzolanicity.

Previous literature has shown the potential of metakaolin in strength enhancement of mortar and concrete (Caldarone, 1994, Wild, 1996 and Curcio, 1998), portlandite consumption (Oriol, 1995 and Wild, 1997), pore refinement (Khatib, 1996 and Kostuch, 1993), suppressing alkali-silica reaction (Walters, 1991) and sulphate resistance (Khatib, 1998). According to a 1996 geological survey (Loh, 1996), it is estimated that there are 110 million tonnes (MT) of raw kaolin reserves in Malaysia. The states of Perak (59 MT), Sarawak (22 MT) and Johor (20 MT) contribute 92% of total kaolin reserves in Malaysia. The normal grade kaolin is utilised as fillers and extenders for paper, paint, plastic and rubber, and for the manufacture of ceramics. However, the prospect of local kaolin as a pozzolanic material is unknown and yet to be explored. Thus, the present study aims to investigate the strength and durability characteristics of concrete incorporated with metakaolin, and to establish the potential of local kaolin in producing an engineered and optimised pozzolanic mineral admixture for high-performance concrete.

EXPERIMENTAL WORK

Materials

Ordinary Portland cement equivalent to ASTM Type 1, single sized 10 mm crushed granite stone and silica sand were used. Metakaolin was obtained by calcining refined kaolin using a rotary electrical furnace in the laboratory. The temperature was uniformly increased from 30^{o}C to 700^{o}C in 3 hours, and then kept constant at 700^{o}C for another 7 hours. The metakaolin, which is in an off-white powdered form, was left to cool in the furnace overnight and later was kept free from moisture in a plastic container.

Physical and chemical properties of cement and metakaolin are presented in Table 1 and Table 2 respectively. Metakaolin was found to have a specific gravity of 2.52, average particle size of 9.5 μm and specific surface area (BET) of 9.5 m^2/g. Chemical analysis shows that the metakaolin is principally composed of silica (57%) and alumina (35%). X-ray diffraction analysis on the raw and thermally treated kaolin (Figure 1) indicates that the local clay consists mainly of kaolinite, illite and mica. Crystallised phases of muscovite, cristobalite and quartz were also detected. Upon calcination, the XRD analysis shows a mainly amorphous material with small quantities of crystallized phases. The decomposition of kaolinite is highly evident at two theta (copper radiation) values of 13^{o}, 21^{o}, 25^{o}, 56^{o} and 63^{o}.

Table 1. Physical properties of cement and metakaolin

Physical properties	Cement	Metakaolin
Colour	Greenish Grey	Light creamy white
Specific gravity (ASTM D 854-92), %	3.11	2.52
Fineness [a], %		
Passing 150 μm	98	94
Passing 75 μm	91	88
Passing 45 μm	77	84
Average particle size D (v, 0.5) [a], μm	23	9.5
Specific surface area, m^2/kg		
Blaine (ASTM C 204-94a)	343	-
Nitrogen adsorption (BET) [b]	4 200	9 500
Standard consistency (ASTM C 187-86), %	27.4	-
Setting time (ASTM C 191-92), min		
Initial	110	-
Final	300	-

a. Obtained from laser particle size analysis, conducted using *Malvern Mastersizer X*.
b. Brunauer-Emmett-Teller method, conducted using *Micromeritics ASAP 2000*.

Table 2. Chemical properties of cement and metakaolin

	Cement	Metakaolin
Chemical analysis (%) [a]		
Silicon dioxide (SiO_2)	20.99	57.4
Aluminium oxide (Al_2O_3)	6.19	35.26
Calcium oxide (CaO)	65.96	0.02
Ferric oxide (Fe_2O_3)	3.86	0.94
Magnesium oxide (MgO)	0.20	0.18
Sodium oxide (Na_2O)	0.17	< 0.01
Potassium oxide (K_2O)	0.60	3.17
Phosphorous oxide (P_2O_5)	0.05	0.09
Titanium oxide (TiO_2)	0.40	0.43
Manganan oxide (MnO)	0.06	< 0.01
Loss on ignition, LOI	1.53	2.52
	100.01	100.01
Bogue potential compounds (%)		
Tricalcium silicate (C_3S)	50.32	
Dicalcium silicate (C_2S)	22.22	
Tricalcium aluminate (C_3A)	11.06	
Tetracalcium aluminoferrite (C_4AF)	11.75	
Equivalent alkalis	0.56	
	95.91	

a. *Philips PW 1480 X-ray spectrometer*

The result of single differential thermal analysis (SDTA) on refined kaolin given in Figure 2 reveals three distinctive regions; a broad endotherm at 100°C to 200°C caused by the removal of adsorbed water, an endothermic peak at 550°C, which is associated to the dehydroxylation of kaolinite, and an exothermic peak at 1000°C due to the recrystallisation of mullite. A substantial weight loss in the region of 500°C to 600°C shown in the thermogravimetric (TGA) curve is also an indicative of kaolinite decomposition. It is interesting to note that although the dehydroxylation temperature obtained from thermal analysis is approximately 600°C, research has shown that the optimum temperature of calcination from a lime-pozzolana strength point of view is higher, at approximately 700°C-800°C (Cook, 1986 and Sabir 2001).

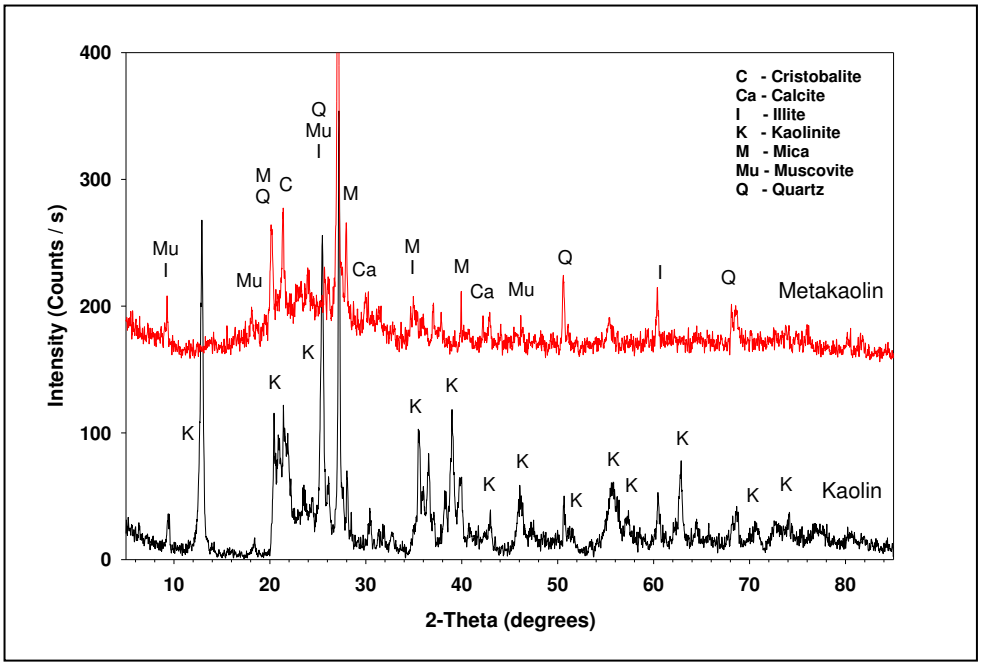

Figure 1. X-ray diffraction pattern of kaolin and metakaolin

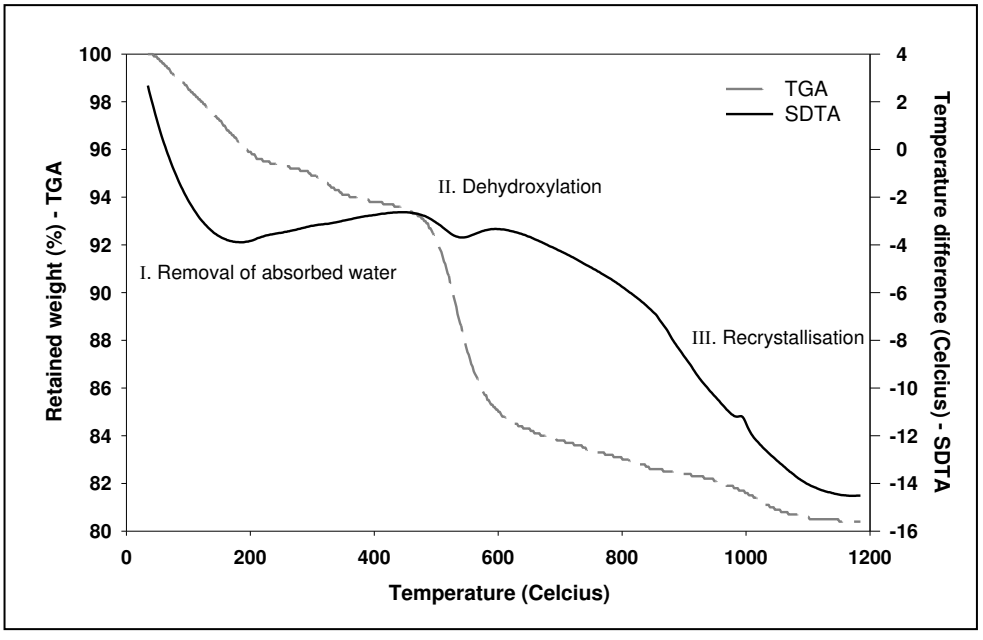

Figure 2. Thermal analysis of refined kaolin[1]

1. Mettler Toledo TGA/SDTA 851^{e}, sample (20-30mg) heated under static atmospheric conditions at 20°C per minute

The silica sand used was of three different sizes: coarse, medium and fine, and was combined in the ratio of 4:2:4 to obtain a fine aggregate which complied with the medium grading of BS 882:1992. The physical properties of the aggregates are shown in Table 3. A polycarboxylic ether based superplasticizer was used as a chemical admixture. The dark brown liquid admixture has a 20% solids content and specific gravity of 1.05. Mixing and curing water was taken directly from tap supply.

Table 3. Physical properties of aggregates

Physical Properties	Coarse Aggregate (Granite stone)	Fine Aggregate (Silica sand)
Specific Gravity	2.57	2.65
Size	5 mm – 10 mm	75 μm – 4.75 mm
Grading	Single sized 10 mm	Medium (BS 882:1992)
Total Water Content (%)	0.25	0.05
Absorption (%)	0.25	0.40
Fineness Modulus	-	2.5

Mixture Proportions

The experimental work covered four concrete mixtures with a fixed water-cementitious material ratio of 0.3. The mixtures are the control (C) and three weight-to-weight metakaolin replacement levels of 5% (MK 5), 10% (MK 10) and 15% (MK 15). All mixtures were designed in accordance to the Sherbrooke mix design method (Aitcin, 1997) for non-air entrained high-performance concrete based on absolute volume. In designing the mixtures, the following parameters were fixed: total cementitious material content of 500 kg/m^3, superplasticizer dosage of 0.8% of total cementitious material, coarse aggregate content of 1050 kg/m^3 and sand to total aggregate ratio of 0.4. The aggregates were assumed to be in saturated and surfaced dry condition and therefore water corrections were made. Additional water contributed by the superplasticizer was also corrected. The mixture proportions are summarised in Table 4.

Table 4. Mixture proportions

Mix	Cement (kg/m^3)	MK (kg/m^3)	Water (kg/m^3)	W/C	Granite stone (kg/m^3)	Silica sand (kg/m^3)	Super-plasticizer (L/m^3)
C	500	-	150	0.3	1050	700	19
MK5	475	25	150	0.3	1050	700	19
MK10	450	50	150	0.3	1050	700	19
MK15	425	75	150	0.3	1050	700	19

A pan mixer with a capacity of 0.2 m^3 was used in the batching process. Materials were fed into the mixer and were mixed dry for about 1½ minutes. Three quarters of the total mixing water was then added followed by superplasticizer and finally the remaining water. Wet mixing was continued for a total period of 5 minutes before discharging. Immediately after the concrete was discharged, various tests on fresh concrete were conducted such as slump test (BS 1881: Part 102: 1983), flow table test (BS 1881: Part 105: 1984), Vebe test (BS 1881: Part 104: 1983), air content test by pressure method (BS 1881: Part 106: 1983)

and density of compacted fresh concrete (BS 1881: Part 107: 1983). The concrete temperature, ambient temperature and ambient relative humidity were also recorded.

Testing Procedures

Table 5 summarises the various types of specimens prepared for this study. Specimens were cast in steel moulds and compacted in three uniform layers by means of a vibrating table. The amount of vibration required to achieve full compaction was based on the Vebe time. After casting, the specimens were covered with wet burlap to prevent moisture loss and to minimise plastic shrinkage. Specimens were demoulded after 24 hours, weighed (in air and water) and wet cured continuously in a water tank, under room temperature until the day of testing. The saturated densities of cube specimen were determined using water displacement method (BS 1881: Part 114: 1983).

Table 5. Testing programme

Test	Specimen	Age at testing (days)
Cube compressive strength (BS 1881: Pt. 116: 1983)	100 x 100 x 100 mm cubes	1,3,7,28,56,90&180
Tensile splitting strength (BS 1881: Pt. 117: 1983)	150 x 300 mm cylinders	3,7,28,56,90&180
Flexural strength (BS 1881: Pt. 118: 1983)	100 x 100 x 500 mm prisms	3,7,28,56,90&180
Static modulus of elasticity (BS 1881: Pt. 121: 1983)	150 x 300 mm cylinders	3,7,28,56,90&180
Initial Surface Adsorption	150 x 150 x 150 mm cubes	7 & 28 [a]
Water absorption	100 x 100 x 100 mm cubes	7 & 28 [a]
Sorptivity test	100 x 200 mm cylinders	7 & 28 [a]

[a.] *After 28 days of full water curing.*

Before testing, the dimensions and saturated mass of each specimen were measured. For the determination of compressive strength, three cubes were tested at each age. For tensile splitting strength, flexural strength and static modulus of elasticity in compression, two specimens were tested at each age. In the determination of static modulus of elasticity, the upper loading level of one-third of the compressive strength was estimated based on the cube compressive strength result. End preparation of all cylinder specimens was done by grinding to maintain uniform end conditions. A compressometer, with an effective gauge length of 150 mm and a dial gauge extensometer, with a sensitivity of 0.001 mm were used as a strain measurement apparatus. A hydraulic driven compression-testing machine, with a maximum capacity of 2000 KN was used throughout. All specimens were tested in moist condition.

For durability studies, three tests were conducted: namely the initial surface absorption (ISAT), water absorption and sorptivity. Specimens for these tests were initially cured in water for 28 days, after which the specimens were taken out from the curing tank and exposed to air. Durability tests were then conducted at ages 7 and 28 days after the initial full water curing. Prior to testing, all specimens were dried in a laboratory oven at 105^{o}C until a constant mass was achieved, taken as when the difference between two successive weightings, performed in an interval of 24 hours, does not exceed 0.1% of the initial mass. ISAT was performed by measuring the absorption of water from a pressure head of 200 mm

into the concrete from the top surface. The flow, in ml/m^2.s was calculated at intervals of 10, 30, 60 and 120 minutes.

Water absorption test was conducted by completely immersing dried cube specimens in water at room temperature for 96 hours. The sorptivity test was carried out by immersing the bottom surface of a cylindrical specimen into a tray of water at room temperature. The depth of immersion was approximately 1-2 mm. The specimen was placed on glass rods to permit free water movement at the bottom surface. The total surface area of water within the tray should not be less than 10 times of the specimen cross-sectional area. Specimens were removed from the tray and weighed at intervals of 5, 10, 30, 60, 120 and 180 minutes. The volume of water absorbed per unit cross-sectional area at each time interval was evaluated and the sorptivity determined from the slope of the graph of the water absorbed against time.

RESULTS AND DISCUSSIONS

Properties of fresh concrete

All mixtures displayed high workability and flowability, despite the fact that the mixtures were designed with a low water/binder ratio and low dosage of superplasticizer. The control mixture achieved the highest slump of 225 mm while the MK 15 mixture had the lowest slump of 205 mm. A slight drop in the flowability of concrete was noted when the amount of metakaolin was increased. On visual inspection, the high flowable mixtures did not exhibit any excessive bleeding or segregation while transporting, placing, compacting and finishing the fresh concrete. In fact, the mixtures incorporating metakaolin showed less bleeding as shown in Figure 3, and little amount of laitance, a white deposit formed on the surface of hardened concrete, compared to the control as shown in Figure 4. The addition of these high fineness metakaolin particles creates a stabilising effect on to the rheology of fresh concrete, reduces bleeding and segregation tendencies by physically blocking up pores between cement particles and by increasing the amount of adsorbed water and contact area between particles.

An increase in air content was observed in the metakaolin mixtures. The fresh concrete densities for all mixtures are slightly above 2400 kg/m^3, which lies in the normal weight concrete range (2200-2600 kg/m^3). A slight reduction was noted when mineral admixtures were used. This was expected because since the mixture proportions are based on the absolute volume method, in the replacement mixtures, the lower specific gravity mineral admixture replaces parts of the cement, thus yielding a slight decline in density of fresh concrete. The hardened density was measured at age 1-day, and is the average measured density of all 30 cubes for that particular mixture.

a) Control **b) MK 15**

Figure 3. Flow of fresh concrete

a) Control **b) MK 15**

Figure 4. Laitance on concrete surface at age 1-day

From the results, it is apparent that the inclusion of metakaolin into the mixtures did not cause any significant loss in workability even when the amount of replacement was increased up to 15%. This outcome was also reflected in previous studies (Caldarone 1994, Balogh 1995, Marsh 1994), whereby it was found that metakaolin did not cause any increase in water demand or superplasticizer dosage in order to maintain the same concrete slump. On the other hand, silica fume which is the current industrial standard as high performance pozzolan, reduces the workability of concrete significantly especially at low water/binder ratio (Duval 1998, Bayasi 1993). According to Caldarone (1994), mixtures produced using metakaolin required 25% to 35% less superplasticizer than silica fume concrete to achieve a similar workability at the same water/cementitious material ratio. Metakaolin, which is described as hydrophilic, promotes rapid dispersion in the mixture. Its larger particle size distribution gives a less sticky and less cohesive nature of fresh concrete, which leads to better finishability compared to silica fume.

Compressive strength

The cube compressive strength results are shown in Figure 5. It can be observed that all the metakaolin mixtures achieved a higher compressive strength than the control from 7 days onwards. At 28 days, the highest compressive strength was achieved by MK 15, followed by MK 10, MK 5 and C. This suggests that the strength enhancement is greater as the level of metakaolin replacement increases. However, at later ages, there was no significant difference in compressive strength recorded between the metakaolin mixtures. At 90 days, the average strength enhancement by the metakaolin mixtures was approximately 13%.

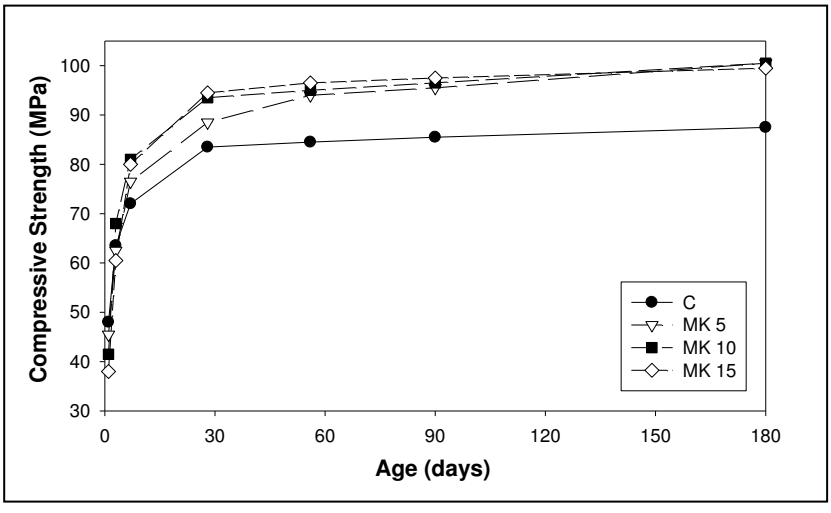

Figure 5. Cube compressive strength development

The gain in compressive strength with time for the control mixture is principally dependent on the rate of cement hydration, while for the metakaolin mixtures are dependent on the combination of the rates of cement hydration and the pozzolanic reaction. Therefore, a relative strength plot as presented in Figure 6, defined as ratio of the strength of the metakaolin mixture to the control mixture at each curing age will be able to provide a comprehensive insight into the rates of reaction in a blended pozzolanic system relative to the plain control system.

Based on the relative strength curve, the metakaolin mixtures did not produce an early strength enhancement brought by the initial acceleration of cement hydration (filler effect) as reported by previous researchers (Caldarone, 1994, Wild, 1996 and Curcio, 1998). Instead, a decrease in compressive strength at the early ages was noted, and this reduction is proportional to the amount of metakaolin replacement. This could be caused by the fact that when cement in concrete is replaced by any mineral admixture, it produces an immediate dilution effect, whereby the early concrete strength would be reduced in approximate proportion to the degree of replacement (Wild, 1996). However, it is also suggested that if the mineral admixture is finely divided, it may behave as fillers and accelerate cement hydration, thus increasing the early compressive strength by producing efficient packing, denser and more homogeneous initial transition zone. The fine particles also act as nuclei for the formation and growth of hydration products. If the finely divided mineral admixture possesses pozzolanicity, then the lime consumption and the formation of additional

cementitious gels will further increase concrete strength by improving the microstructure of the transition zone.

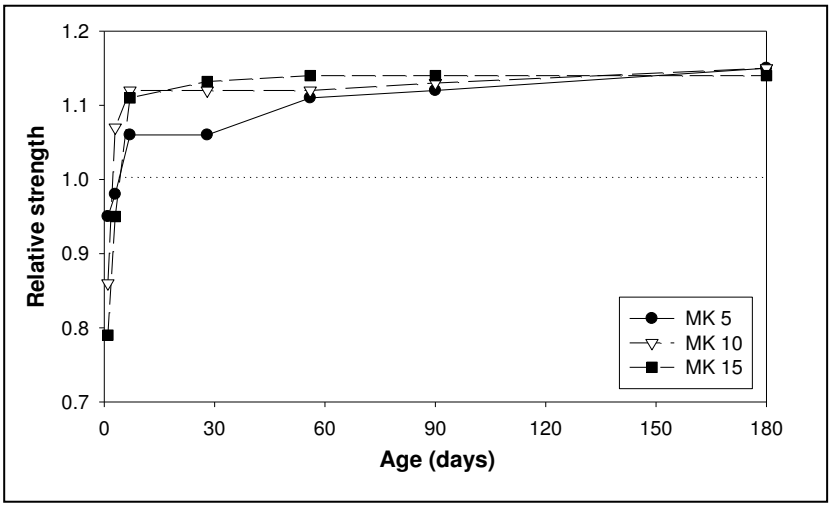

Figure 6. Relative strength for metakaolin concrete

Hence, the strength development of a pozzolanic mixture during the early ages is in fact influenced by three interdependent variables: dilution, filler and the pozzolanic reaction; and the end result will be determined by those that predominate in a particular mixture. In the present study, it seems that the increase in strength resulting from the filler effect did not negate the strength loss due to dilution, even at low replacement levels. The highest gain in relative strength occurred between the ages of 3 and 7 days, suggesting that the role played by metakaolin in rapid removal of calcium hydroxide and acceleration of cement hydration is dominant at this period. Subsequently the increment in relative strength was only subtle and approached a constant value by 90 days. The present study also did not record a maximum in relative strength at any ages. Wild (1996 and 1997) reported a maximum relative strength at 14 days, which corresponds to a minimum in CH content and a maximum in the rate of pozzolanic reactivity. Subsequently relative strength declines and this was attributed to the formation of an inhibiting layer of reaction products surrounding the metakaolin particles. Unfortunately, the present study has been conducted without the 14^{th} day measurement, and thus this trend could not be confirmed in our specimens.

Flexural strength, tensile splitting strength and modulus of elasticity

Figure 7 illustrates the tensile strength development for all mixtures up to the age of 180 days. The incorporation of metakaolin significantly increased the flexural strength of concrete while only slightly improved tensile splitting strength. At 90 days, the average strength enhancement by the metakaolin mixtures was approximately 16% for flexural strength and only 5% for tensile splitting strength. The effect of inclusion of metakaolin onto the tensile strength of concrete is similar to its effect on compressive strength. However, at higher levels of compressive strength, the rate of tensile strength increment decreases. In this study, the average ratio of tensile splitting strength to compressive strength is about 0.06, where as in the case of normal strength concrete, the ratio is in the order of 0.1. This indicates that high strength concrete has a higher degree of brittleness.

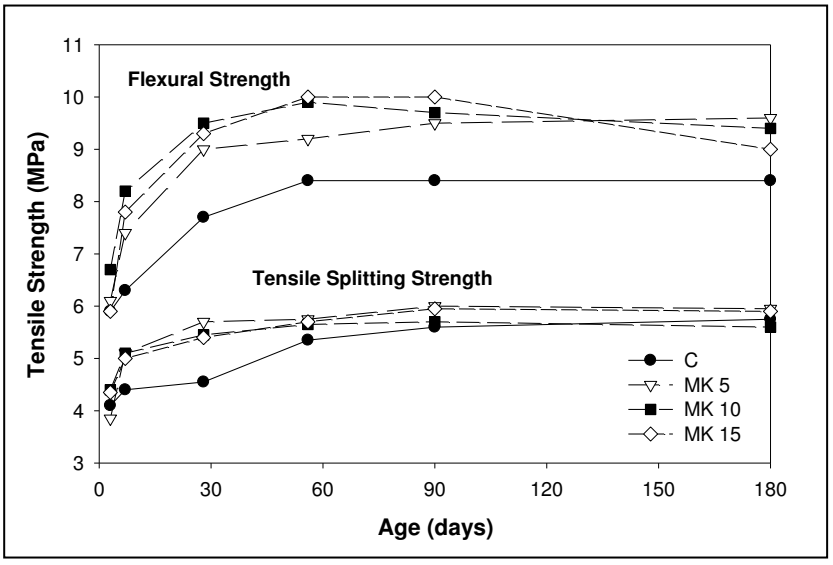

Figure 7. Tensile strength development

In Figure 8, the effect of metakaolin on the elastic modulus of concrete displays similar trends to its effect on compressive and tensile strength. Generally as the concrete strength increases, so does the modulus of elasticity, although the rate of increase is less compared to the rate of increase in strength. This has also been expressed in previous findings of Asselanis (1989). However, the metakaolin mixtures gave a clear indication of enhancement in modulus of elasticity at a much later age (28 days) compared to the compressive and tensile strength (7 days), and the MK 15 mixture gave a lower value of modulus of elasticity than anticipated. At age 90 days, the average enhancement in the metakaolin mixtures was about 4 %.

Initial surface absorption test (ISAT)

The ISAT was performed to investigate the permeability of concrete cover, hence illustrates the durability of concrete when subjected to external chemical attack. Concrete cover is the weakest, most permeable and absorptive part of concrete matrix as compared to the internal microstructure. The near surface concrete is highly heterogeneous in nature due to the relative movement of cement paste and aggregates during compaction and bleeding of mix water. As a result, there is a porosity gradient, whereby the porosity of near surface is higher than that of internal concrete (Basheer, 2001). Therefore, the durability of concrete in general can be characterised by simply determining the water permeability of concrete surface, which is considered as the most critical and vulnerable part towards external fluid ingress.

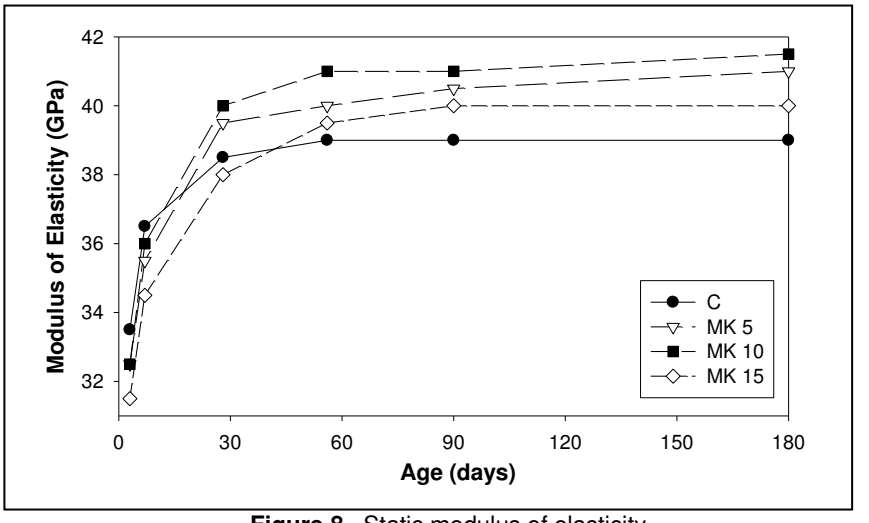

Figure 8. Static modulus of elasticity

The ISAT results for 7 and 28 days are presented in Figure 9. The flow decreases exponentially with time. The rate of water absorption reduces with time because when the outer surface zone is saturated, it becomes more difficult for water to be absorbed by the inner pores. The control mixture showed the highest flow ranging from 0.136 to 0.075 ml/m^2.s for 7 days, and 0.121 to 0.071 ml/m^2.s for 28 days, whereas the MK 10 mixture exhibited the lowest flow, ranging from 0.102 to 0.047 ml/m^{2}s for 7 days and 0.091 to 0.046 ml/m^{2}s for 28 days. Both MK 5 and MK 15 mixtures gave significant flow reductions as compared to the control mixture. From the results, it can be concluded that 10% is the optimum replacement level for metakaolin based on the resistance towards water absorption on the surface.

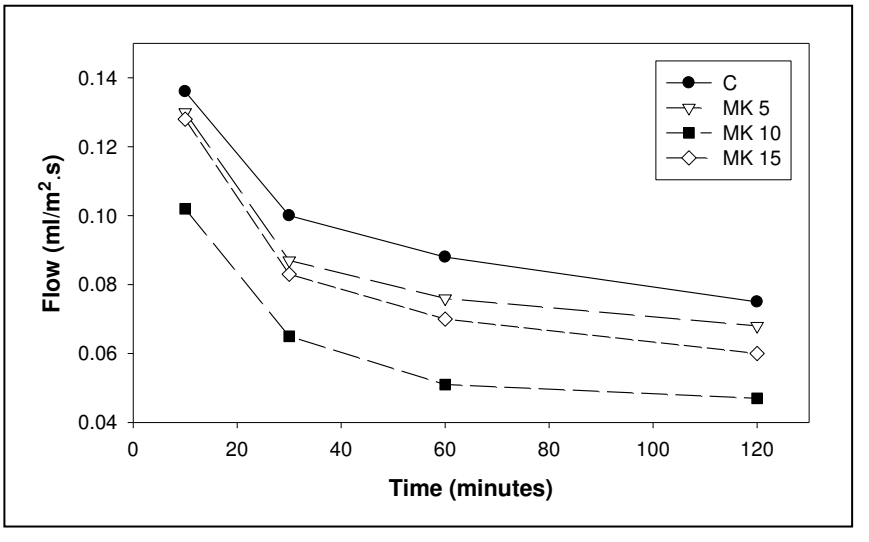

Figure 9a. Initial Surface Adsorption (7d)

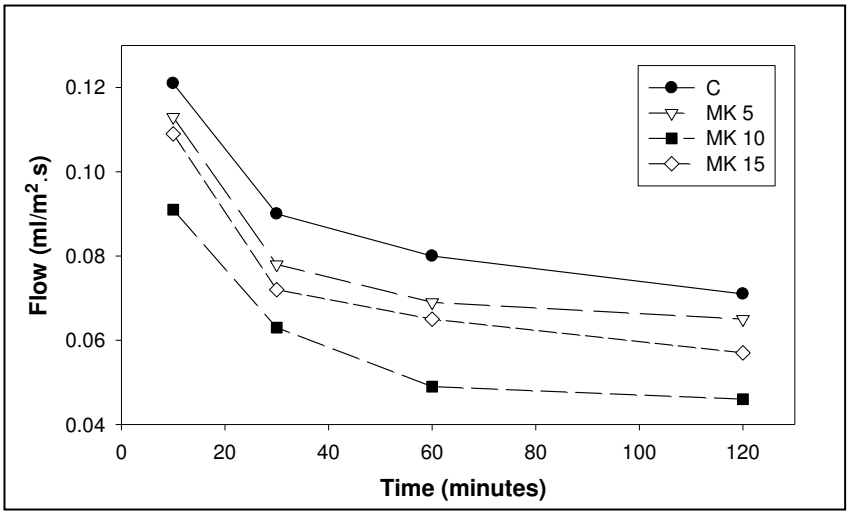

Figure 9b. Initial Surface Adsorption (28d)

Water Absorption Test

The volume of pore space in concrete can be measured indirectly by water absorption and the results are shown in Figure 10. It was found that the mixtures achieved an overall low absorption characteristic (< 10%) due to its low water/cementitious ratio. In addition, the decrease in absorption from 7 days to 28 days was almost insignificant. Since absorption is related to the pore volume in concrete, it is possible to state that the concrete mixtures tested are of low porosity. The control mixture exhibited the highest absorption rate, followed by MK 15, MK 5 and MK 10. A high percentage of water absorbed by the control indicates the importance of pozzolanic material in producing a low permeable concrete. Microstructure of concrete plays a major role in water absorption. The effect of pozzolanic reaction by metakaolin reduced the ease of water absorbed into concrete as dense masses of hydrated products join in to alter the complex matrix that has decreased the pore volume. Metakaolin also acts as filler, creating a discontinuous pore system and thus resulting in a low water absorption into concrete.

Sorptivity Test

The sorptivity test differs from water permeability test because it does not require a water head or pressure head. The value of sorptivity represents the height of water rise in concrete through capillary suction, and is expressed in millimetre/minute ^{½}. A low sorptivity value indicates a high resistance towards water absorption. The decrease in sorptivity is due to several factors. Firstly, as the water invades the pores it encounters smaller pores hence slowing the rate of sorption. Secondly, even if the capillary pores form a strong interconnected network throughout the concrete, for example through the interfacial zone around the aggregates with larger capillary pores, the ingress of water particles may still be slowed as the air-water interface rests at a stable configuration in the pore space. Any further absorption of water can only be transported through gel pores that are much smaller than capillary pores, or by moisture diffusion in both capillary and gel pores (Martys, 1997).

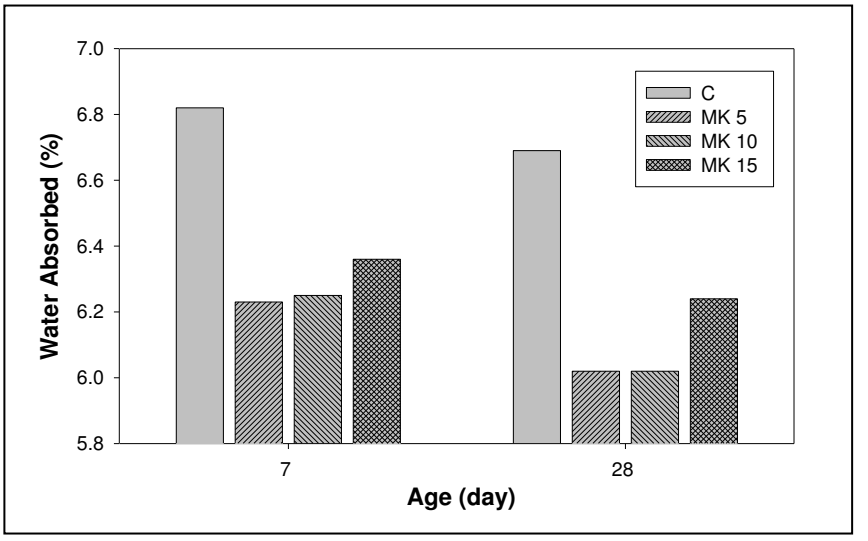

Figure 10. Water absorption

Figure 11 shows the sorptivity results for 7 and 28 days. Generally, all four mixtures have low sorptivity values because they are of high-performance mixtures. MK 10 achieved the lowest sorptivity value, indicating that it has been hydrated completely to give a dense concrete with an interconnected network of capillary pores. Metakaolin acts as an ultra fine filler which causes

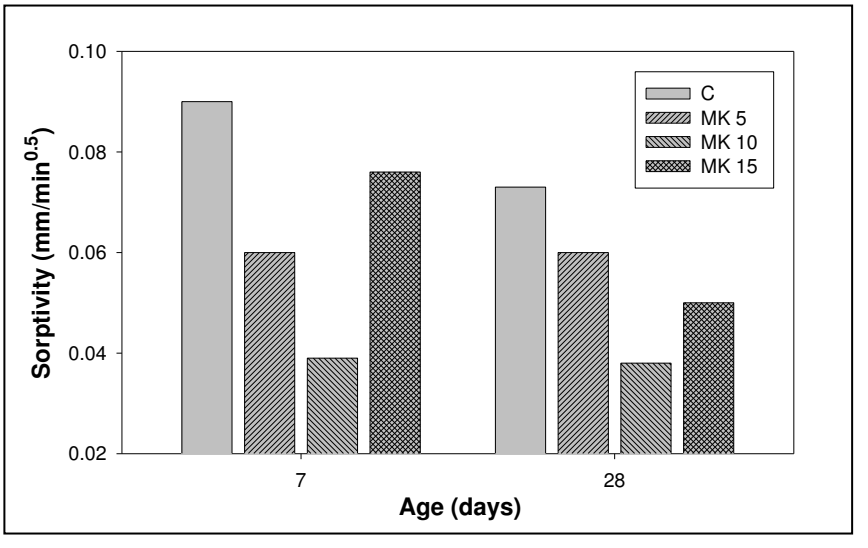

Figure 11. Sorptivity test

partial blocking and segmentation of the pore system. In this case, the capillary pores are only interconnected by gel pores, which are smaller and almost impermeable (Neville, 1993). Following this argument, it is anticipated that higher percentage of metakaolin replacement will produce concrete with greater impermeability. However, the results indicate that this is only true where MK 5 and MK 10 are concerned. At both ages, MK 15

yielded higher sorptivity values than that was expected. The highest sorptivity value shown by the control mixture substantiates the effectiveness of metakaolin in producing low permeability concrete.

CONCLUSIONS

The following conclusions are drawn based on results of the present study: -

1. The incorporation of metakaolin did not significantly affect the workability of concrete in terms of the slump, Vebe and flow parameters. In fact, the metakaolin mixtures displayed less bleeding, less laitance and overall improved finishability. Metakaolin also resulted in a slightly lower concrete density and higher air content.
2. The mixtures incorporating metakaolin exhibited a higher compressive strength, tensile splitting strength, flexural strength and modulus of elasticity compared to the control. All metakaolin mixtures achieved higher strengths than the control from age 7 days onwards. At 90 days, the metakaolin mixtures attained an average enhancement of 13% (compressive strength), 16% (flexural strength), 5% (tensile splitting) and 4% (modulus of elasticity).
3. Metakaolin mixtures also enhanced the durability of concrete by reducing its water absorption characteristics. The test results concluded that the incorporation of metakaolin into concrete significantly decreased the initial surface absorption, water absorption and sorptivity of concrete, when compared to plain OPC control mixture.
4. This study proves that it is feasible to use a local source of normal grade kaolin to produce metakaolin as pozzolan for concrete. This would provide the local construction industry with a cheaper alternative for producing high-performance concrete.

ACKNOWLEDGEMENTS

The authors gratefully acknowledge the financial assistance provied by the National Council for Scientific Research and Development through a research grant under the Intensification of Research in Priority Areas (IRPA) programme under project 02-02-03-0601. The support given by MBT (M) Sdn. Bhd. and Simen Utama Sdn. Bhd. by providing the concreting materials required for this study is greatly appreciated.

REFERENCES

Cook, D. J. (1986) Cement replacement materials, Surrey University Press, R.N. Swamy, Ed., 40-72 pp.

Sayanam, R. A., Kalsotra, A. K., Mehta, S. K., Sing, R. S. and Mandal, G. (1989) Studies on thermal transformation and pozzolanic activities of clay from Jammu region (India). *Thermal Analysis,* 35:99-106.

Ambroise, J., Murat, M. and Pera, J. (1986) Investigation on synthetic binders obtained by middle-temperature thermal dissociation of clay minerals. *Silicate Industries,* 7(8):99-107.

Caldarone, M. A. and Gruber, K. A, Burg R. G. (1994) High-reactivity metakaolin: A new generation mineral admixture. *Concrete International,* 16:34-40.

Wild, S., Khatib, J. M. and Burg R. G. (1996) Relative strength, pozzolanic activity and cement hydration in superplasticised metakaolin concrete. *Cement and Concrete Research,* 26(10):1537-1544.

Curcio, F., DeAngelis, B. A. and Pagliolico, S. (1998) Metakaolin as a pozzolanic

microfiller for high-performance mortars. *Cement and Concrete Research,* 28(6):803-809.

Oriol, M. and Pera, J. (1995) Pozzolanic activity of metakaolin under microwave treatment. *Cement and Concrete Research,* 25(2):265-270.

Wild, S. and Khatib, J. M. (1997) Portlandite consumption in metakaolin cement pastes and mortars. *Cement and Concrete Research,* 27(1):137-146.

Khatib, J. M. and Wild, S. (1996) Pore size distribution of metakaolin paste. *Cement and Concrete Research,* 26(10):1545-1553.

Kostuch, J. A., Walters, V. and Jones, T. R. (1993) High performance concretes incorporating metakaolin: a review. *Proceedings of Concrete 2000: Economic and durable construction through excellence ,* E&FN Spon, R. K. Dhir and M. R. Jones, Ed., University of Dundee, Scotland, 1799-1809.

Walters, G. V. and Jones, T. R. (1991) Effect of metakaolin on alkali-silica reaction in concrete manufactured with reactive aggregates. *Proceedings of the Second International Conference on the Durability of Concrete,* Malhorta V. M. , Ed., Montreal, 941-947.

Khatib, J. M. and Wild, S. (1998) Sulphate resistance of metakaolin mortar. *Cement and Concrete Research,* 28(1):83-91.

Loh, C. H. and Harun, H. C. (1996) Clay resources of Malaysia - An overview of Geological Survey Department's findings to date. *Opportunities in the clay-based industries,* Geological Survey Department, Malaysia, 9-18.

Sabir, B. B., Wild, S. and Bai, J. (2001) Metakaolin and calcined clays as pozzolans for concrete: A review. *Cement and Concrete Composites,* 23:441-454.

Aitcin, P. C. (1997) Sherbrooke MIx Design Method. *One-day short course on Concrete Technology and High-Performance Concrete: Properties and Durability,* University Malaya, Kuala Lumpur, 1-33.

Balogh, A. (1995) High-reactivity metakaolin. *Aberdeen's Concrete Construction,* 40(7).

Marsh, D. (1994) An alternative to silica fume? *Concrete Products.*

Duval, R., and Kadri, E. H. (1998) Influence of silica fume on the workability and the compressive strength high-performance concretes. *Cement and Concrete Research,* 28:533-547.

Bayasi, Z. and Zhou, J. (1993) Properties of silica fume concrete and mortar. *ACI Materials Journal,* 90(4):349-356.

Asselanis, J. G., Aitcin, P. C. and Mehta, P. K. (1989) Effect of curing conditions on the compressive strength and elastic modulus of very high strength concrete. *Cement, Concrete and Aggregates,* 11(1):80-83.

Basheer, PAM. and Nolan, E. (2001) Near-surface moisture gradient and in-situ permeation tests. *Construction and Building Materials,* 15:105-114.

Martys, NS. and Ferraris, C. F. (1997) Capillary transport in mortars and concrete. *Cement and Concrete Research,* 27(5):747-760.

Neville, A. M. (1993) Properties of Concrete (4th edition), Addison Wesley Longman Limited.

LOAD-DEFLECTION ANALYSIS OF PRETENSIONED INVERTED T-BEAM WITH WEB OPENINGS

Cheng Hock Tian[1], Bashar S. Mohammed[2], Kamal Nasharuddin Mustapha[2]
[1]Faculty of Civil & Environmental Engineering, Universiti Malaysia Pahang, Karung Berkunci 12, 25000 Kuantan, Pahang, Malaysia
[2]Department of Civil Engineering, College of Engineering, Universiti Tenaga Nasional, KM7, Jalan Kajang-Puchong, 43009 Kajang, Selangor, Malaysia

Abstract

A precast, prestressed concrete girder with circular web openings allows building service systems (mechanical, electrical, communications, and plumbing) to cross the girder line within the member's depth, reducing a building's floor-to-floor height and the overall height of the structure. These height reductions have the potential to improve the competitiveness of total precast concrete structures versus other types of building systems. The experimental program reported in this paper tested five full-scale inverted-tee girders with circular web openings to failure, to evaluate the openings' effect on girder behavior. The girders failed in a ductile manner due to diagonal cracking above the openings. The tested girders were designed using available recommendations in the existing literatures. It was observed that concrete fractured from tension zones around an opening, with cracks developed vertically towards the beam flanges. A beam would collapse when the cracks reached the flanges. In the present work, an analytical solution is developed for the load-deflection calculation of prestressed beam with web openings at any load stage. The solution assumes a trilinear deflection response characterised by the flexural cracking initiation, steel yielding, and ultimate capacity. Closed form expressions are presented for the case of simple beams subjected to four-points loading. These expressions are modified from present ACI code equations by incorporating appropriate laboratory determined coefficients in order to predict more precisely with some degree of conservativeness on flexural load-point deflection with any extent of uncracked, postcracked, and postyielded region along their spans. Accordingly, a simplified analysis procedure is developed by adopting a trilinear load-deflection response. The effectiveness of the simplified procedure is demonstrated by comparing its results to those of the analytical solution and the experimental values.

Keywords: prestressed concrete; inverted T-beam; web opening

INTRODUCTION

Modern multi-storey buildings always have a stringent requirement on headroom. In order to accommodate building services within the constructional depth of a floor, it is common practice to provide web openings in structural floor beams for passage of services. A large number of research efforts on the structural behaviour of concrete beams with web openings have been reported in the literatures. These researches (Tan and Mansur, 1996; Mansur, 1988) have focused primarily on reinforced concrete beams with multiple web openings and composite beams with rectangular web openings, both with or without reinforcement. Rectangular web openings with aspect ratios ranging from 1.0 to 3.0 and opening depth (d_o) restricted to about 50% of the overall section height (h) are commonly used (Tan and Mansur, 1996). Circular web openings are also popular in commercial buildings for easy installation of water pipes. Only limited research work has been reported on the structural behavior of prestress beams with web openings. Previous researchers (Ragan and Warwaruk, 1967; Barney *et al*., 1977; Dinakaran and Sastry, 1984; Savage *et al.*, 1996;

Pessiki *et al.*, 1997) had tested full-scale, simply supported, uniformly loaded, pretensioned T-beams with web openings. The T-beams they tested have the proportions of one-half of a double tee beam. These members are typically floor beams supporting uniformly distributed gravity loads applied to the top surface in a typical precast structural system. Thompson and Pessiki (2006) tested and analyzed pretensioned inverted T-beam with rectangular openings. The inverted T-beam tested and analyzed in this research is not similar to beams tested and analyzed by Thompson and Pessiki (2006) in term of configurations as well as types of openings.

The use of prestressed beam with web openings as structural elements mandates a comprehensive understanding of how its structural performance can be reliably predicted. In this context, analytic quantification of strength and deflection characteristics of structural components with web openings must be developed through research data collected through controlled laboratory testings. To date, several significant studies (Kennedy and Abdalla, 1992; Abdalla and Kennedy, 1995; Saleh *et al*., 1999; Thompson and Pessiki, 2006) have been published characterising the behaviour of prestressed beam with web openings. This paper is submitted to compliment this body of information and thereby further the engineering communities understanding of deflection behaviour of prestressed beam with web openings.

OBJECTIVE AND SCOPE

Deflection prediction of prestressed beam with web opening is, in part, dependent on empirical performance constants. The empirical component reflects the opening locations, number of openings along the beam as well as material specific composite behaviour of prestressing steel and concrete. Therefore, wherever web opening is exist in lieu of prestressing steel, the measured response may have significant difference if one compare to predicted value using existing deflection equation in ACI 318-99 code (2004). The objective of this paper is to investigate the suitability of using existing analytical procedures for computing deflections using ACI 318-99 code (2004) for predicting the deflection behaviour of prestressed beam with web openings. Load-deflection and failure load results of five simply supported pretensioned inverted T-beams with web openings subject to four-point monotonic loadings are presented. Test results are compared with proposed modified ACI 318-99 code (2004) equation for predicting deflection under all load conditions.

TESTS SET UP AND SAMPLES SPECIFICATIONS

The experimental program was designed to investigate the failure behaviour of pretensioned inverted T-beams with web openings under static loading conditions. Testing was intended to evaluate the flexural strength. Therefore, all beams were designed such that shear strength exceeded flexural strength. Accordingly, flexural failure was expected. Figure 1 and Figure 2 show the configuration of web openings in the pretensioned beams as well as cross-section prestressing steel and shear reinforcement detailings. The materials used, design and fabrication of pretensioned inverted T-beams are described below.

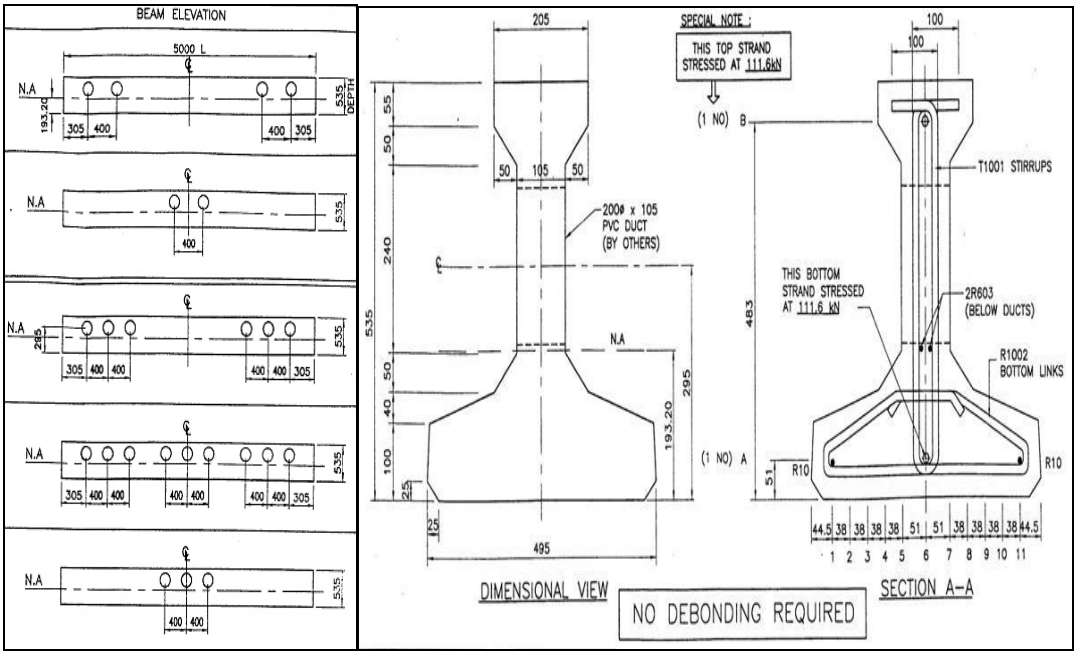

Figure 1. Configuration of web openings inside the pretensioned inverted T-beam and inverted T-beam overall detailed dimensions

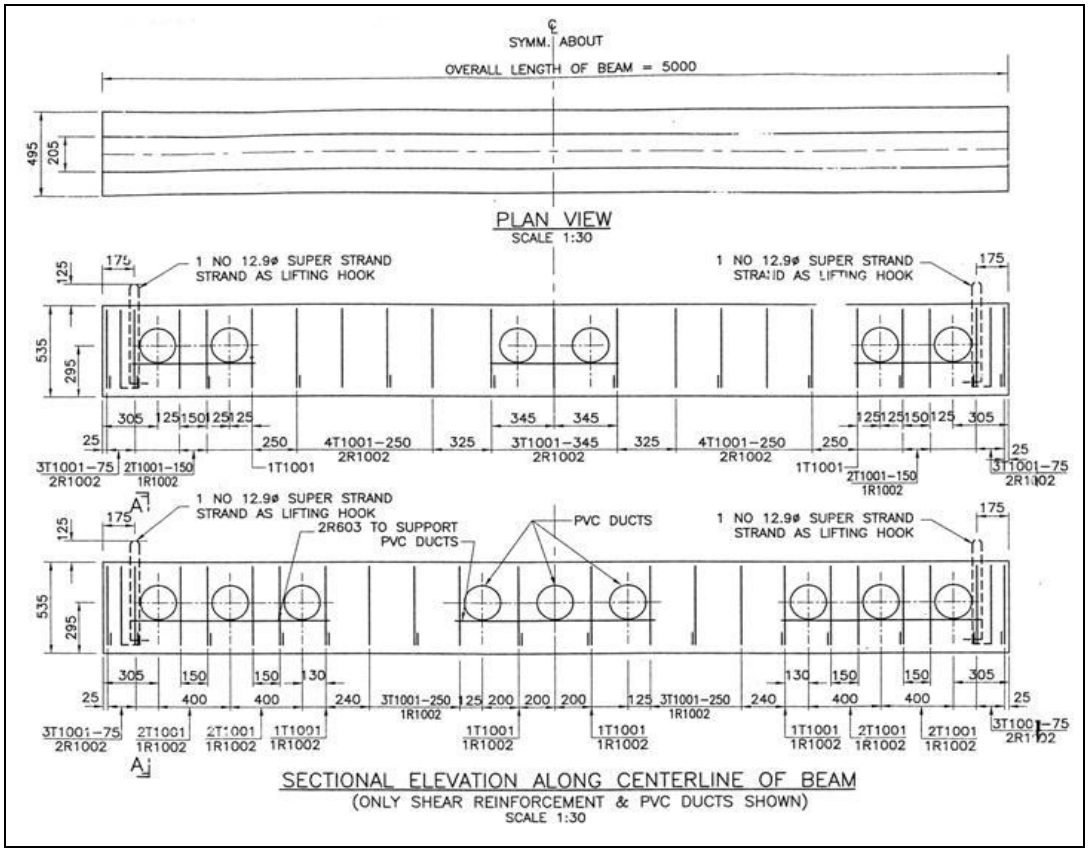

Figure 2. Detailing and location of prestressing steels and shear reinforcements

Materials

The average 28 days concrete cube strength in compression was 53 MPa for all five beams, as evaluated by tests on three cubes specimens for each beam. Figures 3 shows the prestressing steel and shear reinforcement location in the prestressed concrete beams. Straight, bonded, seven-wired super high tensile strand with 12.9mm diameter were used as prestressing tendons, with ultimate strength of 1860MPa. The stirrups for shear reinforcement were made from 10mm rebars with a minimum specified yield strength of 300 N/mm^2. The elastic modulus of the prestressing steel is taken as 200 x 10^3 N/mm^2. Figure 4 shows the fabricated prestressed beams used in the testing program

Figure 3. Prestressing steel and shear reinforcement locations

Figure 4. Pretensioned Inverted T beams with circular web openings fabricated at Hume factory

Testing Set Up

All tests were conducted with a closed-loop hydraulic servo-controlled MTS testing system. The 360 KN jack was capable of both displacement and load control for monotonic or cyclic loading. A four-point loading scheme, with an effective span of 4000 mm and a distance of 1200 mm between the load points was used to limit the presence of shear stress in the mid-span zone. Figure 5 shows the layout of four points bending test of pretensioned inverted T-beam.

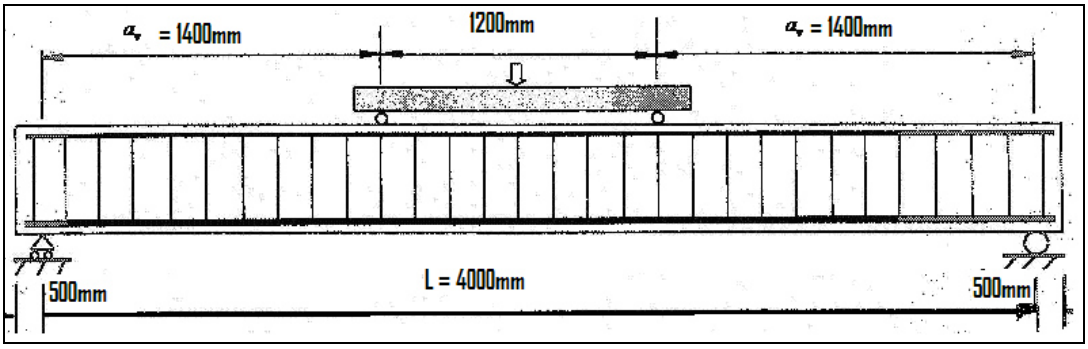

Figure 5. Four-points bending test of pretensioned inverted T-beam

THEORETICAL ANALYSIS: MODEL FOR SEVICEABILITY CHECK

Currently, ACI 318-99 code (2004) adopts models in which deformability of the whole element is defined by means of relations arising from linear analysis, where a transformed value of the cross section moment of inertia is introduced. In practical, an effective constant moment of inertia is determined as a linear combination of the gross moment of inertia (elastic uncracked cross section) and the moment of inertia corresponding to the cracked state of the member. The deformability of structures thus is evaluated by an elastic analysis of members treated as prismatic (ie. with constant cross-sectional properties). These models, are not rigorous; nevertheless, the involved approximations are accepted both for prestressed and reinforced concrete structures, because results obtained are, generally on the safe side. In this paper, the serviceability behaviour of flexural prestressed beam with web openings is analysed both theoretically and experimentally. Predictions of member deflections furnished by the proposed procedure are compared with those given by code (ACI 318-99 code, 2004) models usually adopted in serviceability analysis of prestressed beam. In addition, experimental results of prestressed beam with web openings tested under static loading conditions up to failure are presented and discussed. Finally, analytical results from proposed modified ACI equations (ACI 318-99, 2004) to compute deflection in prestressed concrete beam with web opening are compared with available experimental results to focus on both the effectiveness of the proposed analytical models and their applicability for design purposes. The ACI 318-99 code (2004) recommends the use of Branson's equation to account for the effective moment of inertia after cracking:

$$I_e = \left(\frac{M_{cr}}{M_a}\right)^3 I_g + \left(1 - \left(\frac{M_{cr}}{M_a}\right)\right)^3 I_{cr} \qquad (1)$$

where I_e = secant moment of inertia of the entire beam at any load level; I_g = gross transformed section moment of inertia; I_{cr} = cracked section moment of inertia; M_{cr} = cracking moment; M_a = maximum moment in the beam. Eq.(1) does not properly address uncracked region, postcracking region as well as postyielding deflection for beam with web openings. It is worth to mention here that the prediction of failure load is beyond the scope of this paper.

Proposed Equations For Deflection Prediction

Uncracked region

As per ACI 318-99 (2004), load-point flexural deflection, δ_a for the test set up in Figure 5 is calculated as:

$$\delta_a = \frac{1}{6}\left(3La_v - 4a_v^2\right)\left(\frac{M_a}{I_e E_c}\right) \tag{2}$$

Where M_a = load-point moment; E_c = concrete elastic modulus calculated as per ACI 318-99 (2004); I_e = effective moment of inertia specified in ACI 318-99 (2004) computed from Eq.(1). Note that I_e represents the parabolic "Branson" equation and is assumed constant over beam length L. The form of Eq. (1) implies a linear curvature gradient over the shear span. In reality, part of the shear span is uncracked at a given load. Therefore, the curvature diagram should discontinuous at M_{cr}.

The following equation is proposed for the uncracked region of the beam:

$$\delta_a = \frac{1}{6}\left(3La_v - 4a_v^2\right)\left(\frac{M_a}{\alpha I_g E_c}\right) \tag{3}$$

where α = reduction factor that represents presence of circular web openings along the length of beam. A reduction factor α of 35% was found to be an effective tuning parameter for the deflection prediction as seen in Figure 6 to Figure 15. Further test results would be required to authenticate the proposed value of α.

Postcracking region

In the postcracking region, the following modified relationship is proposed taking into account the effect of circular web opening/openings along the web of a beam.

$$I_e = \left(\frac{M_{cr}}{M_a}\right)^3 \beta I_g + \left(1 - \left(\frac{M_{cr}}{M_a}\right)\right)^3 I_{cr} \tag{4}$$

in which β = experimentally determined reduction coefficient that represents presence of circular web openings along the length of the beam. A reduction factor β of 25% was found to be an effective tuning parameter for the deflection prediction as seen in Figure 6 to Figure 15. Further test results would be required to authenticate the proposed value of β.

Postyielding region

In the postyielding region, the following modified relationship is proposed taking into account the effect of circular web opening/openings along the web of a beam:

$$\delta_a = \frac{1}{6}\left(3La_v - 4a_v^2\right)\left(\frac{M_{cr}}{I_e E_c}\right) \tag{5}$$

$$I_e = \left(\frac{M_{cr}}{M_a}\right)^3 \gamma I_g + \left(1 - \left(\frac{M_{cr}}{M_a}\right)\right)^3 I_{cr} \tag{6}$$

in which γ = experimentally determined reduction coefficient that represents the presence of circular web openings along the length of the beam. A reduction factor, γ of 15% was found to be an effective tuning parameter for the deflection prediction as seen in Figure 6 to Figure 15. Further test results would be required to authenticate the proposed value of γ.

Comparisons between experimental load deflection curves obtained in this study and those predicted by the proposed equations at the load point deflection of the simply supported beam are presented in Figure 6 to Figure 15. The curves show that the proposed equations predict conservative deflection values for the simply supported beams.

Concrete Cracking and Crushing

Concrete cracking and crushing failure sequences for all the five tested beams could be summarized as follow: (1) at an applied load in the range 125kN to 135kN (mid point load) with 2mm to 2.5mm displacement, the bending cracks occur vertically on the tension side of the prestressed beam base; (2) with increasing load, the cracking progresses toward the upper part of the prestressed beam; (3) at applied loading between 160kN to 175kN (mid point load) with displacement in the range of 12mm to 18mm, the cracks reach almost 75% of the prestressed beam height. The prestressing steel at this loading is about 75% to 80% of yield value. More cracks begin to form above the openings in the pure moment region towards the top fiber of the prestressed beam; (4) at 190kN to 200kN central loading with 30mm to 40mm displacement, the prestressing steels yield and crack at the tension side grow relatively large in short period of time; (5) at the same time, yielding at the prestressing steel compression fiber starts follow by completely failure of the beam in a ductile manner. Load-deflection results are shown in Figure 6 to Figure 15. As expected, a ductile flexural failure occurred in all beams associated with yielding of prestressing steel.

The advantage of prestressing steel is demonstrated in the energy absorbed through plastic deformation in the prestressing steel. Although the specimens technically failed at yielding of prestressing steel, the applied load was sustained and moment capacity remained intact until secondary ductile failure occurred by concrete crushing. The load-deflection history for these five samples was characterised by two to three individual cracks in each sample. Cracks within and near the constant moment region were observed to grow in a vertical direction. The orientation became progressively more incline as the distance from the beam centerline increased.

Figure 6. Flexural failure of beam with 9 circular web openings

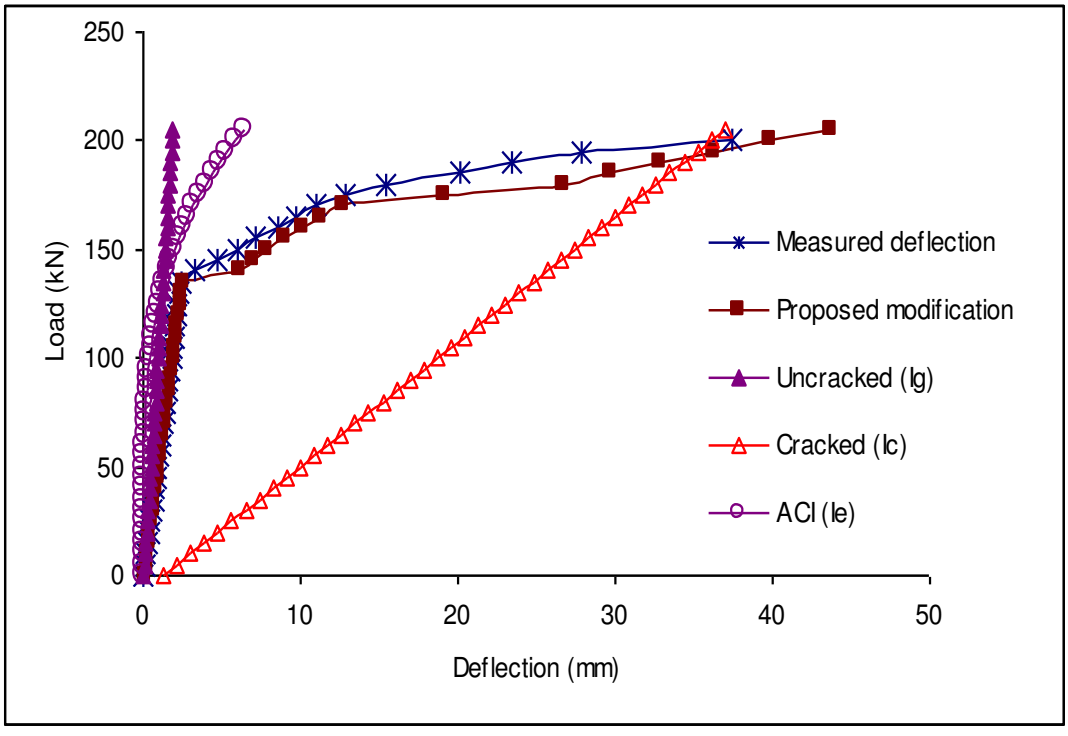

Figure 7. Load-deflection plot for beam with 9 circular web openings

Figure 8. Flexural failure of beam with 3 web openings in constant shear area

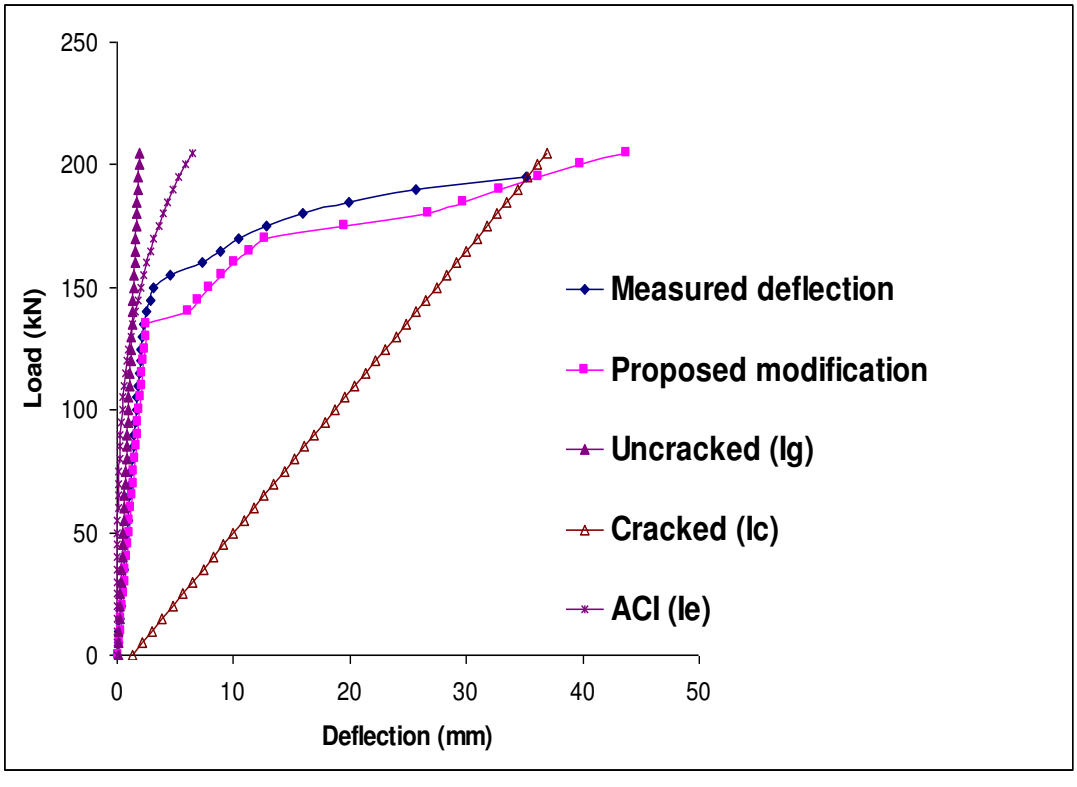

Figure 9. Load-deflection plot for beam with 3 web openings in constant shear area

Figure 10. Flexural failure of beam with 3 web openings in constant moment area

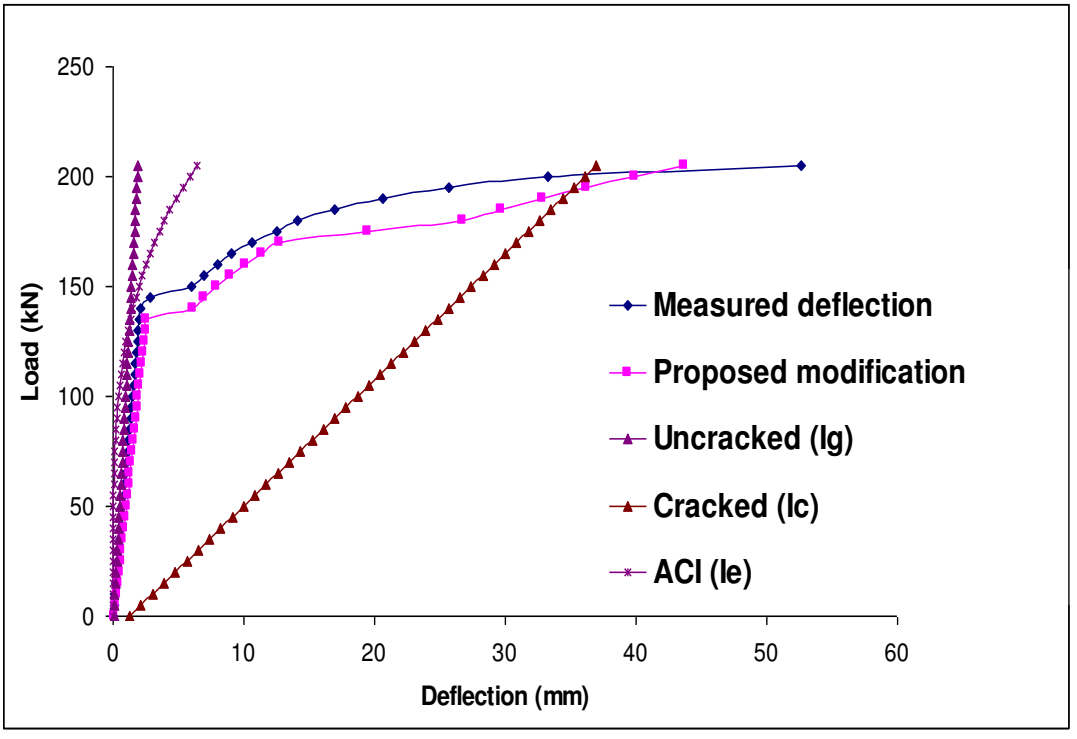

Figure 11. Load-deflection plot for beam with 3 web openings in constant moment area

Figure 12. Flexural failure of beam with 2 web openings in constant moment area

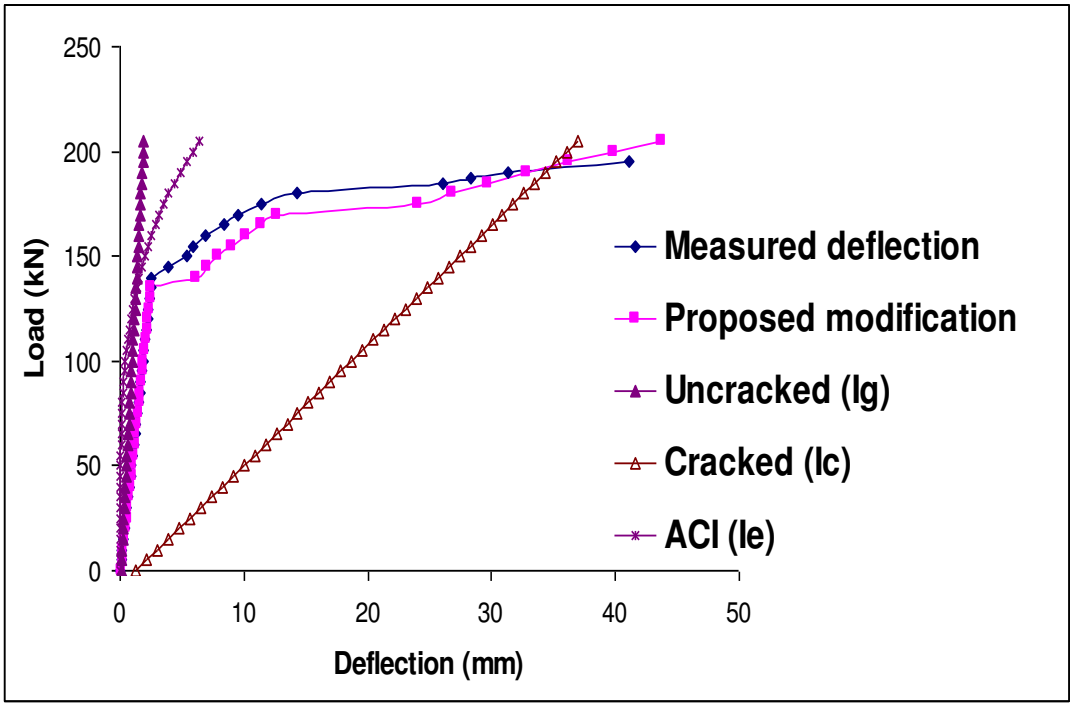

Figure 13. Load-deflection plot for beam with 2 web openings in constant moment area

Figure 14. Flexural failure of beam with 2 web openings in constant shear area

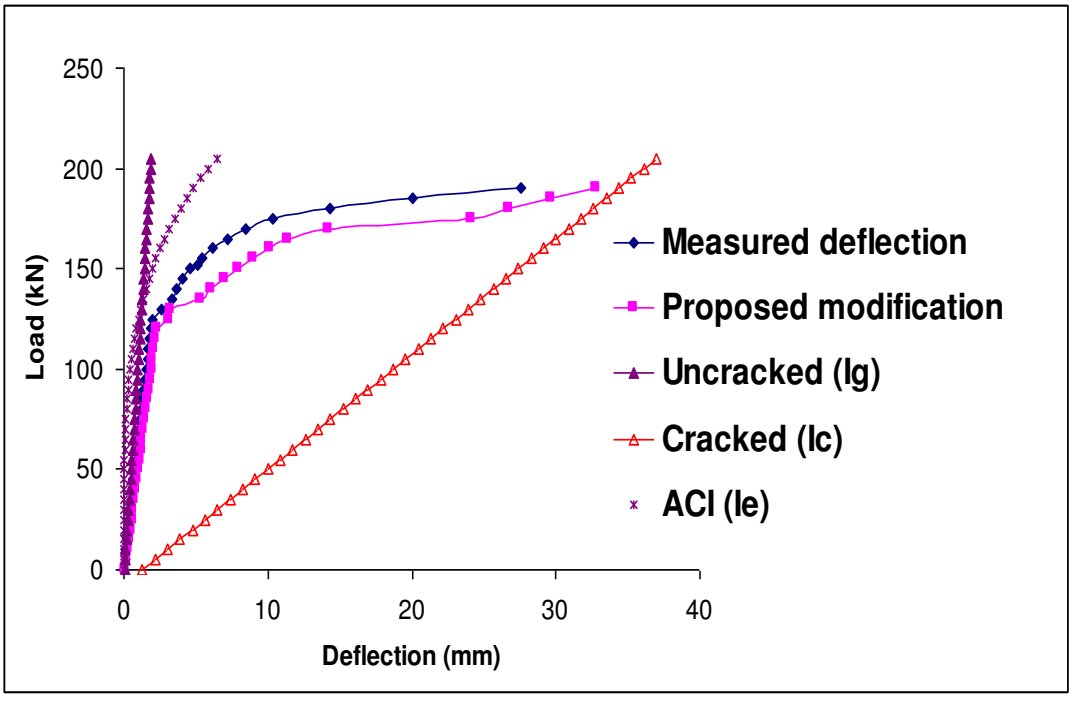

Figure 15. Load-deflection plot for beam with 2 web openings in constant shear area

Deflection Predictions

The proposed equations predict deflections at all moment levels, with high accuracy of about 90% at the uncracked region and ranged between 75% and 85% of average measured values for all tested beams. This accuracy would be well within an acceptable tolerance for concrete deflection prediction. Since I_e is a function of the cube of the compression block thickness, a small error in the calculation of this dimension will significantly affect stiffness and deflection prediction. Also, ACI 318-99 code (2004) assumes I_e to be constant over the length, L, in effect "smearing" the softened effective transformed section. For prestressed beam with web openings, this may be an over-simplication, especially for underreinforced sections where a significant portion of the beam's length remains uncracked.

Analysis Considerations

The design of prestressed beam with web openings need to ensure the beam fail in ductile manners at ultimate limit state. In this case, flexural ductile failure may occur which will cause large deflection at ultimate loading stage. All beams that have been tested demonstrated trilinear failure behaviour as one could examine through load-deflection curve whereby flexural ductile failure in all samples were more gradually rather than immediate and terminal loss in load carrying capacity. Since all beams were designed to be underreinforced in this research, failure occurs in a ductile manner by initial yielding of main presressing steel. This type of behaviour provide ample warning of the imminence of collapse of the beam. As far as flexural analysis is concerned, a region of flexural ductile failure, may, in some circumstances, govern the failure mechanisme. Considering this failure performance together with existence of web openings and prestressing steel, flexural design criteria could considered flexural ductile failure that limit flexural strength. The consequence will be low reinforcement service stress levels resulting in high degree of reserve strength and acceptable compliance with deflection criteria. Additional research is required to establish rational prestressing limit so that the desire failure mode and safety factor are ensured.

CONCLUSIONS

In this study, a simplified analysis is developed to predict the load-deflection response of simple prestressed beam with different configuration of web openings at transverse locations along the entire length of the beams. Based on experimental and analytical verification, one can assume trilinear load-deflection response. Simple equations are, accordingly, developed for calculating the beam effective moment of inertia at any stage. The simple analytical equations greatly simplifies the analysis process since the entire load-deflection response is calculated based on basic linearised equations after determining the section properties that the designer would need to compute in practice anyway. Comparison with present experimental results demonstrate the merits of the analytical and simplified procedures in term of conservativeness. Accordingly, the modified ACI 318-99 code (2004) equations have the potential to be implemented in design practice. The following key conclusions are derived from the research presented in this study:

1) Applying higher amount of shear reinforcement as close as possible beside each circular web openings (approximate 20mm in this research project) could be a key factor in enhancing the shear capacity, controlling the deflection around the opening area, in addition to the delay of crack propagation at the midspan opening section of such beam.

2) Deflection of simply supported prestressed beam with web openings could not be accurately predicted using present available ACI 318-99 code (2004) equations. Deflection stiffness calculated according to ACI 318-99 code (2004) using the Branson effective moment of inertia is overestimated. The prediction process using existing ACI 318-99 equation (2004) has been negatively affected by presence of web openings and wide cracks that appear over the moment constant zone.

3) A proposed reduction factor of 35%, 25% and 15% for second moment of inertia at uncracked region, postcracking region and postyielding region, respectively, in estimating the effective moment of inertia proposed by ACI 318-99 (2004) has been found to be effective in tuning the deflection prediction of simply supported prestressed beam with web openings. Predicted deflection of pretensioned inverted T-beam with circular web openings sections is conservative relative to measured values.

ACKNOWLEDGEMENT

The authors gratefully acknowledge financial supports from Universiti Malaysia Pahang (UMP) through Short-Term Grant (Grant No: FR56398) and Ministry of Science, Technology and Innovation (MOSTI) through e-science fund (Grant No: 03-02-03 SF0115). Thanks are extended to Hume Concrete Product Research Centre (HCPRC) for several useful discussions and generously provided large collection of prestressed beam tests data.

REFERENCES

Abdalla, H., and Kennedy, J.B. (1995) Design of Prestressed Concrete Beams with Openings. *Journal of Structural Engineering*, V. 121, No. 5 (May): 890–898.

ACI Committee 318-1999 (Rev. 2004) *Building Code Requirements for Structural Concrete (ACI 318-99) and Commentary (ACI 318R-99).* Farmington Hills, MI: American Concrete Institute

Barney, G. B., Corley, W. G., Hanson, J. M. and Parmelee, R. A. (1977) Behavior and Design Of Prestressed Concrete Beams with Large Web Openings. *PCI Journal*, V. 22, No. 6 (November– December): pp. 32–61.

Dinakaran, V., and Sastry, M.K. (1984) Behavior of post-tensioned prestressed concrete T-beam with large web openings. *Indian Concrete Journal*, 58(2), 34-38.

Kennedy, J. B. and Abdalla, H., (1992) Static Response of Prestressed Girders with Openings. *Journal of Structural Engineering*, ASCE, 118(2), 488-504.

Mansur, M.A. (1988) Ultimate strength design of beam with large openings. *Journal of Structural Engineering*. 8(2), 107-125.

Pessiki, S., van Zyverden, W., Sause, R. and Slaughter. S. (1997) Proposed Concepts for Floor Framing Systems for Precast/Prestressed Concrete Office Buildings. *PCI Journal*, V. 42, No. 5 (September–October): pp. 66–76.

Ragan, H. S., and Warwaruk, J. (1967) Tee Members with Large Web Openings. *PCI Journal*, V. 12, No. 4 (August): pp. 52–65.

Saleh Mohsen, Tadros, Maher K., Einea, Armin, Fischer, Larry G., Foster, E. Terence (1999) Standardized Design of Double Tees with Large Web Openings, *PCI Journal*, V.67, No. 4, November –December 1999, pp. 68-78.

Savage, J. M., Tadros, M. R., Arumugasaamy, P. and Fischer, L. G. (1996) Behavior and Design of Double Tees with Web Openings. *PCI Journal*, V. 41, No. 1 (January–February): pp. 46 – 62.

Tan, K. H. and Mansur, M.A. (1996) Design procedure for reinforced concrete beams with large web openings. *ACI Structural Journal*, Vol. 93, No.4, July-Aug., pp. 404-411.

Thompson, James M., and Pessiki, S. (2006) Experimental Investigation Precast,Prestressed Inverted Tee Girders with Large Web Openings. *PCI Journal*, V.109, No.2, November-December 2006, pp

EMPIRICAL MODELLING OF THE INFLUENCE OF UNIT WATER ABSORPTION ON BRICKWORK STRENGTH

Badorul Hisham Abu Bakar, Chow Shiao Teng, Megat Azmi Megat Johari
School of Civil Engineering, Universiti Sains Malaysia

Abstract

Unit water absorption is one of the major factors influencing strength and durability performance of brickwork structures. The moisture transfer mechanism between mortar joint and brick unit would lead to a reduction in the water content of fresh mortar, thereby producing poor and porous mortar joint which would affect the brickwork's strength, durability, serviceability and causes frost damage in seasonal regions. This paper investigates the effect of unit water absorption on the strength of brickwork. An empirical model was developed to predict the compressive strength of brickwork based on the unit water absorption, unit strength and mortar strength obtained from laboratory tests. Comparison between the developed model and other established models was also made. Experimental works were conducted on 60 specimens including individual bricks and brickwork prisms made up of calcium silicate, clay and cement sand bricks in order to obtain the brick compressive strength, mortar strength, unit water absorption and initial rate of absorption. Brickwork were constructed from four-stack units as prisms and were loaded at the age of 14-day after being cured under the polythene sheet. Based on the test results, empirical model of the brickwork wall compressive strength was developed by means of regression analysis using MINITAB R14. The multiple regression analyses revealed that unit with high water absorption contributes to the reduction in strength of brickwork wall. Comparison between all models shows that EC 6 and BS 5628 underestimate the wall's compressive strength, while Mann's model overestimated the brickwork strength.

Keywords: Unit water absorption, compressive strength, empirical modelling, regression analysis, comparison: EC 6, BS 5628, Mann's model.

INTRODUCTION

Brickwork is a non-homogeneous and anisotropic material, which exists in many forms and comprising of units with varying shape, size and physical characteristic and mortar joint. Examples of unit used in brickwork are such as bricks, blocks, ashlars, adobes, irregular stones, etc. The properties of brickwork are strongly dependant upon the properties of its constituent. Its compressive strength depends on the geometry and type of the units, brick strength, mortar grade, slenderness ratio, workmanship, etc. Apart from that, an interaction between brick and mortar element of brickwork due to different water absorption characteristics of brick also influences the compressive strength of brickwork wall.

Water absorption is an important characteristic that requires attention in the construction of brickwork structures as it plays a significant role in the strength and durability performance of brickwork. The unit water absorption has been discovered to have significant implication on the development of brickwork bond, which is developed by mechanical interlocking of cement hydration products growing in the brickwork pores on the unit surface and connected to the mortar matrix (Goodwind and West, 1982). The migration of water from fresh mortar to brickwork unit may reduce or interrupt the hydration process of mortar consequently impair the crystallization of C-S-H, ettringite and

calcium hydroxide. As a result, mortar joint contains more unhydrated cement grain. The loss of moisture in mortar leaves voids in mortar, which is later filled by air, and leads to weak and porous mortar joint, which is often an inherent weakness of brickwork structure. Henry (2001) commented that although mortar accounts for as little as 7% of the total volume of brickwork but its influences performance far more than this proportion indicates. Mortar requires certain properties prior to setting, particularly workability. Hardened mortar has to be sufficiently strong to develop adequate adhesion to the units and also to set without excessive shrinkage, which will affect the performance of brickwork and cause cracking of the units. Lawrence and Cao (1988) also explained that the unit with the high water absorption would remove too much water from the mortar thus reduce the degree of hydration of mortar and the amount of hydration products deposited in the pores of the unit. Consequently, shrinkage cracks may be induced in the mortar weakening the unit and mortar interface. The moisture transfer mechanism between the unit and mortar leads to reduction in the water content of the bonded mortar, thereby causing shrinkage. This leads to strength reduction and may also affect the durability, performance and serviceability of brickwork structures.

Numerous experimental investigations have been carried out over the years to examine the variables affecting brickwork strength and to develop models for brickwork strength prediction. Table 1 summarizes the detail of models developed by previous researchers and listed the predictors (independent variables) contributing to brickwork strength. It was observed that none of the listed models considered the effect of unit water absorption in the compressive strength prediction. Since water absorption also plays an important role in brickwork strength and performance, a new model considering the effect of unit water absorption in term of total absorption and initial rate of absorption (IRA) is important.

In determining the characteristic strength of brickwork, f_{wc} using standard format bricks, BS 5628 relates the strength of unit with the type of mortar to be used. These values are derived from research data carried out on individual unit, small wall unit (wallettes) and full-scale testing of storey height wall. Linear interpolation between values is allowed to calculate as realistic results as possible. Eurocode 6 proposes three methods to determine the characteristics strength of unreinforced brickwork. The first two methods suggest using experimental test on brickwork whereas the third method suggests applying the proposed formulae. In the latter case simple empirical relationships involving the compressive strength of the mortar (f_{mc}) and bricks (f_{bc}) should ideally provide conservative estimates of f_{wc}. The proposed model is deemed valid provided that the brickwork is built in accordance with EC6 and the coefficient of variation (COV) of f_{bc} does not exceed 25%. For general purposes, it is proposed that:

$$f_{wc} = Kf_{bc}^{0.65} f_{mc}^{0.25} \tag{1}$$

Where;

f_{wc}=brickwork compressive strength
f_{bc}=unit compressive strength
f_{mc}=mortar compressive strength

The compressive strength are given in MPa and $f_{mc} < \min(20\ \text{MPa}, 2f_{bc})$. The constant multiplication factor K depends on specified features of the bricks, mortar and construction details, such as the presence of longitudinal joints, and is in the range of $0.4 < K < 0.7$.

Mann's model was developed based upon experimental tests on 925 brickwork and the relationship between brickwork strength, brick strength and mortar strength. Using the experimental results, the model was derived using statistical evaluation and potential function as follows:

$$f_{wc} = 0.83 f_{bc}^{0.67} f_{mc}^{0.33} \quad (2)$$

This paper describes the effects of unit water absorption on brickwork built from different types of units with high water absorption. In addition, a new model for brickwork strength prediction with consideration of the unit water absorption effect will be developed and compared with other established models. It was anticipated that the accuracy of the established models might be affected.

Table 1. Summary of models developed by previous researchers

Model	Reference	Predictor variables included in the model
1	BS 5628 (1992)	Brick strength, mortar designation
2	Eurocode 6 (1995)	Brick strength, mortar strength
3	Hendry and Malek (1986)	Brick strength, mortar strength
4	Dymiotis and Gutledere (2002)	Brick strength, mortar strength, joint thickness, wall thickness, wall height, brick dimension, no of course, volume of perforation/overall brick volume
5	Baur et. al. (1978)	Brick strength, mortar strength
6	Atkinson et. al. (1990)	Brick strength, mortar strength, percentage of solid volume in the unit joint thickness and brick dimension.
7	Pande et. al. (1994)	Brick strength, gross area, net area, stress factor
8	Francis et. al. (1971)	Axial compressive stress, Poisson ratio of brick and mortar
9	Grimm (1975)	Brick strength, mortar strength, material size factor, slenderness factor, workmanship factor
10	Mann (1982)	Brick strength, mortar strength

EXPERIMENTAL DETAIL

Three types of brickwork units were used in this investigation. They are calcium silicate, cement-sand and fired-clay bricks. The nominal size of brickwork unit is 215 mm x 102.5 mm x 65 mm. Figure 1 illustrates the brickwork units used throughout the experimental works.

Figure 1. Brickwork unit used in the investigation
(Calcium silicate-left, clay brick-centre, cement sand brick-right)

The same batch of sand was used throughout the investigation. Sieve analysis performed on the sand indicates compliance with BS 1200 (1976) was carried out and found that the quality of sand used was proven to be satisfactory within the upper and lower limit. Ordinary Portland Cement (OPC) complying BS 12 and white hydrated building lime, in accordance with BS 890 (1995) was used throughout the experimental work. The dropping ball test, in accordance with BS 4551 (1980) was used to check the consistency of the mortar and water/cement ratio during the mixing process. According to BS 4551, the requirement for a standard consistency of mortar is 10 ± 1 mm penetration of the dropped ball. The standard consistency of mortar was maintained throughout the project. Mortar designation 1: ½: 4½ as stated in Table 1 of BS 5628 (1992): Part 1 was adopted for the whole experimental work.

The compressive strength of a brickwork unit/ brick indicates its ability to resist crushing. In this investigation, the compressive strength of calcium silicate, clay and cement sand bricks were determined using the Universal Testing Machine. The bed face of the brick is loaded at a rate of 35 N/mm^2/min to about half its expected strength with a gradual transition to a rate of 15 N/mm^2/min thereafter to failure in accordance with BS 3921. Bricks were immersed in water at specified temperature and period prior to loading on bed faces using 4 mm plywood plates to obtain even surface on both directions. For calcium silicate bricks, the bricks were immersed in water at a temperature of 20 ± 5°C for 18 ± 2 hours in accordance with Appendix B of BS 187: 1978 prior to loading on bed face. For clay bricks, the compressive strength of bricks was obtained in accordance with BS 3921 (1985). Prior to loading on bed face, the bricks were immersed in water for 24 hours or saturated by 5 hours boiling. According to Shrive (1991), moisture content is defined as the mass of water per unit volume in the unit. The moisture content may be expressed in absolute terms with the value in the range of 50-60 kgm^{-3} being typical for units on site, or in relative terms (relative to the density of the unit when dry) with typical value of 2-3%. The water absorption characteristic of unit is commonly assessed by two parameters, namely total absorption and initial rate of absorption (IRA). Total absorption is the amount of water required to saturate the unit and fill the pores, while IRA is a measure of the mass of water absorbed per unit area per unit time (kgm^{-2}min^{-1}). The pores in brickwork units function as

capillaries and draw water into the unit. Thus IRA is a measure related to the pore-size distribution of the unit. Water absorption behaviour of brickwork units affects the performance of mortar and the deformation of brickwork. Therefore, water absorption tests are essential in monitoring the performance of brickwork units. In this investigation, 5-hour boiling test and IRA test were conducted to measure the total absorption and initial rate of absorption of brick units. Mortar cubes of 100 mm x 100 mm x 100 mm were prepared at the same time to obtain the compressive strength of brickwork mortar in accordance with BS 5628: Part 1 and Part 3. For each batch of prisms, three mortar cubes were made and tested the same day as the brickwork prisms i.e. at 14 day. All mortar cubes were cured in curing tank until the testing day to prevent moisture loss.

Twenty prisms were constructed from four bricks stack-bonded and laid up with 10 mm mortar joints from each type of brickwork unit. They were tested at the age of 14-day to obtain the brickwork wall compressive strength. The selection of the number of units was based upon the concept that due to frictional restraint at the test machine-prism interface, at least three joints would be required to attain representative measurement of full-scale brickwork behaviour. All brickwork prisms were cured until the testing day using polythene sheet to prevent loss of moisture from the mortar to the atmosphere, which would impair the hydration process and reduce the performance of brickwork prisms.

During testing, the prism was aligned accordingly in the testing machine. 6 mm thick plywood sheets were placed between the test specimens and the platens of the machine to distribute the load evenly. Figure 2 shows the set up of compression test for the brickwork prism.

Figure 2. Compression test of brickwork prism

EXPERIMENTAL RESULTS

The summary for compressive strength test, water absorption test and IRA test for calcium silicate, clay and cement sand bricks are detailed in this section. For this research, 60 specimens (20 for each type of bricks) were tested and the mean value of data set for individual bricks, mortar cubes and brickwork prisms is as shown in Table 2. The mean compressive strength of calcium silicate, clay and cement sand brick is 24.79 N/mm^2, 30.51 N/mm^2 and 6.53 N/mm^2, respectively. Clay brick was observed to have the highest compressive strength compared to other types of brick, where its strength is higher by 23.07

% and 36.7 % higher than calcium silicate and cement sand bricks, respectively. The variation in brick's compressive strength can be explained by the differences in physical properties of constituents, method of manufacturing and degree of burning for every type of bricks. For instance, higher degree of burning in the manufacturing of clay brick resulted in an increase on its compressive strength. In contrary, the constituents of cement sand brick contribute to its porous texture, which leads to reduction in compressive strength. However, the variation of compressive strength for cement sand bricks is less than other bricks and it showed that the values is more consistent and reliable. In addition, the variation of compressive strength of all prisms also seem to be in the acceptable range as opposed to the individual bricks.

The properties of mortar for each batch of mixing during the building of brickwork prisms were determined by dropping ball test and compressive strength test. The result of dropping ball test in Table 3 shows that the consistency of the fresh mortar is between 4.50 and 10.98 mm from the range of water/cement ratios of 0.45 and 0.80. The water/cement ratio with the range of 0.78 to 0.80 was adopted throughout the project to maintain the standard consistency of 10 ± 1 mm with reference to BS 4551 (1980). The compressive strength test results of mortar cubes for calcium silicate, clay and cement sand brickwork prism with the dimension of 100 mm x 100 mm x 100 mm were obtained which was cast at the same time of building the prisms and cured in curing tank until testing day. The compressive strength of mortar cubes for calcium silicate, clay and cement sand brickwork prism lie between 10.87 and 14.53 N/mm^2, 11.20 and 13.07 N/mm^2 and 10.00 N/mm^2 and 12.17 N/mm^2, respectively. Apart from that, the mean compressive strength is 11.60 N/mm^2, 12.46 N/mm^2 and 11.09 N/mm^2, respectively. Small variation was observed in the strength of mortar cubes as all batches of mortar cubes were produced based on the same mortar designation of 1: ½: 4½ (cement: lime: sand).

IRA test shows the initial rate of absorption of brickwork units. From the test, we can measure the speed of the water is drawn into the units from the mortar. Table 2 presents the test results of IRA test for calcium silicate, clay and cement sand brick. From the test results, it was observed that all types of brickwork units used in the project have relatively low IRA, which falls within the range of 0.016 kg/m^2/min and 0.024 kg/m^2/min. The mean IRA for calcium silicate, clay and cement sand brick is 0.016 kg/m^2/min, 0.051 kg/m^2/min and 0.024 kg/m^2/min, respectively, whereas, the range of IRA for each type of bricks lie between 0.008 kg/m^2/min and 0.028 kg/m^2/min, 0.029 kg/m^2/min and 0.113 kg/m^2/min and 0.007 kg/m^2/min and 0.038 kg/m^2/min, respectively.

Fired-clay brick was found to exhibit the highest initial rate of absorption (IRA) and unit water absorption (WA). The variation in IRA for all types of bricks can be explained by their pore size distribution e.g. higher initial rate of absorption was observed in cement sand brick, which is porous in texture and has relatively high pore distribution. In this project, the bricks used need not to be 'docked' as the initial rate of water absorption (suction) is low and less that 1.5 kg/m^2/min. Surprisingly, the percentage of water absorption for cement bricks is less than fired-clay bricks and not much different with calcium silicate bricks. This could be associated with the differences in the pore size of the bricks either subjected to capillary action or not.

Apart from that, illustrations of the failure modes of the test specimens are shown in Figures 3 and 4. Figure 3 shows the failed compression specimens for individual brick unit and mortar cube, while Figure 4 presents the cracking pattern for three types of brickwork prisms. It was observed that all types of brickwork prisms used in the investigation fail in compression with tensile cracks propagated through the units and the mortar in the direction

of the applied load. The cracks are caused by secondary tensile stresses resulting from the restrained deformation of the mortar in the bed joints of the brickwork (Mckenzie, 2001).

Table 2. Summary of test results for calcium silicate, clay and cement sand bricks

Parameter	Calcium Silicates bricks			Fired-clay bricks			Cement sand bricks		
	Smallest value in data set	Greatest value in data set	Mean	Smallest value in data set	Greatest value in data set	Mean	Smallest value in data set	Greatest value in data set	Mean
Brick Compressive strength, f_{bc} N/mm^2	18.36	28.89	24.79	24.74	36.86	30.51	5.74	7.09	6.53
Water absorption, WA %	9.64	14.63	11.93	17.78	23.12	20.78	11.11	15.34	12.77
IRA, kg/m^2/min	0.008	0.028	0.016	0.024	0.113	0.051	0.007	0.040	0.024
Mortar Compressive strength, f_{mc} N/mm^2	10.87	14.53	11.60	11.20	13.07	12.46	10.00	12.17	11.09
Prism Compressive strength, f_{pc} N/mm^2	13.63	17.44	15.12	12.58	19.38	15.08	4.66	5.91	5.24

Table 3. Result of dropping ball test

w/c ratio	Penetration (mm)
0.45	4.50
0.60	7.80
0.78	9.86
0.80	10.98

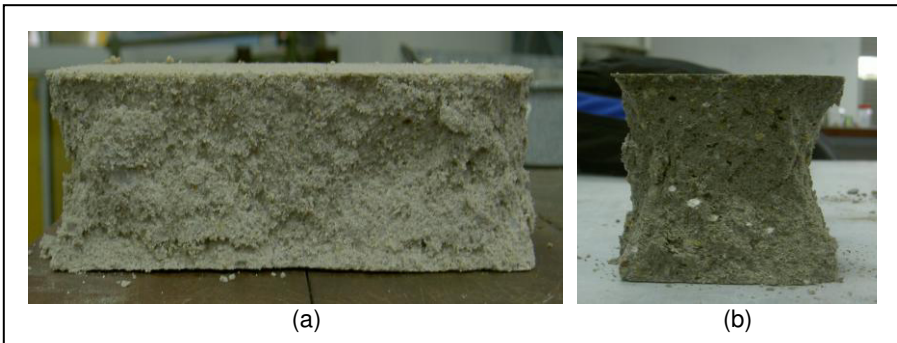

(a) (b)

Figure 3. Failure mode of (a) brick unit (b) Mortar cube

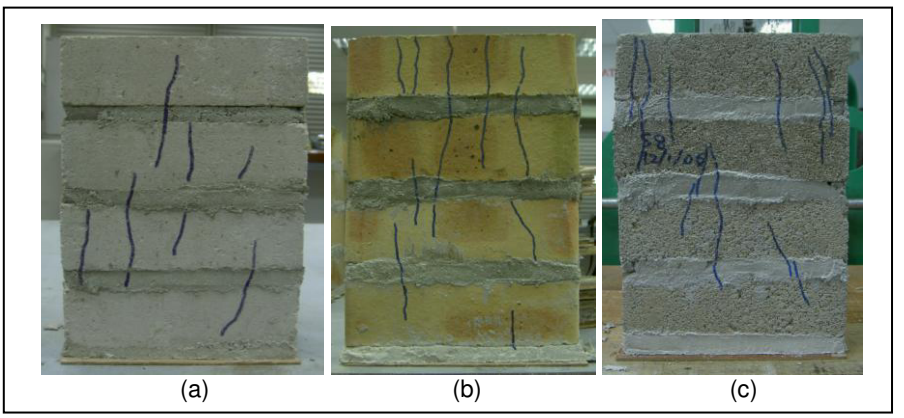

Figure 4. Failure mode of brickwork prisms for (a) Calcium silicate brickwork (b) Clay brickwork and (c) Cement sand brickwork

MODELLING WITH MINITAB R14

In this research, empirical modelling of brickwork compressive strength with statistical software MINITAB R14 was conducted. It is a powerful and flexible statistical software program that provides a wide range of basic and advanced data analysis capabilities. The comprehensive capabilities include data management, advanced graphics, command language, basic statistics, regression analysis, analysis of variance, statistical process control, measurement system analysis, design of experiments, reliability/survival analysis, power and sample size, multivariate analysis, forecasting, non-parametric, tables and simulation and distributions. Apart from that, MINITAB provides advanced graphics capabilities that give the critical ability of data, reveal underlying patterns, makes informed decisions and evaluation on the model's effectiveness. Several multiple regression analyses were performed based on 60 lab data obtained from the experimental works in which the experimental predictor variables (f_{bc}, f_{mc}, WA, IRA) were input. The relationship between response variable (prism's compressive strength) and the predictor variables (unit compressive strength, mortar compressive strength and unit water absorption) was examined. Least square method, which involved best fitting line with minimized sum of squared deviation, was adopted. In addition, analyses were performed based upon two form of regression model, namely linear form and exponential form (linearized form) where:

$$\text{Linear form: } Y' = \beta_o + \beta_1 X_1 + \beta_2 X_2 + \ldots. + \beta_k X_k \quad (3)$$

$$\text{Exponential form: } \text{Log } Y' = \text{Log } \beta_o + \beta_1 \text{LogX}_1 + \beta_2 \text{LogX}_2 + \ldots. + \beta_k \text{LogX}_k$$

$$\text{Or} \qquad Y' = \beta_o X_1^{\beta 1} X_2^{\beta 2} \ldots. X_k^{\beta k} \quad (4)$$

The combinations of predictor variables used in the modelling process are listed in Table 4. Nine combination sets of predictor variables were attempted for models in linear and exponential form. Table 4 also summarised the coefficient of determination of all candidate models. Prior to regression analysis, matrix plot of variables was performed to investigate

the relationship and correlation between variables. After the regression analysis, t-tests (hypothesis testes) were carried out to determine the significance and usefulness of candidate models and predictor variables. These involved the comparison of the calculated t-statistic for each model or term with the value corresponding to the 5% probability threshold value for the t-distribution. If t-test reveals that the actual t-statistic is lower than the threshold value, conclusion can be drawn that the particular model or term is not significant. For t-test on predictor variables, the insignificant predictor variable is dropped and regression is then repeated utilising the remaining terms until all terms are significant. The selection of the best model based on several factors, both statistically and non-statically. e.g. coefficient of determination (r^2), results of t-tests, residual analysis, etc. For a perfect model, r^2 should approach unity (Draper and Smith, 1998).

The summary of regression analysis in Table 4 shows that the exponential form of predictor expression resulted in higher coefficient of determination, r^2. This indicates the models in exponential form are the better models in comparison to the model in linear form. Further discussion in this paper will focus on the following expressions, which are associated with higher degree of coefficient of determination (r^2).

Models in exponential form:

Combination set 1: $\text{Log } f_{pc} = 0.218 + 0.743 \log f_{bc} - 0.206 \log f_{mc} - 0.0220 \text{ WA} - 0.0869 \log \text{IRA}$ (5)

Combination set 5: $\text{Log } f_{pc} = 0.197 + 0.741 \log f_{bc} - 0.217 f_{mc} - 0.0928 \text{ IRA}$ (6)

Combination set 6: $\text{Log } f_{pc} = -0.0268 + 0.729 \log f_{bc} - 0.0976 \text{ IRA}$ (7)

Combination set 8: $\text{Log } f_{pc} = 0.041 + 0.734 \log f_{bc} - 0.0461 \text{ WA} - 0.0847 \text{ IRA}$ (8)

Further evaluations on the candidate models are shown in Table 5 and 6. Hypothesis test (t-test) on models and predictor variables indicates that Eqn. 7 is the best model in predicting the brickwork compressive strength. Thus, the final model selected is

$$\text{Log } f_{pc} = -0.0268 + 0.729 \log f_{bc} - 0.0976 \text{ IRA or}$$

$$f_{pc} = 0.9402 \, f_{bc}^{0.729} \, \text{IRA}^{-0.0976}$$

Where f_{pc} = prism's strength, f_{bc} = brick compressive strength, f_{mc} = mortar compressive strength,
IRA = brick's initial rate of absorption, WA = water absorption

Table 4. Summary of regression analysis

Combination No.	Predictor variables included	Coefficient of determination, r^2 (%)	
		Linear form	Exponential form
1	f_{bc}, f_{mc}, WA, IRA	87.20	94.60
2	f_{bc}, f_{mc}, WA	84.70	94.10
3	f_{bc}, WA	84.50	94.00
4	fm_c, WA	18.00	19.50
5	f_{bc}, f_{mc}, IRA	87.20	94.60
6	f_{bc}, IRA	87.00	94.50
7	f_{mc}, IRA	13.40	15.80
8	f_{bc}, WA, IRA	87.00	94.50
9	f_{mc}, WA, IRA	18.90	21.30

Table 5. Hypothesis test- usefulness of the models

Combination set no.	Equation no.	F	P
1	5	240.72	0.000
5	6	326.45	0.000
6	7	486.25	0.000
8	8	320.00	0.000

Table 6. Hypothesis test- usefulness of the predictors

Predictor	p-value			
	Eqn. 5	Eqn. 6	Eqn. 7	Eqn. 8
log f_{bc}	0.000	0.000	0.000	0.000
log f_{mc}	0.298	0.255	-	-
log WA	0.816	-	-	0.617
log IRA	0.023	0.001	0.001	0.027

Simulation of the brickwork strength based on the developed model

Based on Eqn. 7, the effect of water absorption on the compressive strength of brickwork wall was simulated. Test results of 60 specimens obtained from experimental works were input into Eqn. 7 for the simulation session. Brickwork strength estimated by Eqn. 7 which has taken into consideration the effect of unit water absorption enable us to see how far unit water absorption would influence the brickwork strength. Apart from that, the simulation process shows the differences between measured strength and developed model. Figure 5 shows the histogram of brickwork strength for Eqn. 7 and measured strength. It was observed that Eqn. 7, which consists of brick strength and IRA as its predictor variable gives lower brickwork strength. The histogram was found approximately in bell shape with small discrepancy between the two curves. The mean strength obtained from test specimens and Eqn. 7 was 11.81 N/mm^2 and 11.76 N/mm^2, respectively, while the standard deviation is 4.849 N/mm^2 and 4.727 N/mm^2**,** respectively. This shows that unit water absorption

contributes to the reduction of compressive strength in brickwork wall. Therefore, consideration of the effect of water absorption on the strength prediction should be made to provide a better safety margin in the construction of brickwork structures.

Comparison with other established models

Figure 6 shows the brickwork strength predicted by Eqn. 7, BS 5628, EC 6 and Mann's formula. Strength predicted by all models was plotted against the measured brickwork strength by inputting the experimental results of 60 test specimens into the following equations. The strength of brickwork predicted by BS 5628 was calculated by interpolation of the characteristic strength on Table 2.2 (a) of section 2.5.1: BS 5628: Part 1: 1992 based on type (ii) mortar designation.

EC 6 : $f_{wc} = 0.70\, f_{bc}^{0.65} f_{mc}^{0.25}$

Mann : $f_{wc} = 0.83\, f_{bc}^{0.67} f_{mc}^{0.33}$

Eqn. 7 : $f_{wc} = 0.9402\, f_{bc}^{0.729}\, IRA^{-0.0976}$

Discrepancies are observed between all curves. The slope of Mann's curve was found to be greater than Eqn.7's curve**,** while the curves corresponding to EC 6 and BS 5628 was noticed to give lower values. Statistical analysis also revealed the mean strength predicted by EC 6 and BS 5628 were respectively 31.69 % and 80.10 % lower than the strength attained by Eqn. 3. Meanwhile, the strength estimated by Mann's equation was found to be 14.41 % higher. However, the prediction of Eqn. 7 may not be faired to compare with other models because the data used is only limited to this investigation. Therefore, the Eqn. 7 should be further validate using data from other researches.

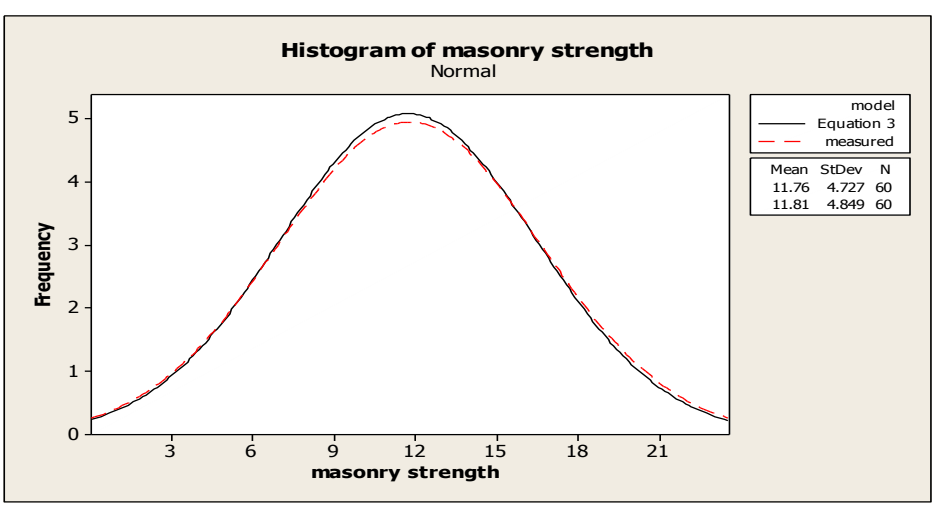

Figure 5. Histogram of brickwork strength

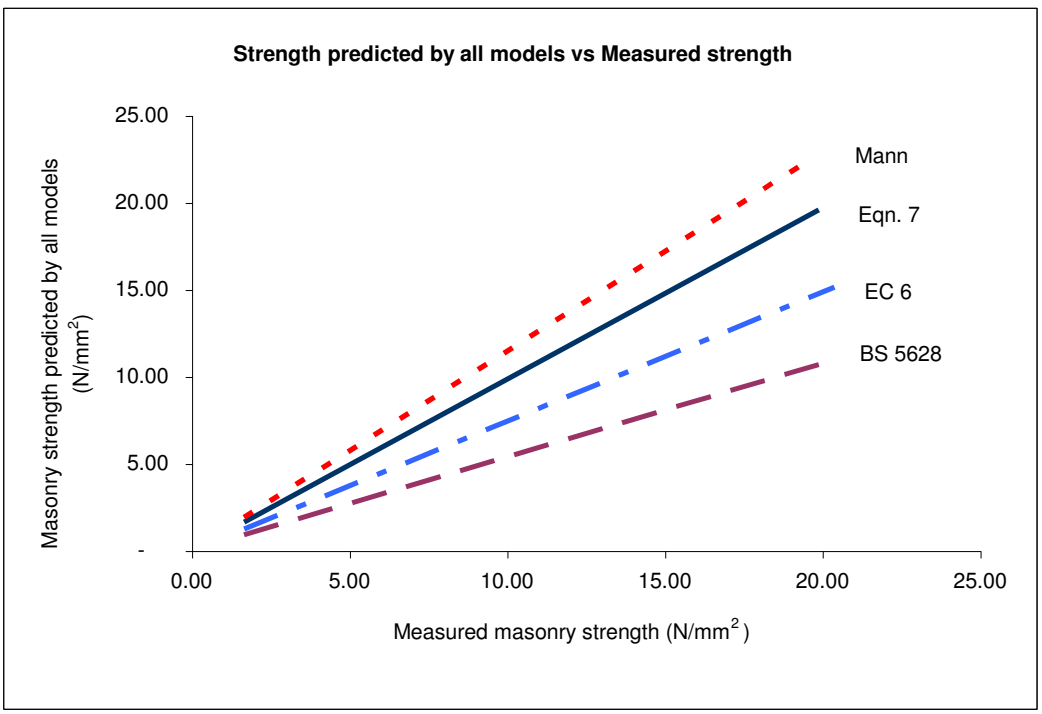

Figure 6. Graph of strength predicted by model vs. measured brickwork strength

CONCLUSIONS

From the experimental results, conclusion can be made that the ultimate compressive strength of the prism, which is a composite of mortar and brick is considerably less than the individual brick unit. It can however be higher than the mortar strength. This coincides with Schneider's theory (1987) in which when brick and mortar are combined as a composite material, they will demonstrate a lower combined strength as the strength and stiffness properties of the mentioned material are different. The summary of test results also revealed that among calcium silicate, clay and cement sand bricks, clay bricks has the highest compressive strength, water absorption, initial rate of absorption and prism strength, followed by calcium silicate and cement sand bricks.

The model developed in this research is $f_{wc} = 0.9402\ f_{bc}^{0.729}\ IRA^{-0.0976}$. The outcome of regression analyses indicated that of the predictor variables evaluated, brick compressive strength and IRA are the important factors influencing the prism strength. These factors are the basis of expressions for the estimation of brickwork strength based on regression analysis using statistical software, MINITAB R14. Inclusion of other parameters, e.g. mortar strength, water absorption only slightly improved the accuracy of prediction. Moreover, these parameters were found insignificant in the model from the hypothesis testes. Therefore, only brick strength and IRA were included as the predictor variables. Even though the coefficient of determination of the final model is quite high (94.5 %), it is to note that the expression apply to the data collected cannot be considered generally applicable. In a statistical sense, the test sample was small; additional data could significantly influence the coefficient of determination and causes a change in the expression. Larger sample size is required to build a model with higher accuracy. In addition, the simulation on the effect of

water absorption on the strength of brickwork wall shows that unit water absorption contributes to the reduction of compressive strength in brickwork wall. Therefore, unit water absorption should be considered in the estimation of brickwork strength to provide a better safety margin in the construction of brickwork structures. However, the influence of mortar strength should be further investigated because most of all models considered mortar strength as an important factor to the strength contribution.

ACKNOWLEDGEMENTS

The authors would like to thank the Construction Industry Development Board Malaysia (CIDB) for the financial support.

REFERENCES

Atkinson, R.H., Kingsley, G.R. and Yan, G.G. (1990) A database for compressive stress-strain behaviour of masonry. *Fifth North American Masonry Conference*. Volume 2: 581–593.

Baur, J., Noland, J.L. and Chinn, J. (1978) Compression tests of clay-unit stackbond prisms. *North American Masonry Conference*. Volume 25:1-25

British Standards Institution (1976) Specification for Building Sands from Natural Sources. London, BS 1200.

British Standards Institution (1978) Specification for Calcium silicate (Sandlime and Flintlime) bricks. London, BS 187.

British Standards Institution (1980) Methods of testing: Mortar, screeds and plasters. London, BS 4551.

British Standards Institution (1985) *British Standard Specification for Clay Bricks*. London, BS 3921.

British Standards Institution (1995) Specification for Building limes. London, BS 890.

British Standards Institution (1992) Structural use of unreinforced masonry, Part 1: Code of practice for use of masonry. London, BS 5628.

British Standards Institution (1996) *Specification for Portland cement.* London, BS 12.

CEN Technical Committee 250/SC6 (1995). *Design of Masonry Structures (ENV 1996.1)*. CEN, Brussels, Eurocode 6.

Draper, N.R. and Smith, H. (1998) *Applied regression analysis*. New York: Wiley series in probability and statistics.

Francis, A. J., Horman, C.B. and Jerems, L. E. (1971) The effect of joint thickness and other factors on the compressive of brickwork. Proceedings of the Second International

Brick Masonry Conference. *British Ceramic Research Association*: 31-37.

Goodwind, J.F. and West, W.H. (1982) *A review of the literature on brick/mortar bond*. Proceedings of the British Ceramic Society. Vol. 30, No. 23, pp23-37.

Grimm, T. (1975) *Strength and related properties of brick masonry*, J. Struct. Div. Am. Soc. Civ. Engr. Volume 107: 217-232.

Henry, A.W. (2001) Masonry walls: materials and construction. *Magazine of Construction and Building Materials.* Vol. 15: 323-330.

Hendry, A.W. and Malek, M.H. (1986) Characteristic compressive strength of brickwork walls from collected test results. *Masonry Int.* Volume 7: 15-24

Lawrence, S. J. and Cao, S. (1988) The Influence of some factors on the tensile bond strength of masonry. *Proceeding of the 10th International brick and block masonry conference*, Calgary, Canada, pp 929-938.

Mann, W. (1982) *Statistical evaluation of tests on masonry by potential functions*. Sixth International Brick Masonry Conference, pp 77-83.

Mckenzie, W.M.C. (2001). *Design of structural masonry*. New York: Palgrave.

Pande, G.N., Kralj, B. and Middleton, J. (1994) Analysis of the compressive strength of masonry given by the equation $K (fb)^{\alpha}(fm)^{\beta}$. *Struct Eng*. Volume 72, No.1 :7 –12.

Shrive, N.G. (1991) *Material and Material Testing- Reinforced and Prestressed masonry*. UK: Longman Scientific & Technical.

Schneider, R.R. and Dickey, W.L. (1987). *Reinforced Masonry Design*. United States: Prentice- Hall Inc.

NUMERICAL STUDY ON THE PERFORMANCE OF SHELL FOOTING

Bujang B.K. Huat[1], Thamer Ahmed Mohammed[1], Adel Al-Raziqi[2]
[1]Department of Civil Engineering, Universiti Putra Malaysia 43400 Serdang, Selangor, Malaysia
[2]Department of Civil Engineering, Thamar University, Yemen

Abstract

This paper describes a study on the performance of shell footings using a non-linear finite element analysis with a finite element code, PLAXIS. The shell footing is found to have a better load carrying capacity compared with the conventional slab (flat) footing of similar cross sectional area. The FE analysis also showed a reasonably good agreement with the laboratory experimental results. The effect of adding edge beams at the bottom of the shell footings has been studied numerically, and found to be beneficial in increasing the load carrying capacity of the footing. The effect of increasing the embedment ratio is also studied and found to increase the load carrying capacity of the shell footings.

Keywords: finite element analysis, flat footing, foundation, shell footing

INTRODUCTION

Concept of shell is not new in foundation design, considering construction in past with inverted brick arch foundation in this category. The use of inverted brick arches as foundation has been in practice in many parts of the world for a long time. Shells in modern foundation engineering however are relatively still newcomer. Shell footings have been found to be economical foundations in areas having high material to labor cost ratio (Kurian, 1977, 1982). Shell foundation is economical and has greater load carrying capacity compared with flat shallow foundations. Moreover, shells are essentially thin structures, thus structurally more efficient than flat structures. This is an advantage in situation involving heavy super structural loads to be transmitted to weaker soils. Shell footing is limited to a few geometries, such as conical, pyramidal, hypar and spherical footings, and these footings are shown in Figures 1 – 4 respectively.

The conical shell (Figure 1) is the simplest form of shell, which can be employed in foundation engineering due to its singly curved surface. Due to its circular plan, the use of conical shell footing is restricted to an isolated footing only.

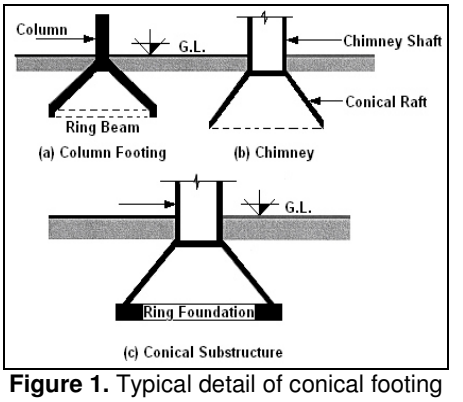

Figure 1. Typical detail of conical footing

A pyramidal shell (Figure 2) is a combination of four inclined trapezoidal plate elements. Since the pyramid can be portrayed as square or rectangular in plan, multiple units of pyramidal shell foundation can be jointly integrated to act as combined or raft foundation.

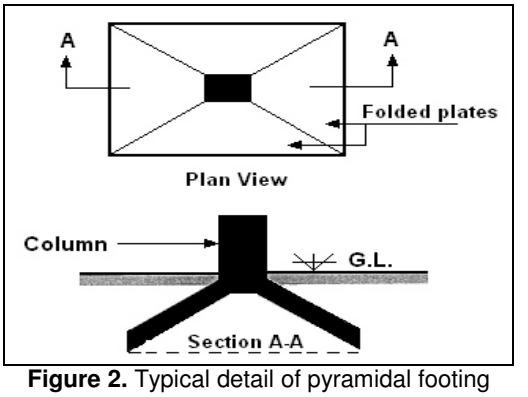

Figure 2. Typical detail of pyramidal footing

The hyperbolic paraboloid (hypar) shell (Figure 3) is a doubly curved anticlastic shell, which has translation as well as ruled surfaces. This footing has potential to be employed in a wide range of application in foundation engineering.

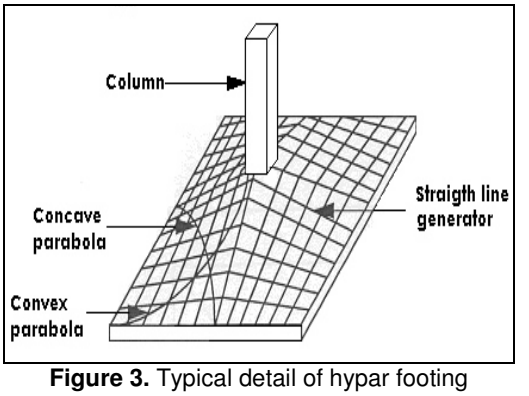

Figure 3. Typical detail of hypar footing

Spherical shells (Figure 4) do not posses straight-line property, which makes its construction more complex. It can only be used as an isolated footing.

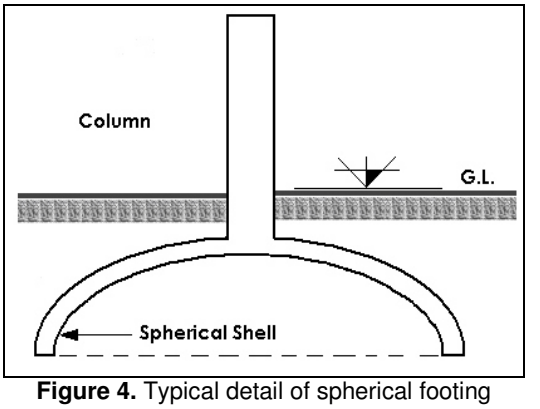

Figure 4. Typical detail of spherical footing

Experimental and theoretical investigations reported the evaluation of structural behavior for shell structure, such as the membrane stresses, bending moments, shear, and deflections. For theoretical analysis, mathematical formulations, namely finite difference technique and finite elements analyses were utilized. In some studies, linear Winkler and Pasternek soil model was used to simulate the soil behavior under different types of shell foundations. In few studies, the distribution of the soil contact pressure on shell footing was also examined. The results indicated a non-uniform contact pressure distribution along the soil-shell interface. However, the structural design of shell foundation is currently based on membrane theory, in which the soil contact pressure distribution is assumed to be uniform (Fareed & Dawoud, 1979, Melerski, 1988, Paliwal & Rai, 1986, Paliwal & Sinha, 1986).

The ultimate strengths of the shell footings were also investigated both experimentally and theoretically; and comparisons were performed with conventional flat foundation. All studies reached the same conclusion concerning the saving achieved in the construction materials and the good structural performance of the shell footing. The findings of these investigations have direct impact on the construction cost of shell footings as compared to the conventional flat counterparts (Kurian, 2000).

Abdel-Rahman and Hanna (1990), Abdel-Rahman (1996), and Hanna and Abdel-Rahman (1998) reported experimental results on model shell footings on sand for plain strain condition. Maharaj (2004) conducted a finite element analysis for conical shell footing to study the effects of increasing soil modulus.

In the present study, a triangular shell footing was adopted being the most suitable shape for strip load bearing wall application. The study aimed to examine the interaction between the triangular shell footing and soil using a non-linear finite element (FE) analysis code. The effects of adding edge beams at the bottom of the footing, and depth of embedment of the footings, on the load carrying capacity of the footing were investigated using the FE analysis.

FINITE ELEMENT MODEL

The triangular shell footings and the soils were modeled and analyzed using the commercial finite element software PLAXIS, developed by PLAXIS BV, Netherlands. The program ‘PLAXIS’ uses the incremental tangent stiffness approach in the analysis, in which the load is divided into a number of small increments, which are applied simultaneously. During each load increment, the stiffness properties appropriate for the current stress level are employed in the numerical analysis. Experimental results on model shell footing from earlier work of Abdel-Rahman (1996) are used to validate the finite element modeling of the present study.

Three footing models; one flat (slab) footing and two triangular shell footings (1 & 2) were selected for the analysis, and compared with the experimental results obtained earlier by Abdel-Rahman (1998). The cross sections of the model footings are shown in Figure 5.

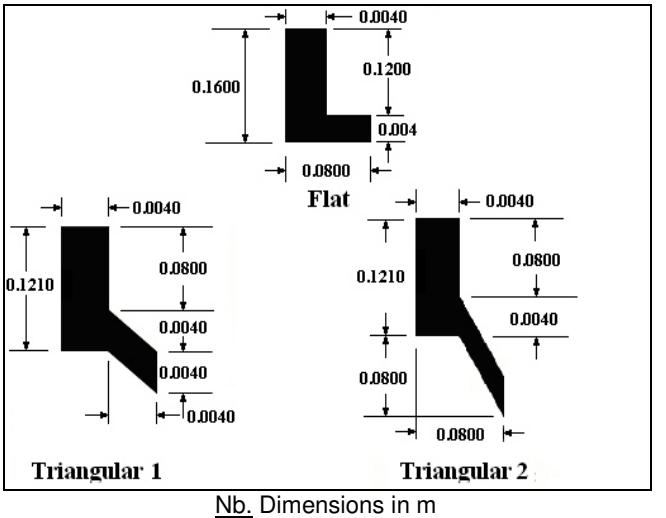

Nb. Dimensions in m

Figure 5. Details of half sections of flat and triangular shell model footings

The cross sectional properties of the three models shown in Figure 5 are listed in Table 1. These properties are used as input for modeling the footings by the program PLAXIS. The soil is modeled using the Mohr-Coulomb model; the properties of which are shown in Table 2.

Table 1. Cross-sectional properties of the model footings

Properties \ Types	Flat	Triangular 1	Triangular 2
Cross Section Area (m^2)	0.00320	0.00328	0.00453
Moment of Inertia, I (mm^4)	4.27E-7	4.77E-7	6.034E-7
Modulus of Elasticity, E_{sh} (kN/m^2)	209E6	209E6	209E6
Poisson Ratio, υ	0.3	0.3	0.3
Material Type	Elastic	Elastic	Elastic
Flexural Rigidity, EI	89.173	99.696	126.110
Axial Stiffness, EA	668800	7482200	9457250

Table 2. Soil (sand) properties

Properties	Value	Unit
Unsaturated Unit Weight	17	kN/m^3
Saturated Unit Weight	18	kN/m^3
Permeability Coefficient, $k_x=k_y$	1.00	m/day
Young's Modulus, E	4E4	kN/m^2
Poisson Ratio, υ	0.3	none
Cohesion Coefficient, c	0.001	kN/m^2
Friction Angle, ϕ	33.68	Degree
Dilatancy Angel, ψ	2.00	Degree
Material Model	Mohr-Coulomb Model	none

The geometry of the mesh for plain strain condition is symmetrical about the centerline, therefore only one half of the cross section passing through the axis of symmetry of the footing is considered. The nodes along the bottom and both sides of the section are considered as pinned supports, i.e., no movement is allowed in both vertical and horizontal directions, which called in the program as Standard Fixities. The soil and the footing were modeled using 15-noded linear strain quadrilateral elements 'LSQ' with quadratic variations for the displacement along the sides of the element.

Figure 6 shows the typical generated and deformed mesh. Figure 7 shows the load – settlement curves of the finite element (FE) models. Superimposed on Figure 7 is the load – settlement of the laboratory experiment. In general there is a good agreement between the FE model and that of the laboratory. However, the results of the FE analyses are generally higher than that of the laboratory experiments. The difference is about 8%, 11% and 27% for the flat, triangular shell 1 and triangular shell 2 footings, respectively. This is inherent since the FE analysis is done in 2 dimensions while the experimental study is for a 3 D model. However both the laboratory and FE models clearly show that load carrying capacity of the triangular shell, with a similar cross sectional area, is higher than the flat footing. Shell footing ensures better enclosibility of the soil inside the space of the footing by preventing the soil from flowing outward. This can be very significant, particularly when the soil is poor. A similar conclusion is made by Abdel-Rahman and Hanna (1990), and Hanna and Abdel-Rahman (1998).

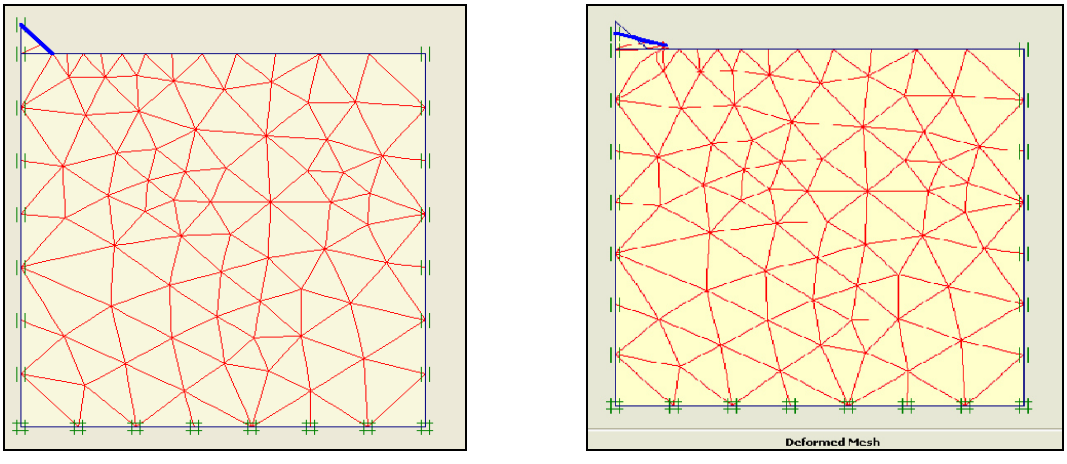

(a) Generated mesh of triangular shell footing 1 (b) Deformed mesh of triangular shell footing 1

Figure 6. Typical generated and deformed mesh

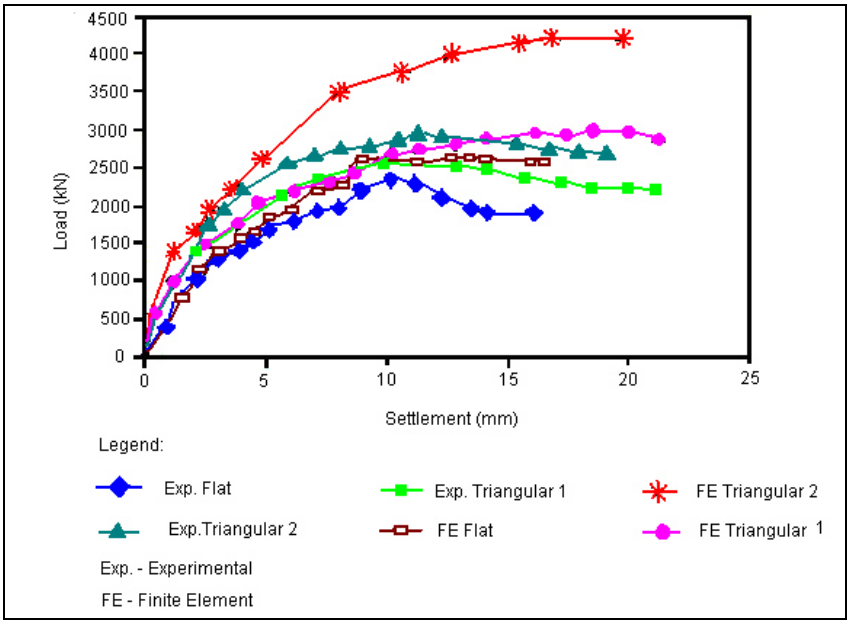

Figure 7. Load-settlement curves of the FE and experimental model of the flat (slab) and triangular shell footings.

FE STUDY ON THE EFFECT OF EDGE BEAMS AND DEPTH OF EMBEDMENT

The presence of an edge beam at the toe of the shell would reduce the soil pressure and increase the bearing capacity (Jain et al, 1977). To examine this, as well as the effect of embedment ratio, a finite element analysis using the finite element code, PLAXIS, is done to study the load - settlement behavior of shell footing model with different edge beams. Five edge beam configurations were considered, namely Type 1, 2, 3, 4 and 5, and these are shown in Figure 8. Type 1 footing is a triangular shell footing without the edge beam; Type 2 footing is with a double edge beam; Type 3 footing is with single edge beam; Type 4 footing is with a vertical edge beam; and Type 5 footing is with inclined edge beam. Embedment ratio, R is 1 for fully embedded footing, and R = 0 for footing with no embedment. In this case only the Type 1 footing was studied. The cross sections of the models are shown in Figure 9. Table 3 summarizes the cross sectional properties of the model footings. The sandy soil is modeled using the Mohr Coulomb model, as shown Table 2.

Table 3. Cross-sectional properties of new shell footing models.

Properties \ Types	Type1 Footing	Type2 Footing	Type3 Footing	Type4 Footing	Type5 Footing
Cross Section Area (m^2)	0.250	0.440	0.329	0.388	0.346
Moment of Inertia, I (mm^4)	4.00E-3	7.00E-3	5.54E-3	6.50E-3	5.00E-3
Modulus of Elasticity, E_{sh} (kN/m^2)	2E7	2E7	2E7	2E7	2E7
Poisson Ratio, υ	0.3	0.3	0.3	0.3	0.3
Material Type	Elastic	Elastic	Elastic	Elastic	Elastic
Flexural Rigidity, EI	8E3	14E4	11E4	13E4	10E4
Axial Stiffness, EA	5.00E6	8.80E6	6.50E6	7.76E6	6.90E6

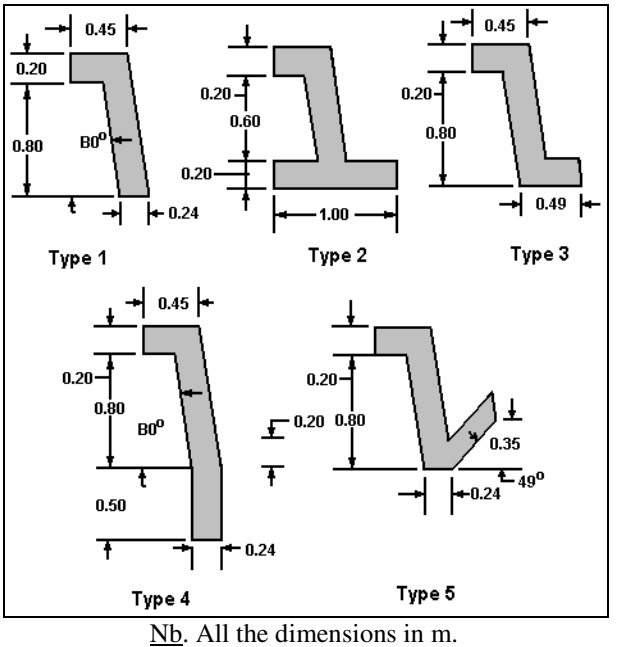

Nb. All the dimensions in m.

Figure 8. Details of half sections of shell footings with various edge beams

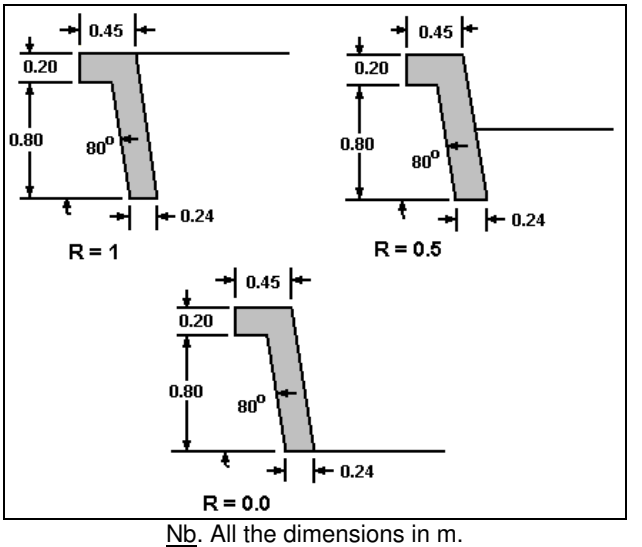

Nb. All the dimensions in m.

Figure 9. Type 1 footing with various embedment ratio, *R*.

Figure 10 shows the effect of adding an edge beam at the bottom of triangular shell footing on load-settlement curve of the footing. Footing of Type 1 (i.e. without edge beam), and Type 2 (with double edge beam) are considered in this case. The initial portion of the two curves overlaps each other up to load of about 100 kN. After this load, the load carried by shell footings with the double edge beam is significantly higher than the footing without the edge beam; almost double at settlement of 10 mm. This shows that there is a significant improvement in settlement-load carrying capacity of the footing when added with the edge beam.

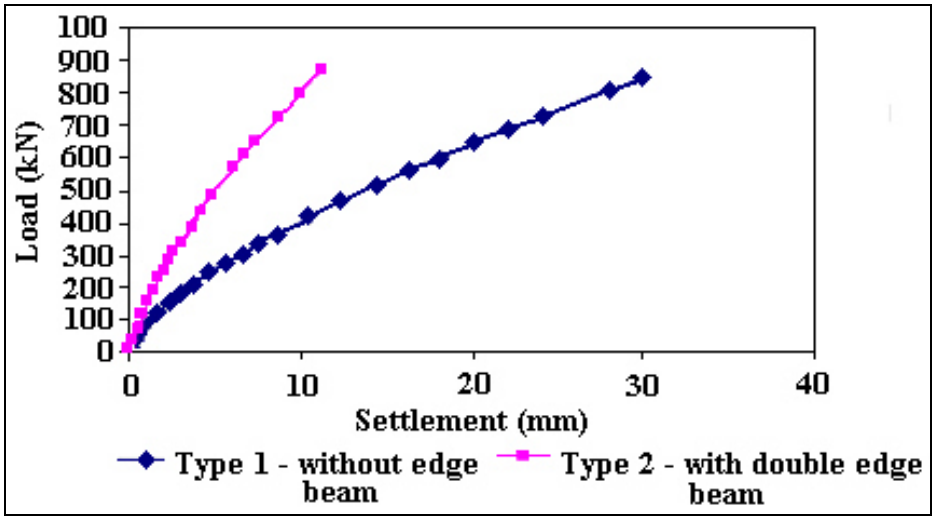

Figure 10. Load -settlement curve at the shell footing with and without the edge beam.

Figure 11 shows the comparison of the load carrying capacity of the triangular shell footings with the various edge beam configurations, i.e. for Type 2, 3, 4 and 5. As shown footing with the double edge beam (Type 2), single edge beam (Type 3), and inclined edge beam (Type 5) show better load-settlement characteristics compared with the footing having vertical edge beam (Type 4).

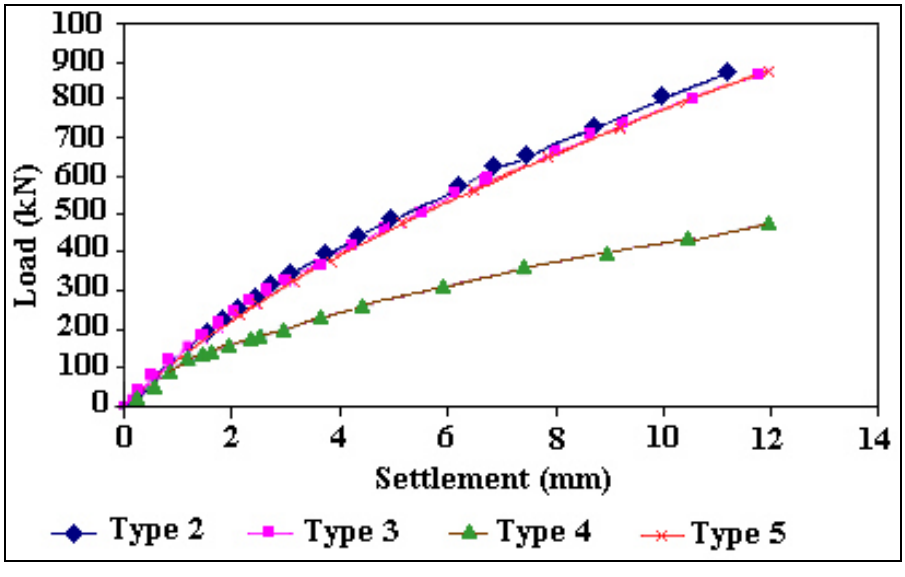

Figure 11. Effects of various configuration of edge beam on the triangular shell footing

Figure 12 shows the effect of embedment ratio on the load-settlement behavior of the shell footings. From Figure 12 it be seen that the load-settlement curve for the three-embedment ratios (i.e. from fully embedded to no embedment) overlaps each other until

about 300 kN. After this load, the load carried by the embedded shell footing is more than the footing without embedment. For example at settlement of 30 mm, the load of the fully embedded footing was 30% higher than the un-embedded footing. This shows the benefit of fully embedded the footing on the load carrying capacity of the shell footing.

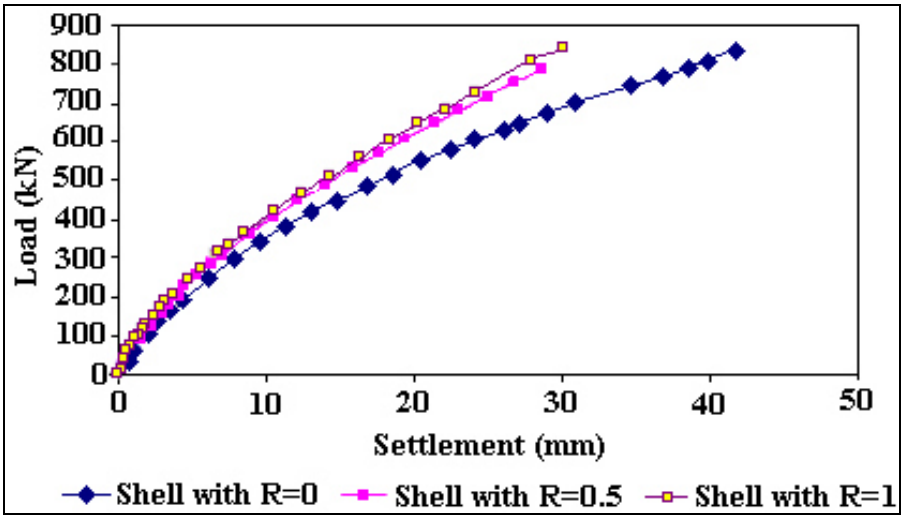

Figure12. Effect of the embedment ratio on the load carrying capacity of the triangular shell footings

CONCLUSIONS

A non-linear finite element analysis using finite element code, PLAXIS, was carried out to study the geotechnical behavior of the triangular shell footings. From the finite element results, it was found that the shell footing had a better load carrying capacity compared with the slab (flat) footing for a similar cross sectional area. The FE analysis also showed a reasonably good agreement with the laboratory experimental results; with a discrepancy of within 8 to 27%.

The effect of adding edge beams at the bottom of the shell footings has been studied numerically, and found to be beneficial in increasing the load carrying capacity of the footing.

Fully embedded shell footing is shown to have a better load carrying capacity compared with the un-embedded footing.

REFERENCES

Abdel-Rahman, M., and Hanna, A.M. (1990). Ultimate Bearing Capacity of Triangular Shell Footings on Sand. *Journal of Geotechnical Engineering*. ASCE, 116(12): 1851-1863.

Abdel-Rahman, M. (1996) *Geotechnical behavior of shell foundations*, Ph.D Thesis, Department of Civil Engineering, Concordia University, Montréal, Canada.

Fareed, A., and Dawoud, R.H. (1979) Cylindrical shells on elastic foundation. *World Congress on Shell and Spatial Structures*. Madrid, Spain. 3: 5.33- 5.46.

Hanna, A.M. & Abdel-Rahman, M. (1998) Experimental investigation on shell foundations on dry sand. *Canadian Geotechnical Journal.* 35(6): 828-846.

Jain, V.K., Nayak, G.C. & Jain, O.P. (1977) General behavior of the conical shell foundation. *Proceedings of 3rd International Symposium on Soil Structure Interaction*. University of Roorkee. India. 2: 53-61.

Kurian, N.P. (1977) Economy of hyperbolic paraboloidal shell footings. Geotechnical Engineering. 8 (1): 53-59.

Kurian, N.P. (1982) Modern foundations - Introduction of advanced techniques. Tata McGraw-Hill, New Delhi.

Kurian, N.P. (2000) Shell foundations – The Asian Choice. New Building Materials and Construction World.

Maharaj, D.K. (2004) Finite element analysis of conical shell foundation. *Electronic Journal of Geotechnical Engineering*, 9A(348)

Melerski, E. (1988) Thin shell foundation resting on stochastic soil. I. *Structural Engineering*. ASCE. 114 (12): 2692-2709.

Paliwal, D.N. & Rai, R.N. (1986) Shallow spherical shell on Pasternak foundation subjected to elevated temperature. *J. Thin-walled structures,* 5 (S): 343-349.

Paliwal, D.N. & Sinha, S.N. (1986) Static and dynamic behaviour of shallow spherical shells on Winkler foundation. *J. Thin-walled structures,* 4 (6): 411-422.

Effect of Surface Cover on Infiltration Rate and Stability of a Cut Slope in Unsaturated Residual Soil

Bujang B. K. Huat[1], Faisal Hj. Ali[2], S. Mariappan[2]
[1]Department of Civil Engineering, University Putra Malaysia, 43400 UPM Serdang, Selangor, Malaysia
[2]Department of Civil Engineering, University of Malaya, 50603 Kuala Lumpur, Malaysia

Abstract

Rainfall has been considered the cause of the majority of slope failures and landslides that happened in regions experiencing high seasonal rainfalls. Basically, it is well known that infiltration impairs slope stability, but since it is often not measured off directly from the field, its assessment often relies on vague correlation with rainfalls and runoff. Conventionally, infiltration of water is not included in the slope stability analysis. However, most of the slope failure and landslides occurred after prolonged heavy rainfall or antecedent rainfall. The mechanism of the failures was mainly due to the lost of matric suction of soils by rainwater. When the rainwater infiltrates into the slopes, it will start to saturate the soil, thus reducing the matric suction. The rate of water infiltration into the soil and its effect on suction is expected to be influenced by the types of surface cover, soil porosity, weathering grades and angle of the soil slopes. This paper presents results of a field study on the effect of surface cover on the water infiltration rate into a cut slope of unsaturated residual soil. A parametric study is also done to examine the effect of surface cover on the factor of safety of soil slope using the Seep/W and Slope/W programs. The soil infiltration rate as measured from the field test shows an increase from the fully vegetated slope with geosynthetic net, to cut grass slope with geosynthetic net, to geosynthetic net and to bare surface slope only. For a particular surface cover/condition, soil of weathering grade III had higher infiltration rate compared to soils of intermediate grade (IV – III), grade IV and grade V. The factor of safety obtain from analysis by incorporating matric suction, is much higher than the factor of safety obtained from the conventional slope stability analysis without matric suction. There is a trend of reduction in factor of safety with rain, in particular for slopes with the lesser cover.

Keywords: Cut slope, landslide, residual soil, vegetation

INTRODUCTION

Rainfall has been considered the cause of the majority of slope failures and landslides that happened in regions experiencing high seasonal rainfalls (Brand 1984, Shaw-Shong 2004). Basically, it is well known that infiltration impairs slope stability, but since it is often not measured off directly from the field, its assessment often relies on vague correlation with rainfalls and runoff. Correlation between rainfall and infiltration involves large number of factors such as rainfall duration and intensity, slope surface cover, degree of saturation, slope angle, permeability ratios and perched water table. Conventionally, infiltration of water is not normally included in slope stability analysis. Many of the steep slopes were designed based on experiences and most of the slopes failure or landslides occurred after prolonged heavy rainfall or antecedent rainfall. The mechanism of the failures was mainly due to the lost of matric suction of soils by rainwater. When the rainwater infiltrates into the slopes, it is known that it will start to saturate the soil, thus reducing the matric suction. The wetting front of rainwater will continue to move into the soil even after the rain stopped. Movement of the wetting front stops when an equilibrium or steady state condition is achieved.

Matric suction is one of the main stress variables in unsaturated soil theory (Fredlund & Morgenstern 1977, Fredlund & Rahardjo 1987). The existence of matric suction will increase the strength of the soil. A deep ground water table condition is normal in hilly area of the tropical countries. In this case, the negative pore water pressure or matric suction plays an important role in controlling the soil shear strength and consequently the stability of many steep slopes. Shallow landslides often occur in steep residual soil slopes after heavy and prolonged rainfall. When water starts to infiltrate into the soil, the matric suction especially near the ground surface will slowly reduce and become zero as the soil approaches saturated condition. The significant reduction in matric suction is known to cause a decrease in the soil shear strength that subsequently produces shallow landslides.

Studies on water infiltration have always been part of hydrology. Water infiltration forms the link between surface and subsurface hydrology. Infiltrated water must be quantified and subtracted from the surface runoff in flood prediction studies and surface water management. Numerous researchers have actually incorporated infiltration into the slope stability analysis of the residual soil, e.g. Othman (1989), Anderson (1991), Affendi & Ali (1994), Suhaimi (1997) and Ali & Rahardjo (2004). In most of the analysis of slope stability, the infiltration rate of the water into soil is assumed uniform throughout the slope. The soil is also assumed homogeneous except in some layered bedding problem.

This paper presents results of a field study on the effect of surface cover on the water infiltration rate into a cut slope of unsaturated residual soil. A parametric study is also done to examine the effect of surface cover on the factor of safety of soil slope using the Seep/W and Slope/W programs.

FIELD SITE

The field site was a cut slope of approximately 40m high along a link road near the Kuala Lumpur International Airport, Sepang, Malaysia. The slope basically comprise of residual soils of weathered sandstone. The soils are generally yellowish brown in color and consist mainly of fine sands and silts. Table 1 shows the cut slope was mapped for the weathering grades, based on the commonly used classification of Little (1969), and Kamoo and Mogana (1988).

Table 1. Classification of weathering profile over sedimentary and meta-sediment rock in Peninsular Malaysia (Komoo & Mogana 1988)

Weathering classification		Description
Term	**Zone**	
Residual soil	VI	All rock material is converted to soil. The mass structure and material fabric (texture) are completely destroyed. The material is generally silty or clayey and shows homogenous color.
Completely weathered	V	All rock material is decomposed to soil. Material partially preserved. The material is sandy and is friable if soaked in water or squeezed by hand.
Highly weathered	IV	The rock material is in the transitional stage to form soil. Material condition is either soil or rock. Material is completely discolored but the fabric is completely preserved. Mass structure partially present.
Moderately weathered	III	The rock material shows partial discoloration. The mass structure and material texture are completely preserved. Discontinuity is commonly filled by iron-rich material. Material fragment or block corner can be chipped by hand.
Slightly weathered	II	Discoloration along discontinuity and may be part of rock material. The mass structure and material texture are completely preserved. The material is generally weaker but fragment corners cannot be chipped by hand
Fresh rock	I	No visible sign of rock material weathering. Some discoloration on major discontinuity surfaces.

Figure 1 shows a cross section of the cut slope. Based on the geological formation, the cut slope profile falls under the following weathering grades:

Berm 1 – Weathering grade V
Berm 2 – Weathering grade IV
Berm 3 – Intermediate weathering grade of IV and III
Berm 4 – Weathering grade III

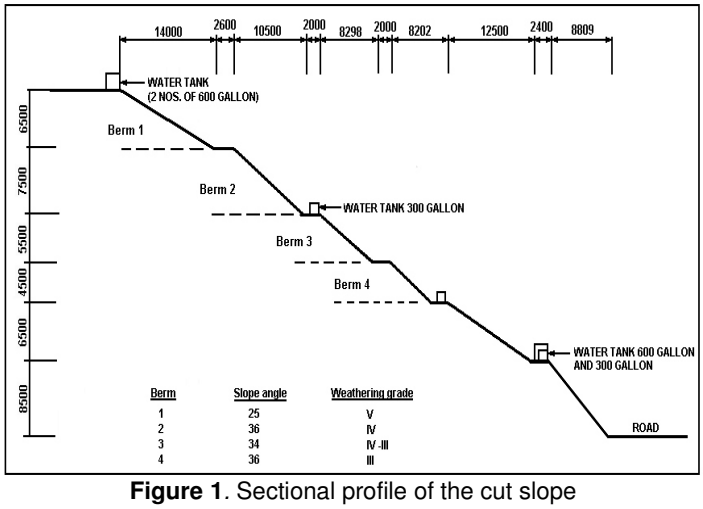

Figure 1. Sectional profile of the cut slope

In order to have a better control of the timing as well as intensity of the rain, as oppose to the unpredictable nature (in term of time, intensity and duration) of natural rain, an artificial rain simulation system using a sprinkler method was designed and setup in the field. The rain simulator system was designed to provide continuous artificial rain during the course of the study.

A 122.4mm/hour (3.4 x 10^{-5} m/s) rainfall was the highest recorded rainfall in five years (1995 – 2000) at the Subang Rainfall Station by the Metrological Department of Malaysia, which is close to the field site, for the 1st hour rain. The rain simulator was designed to impart the same intensity of rainfall for duration of 150 minutes (2 ½ hours). The rain simulator system basically comprise of water tanks, pumps and piping systems, sprinklers, flow meters and v–notch collection drains. The sprinkler system comprised of a 4.57m x 4.57m (15' x 15') sprinkling frame, made of steel tubes, PVC piping and sprinkler heads as shown in Figure 2. Figure 3 shows a rainfall simulation in progress. Note that polythene sheets were used to enclose sides of the sprinkling/catchments area to minimize loss of water and direct surface run off to the collection drain. Figure 4 shows a close up view of the sprinkler head.

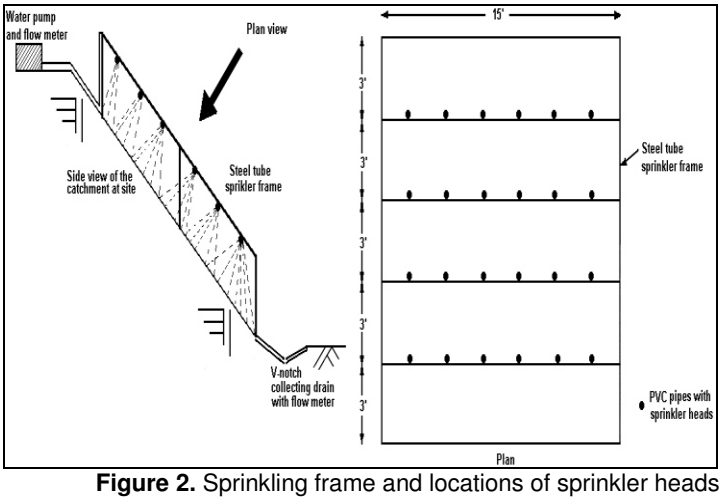

Figure 2. Sprinkling frame and locations of sprinkler heads

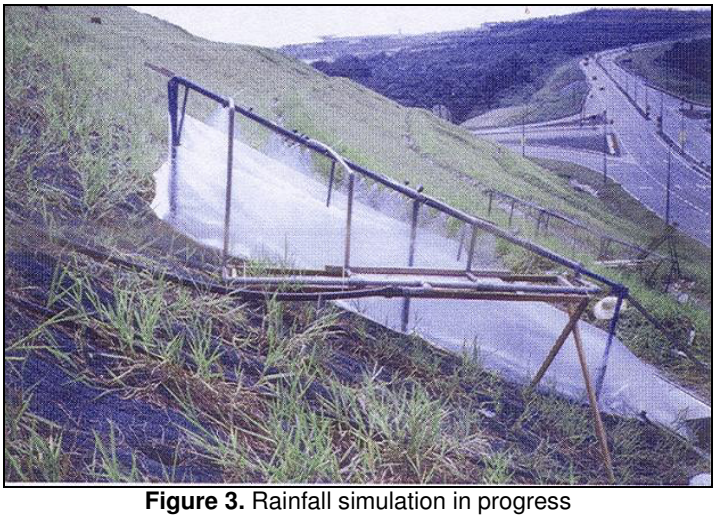

Figure 3. Rainfall simulation in progress

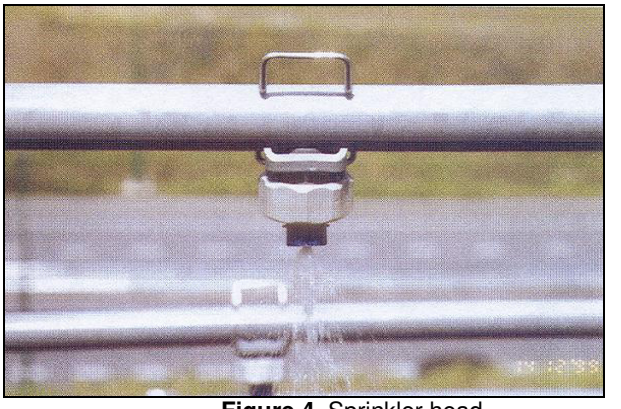

Figure 4. Sprinkler head

To monitor the rate of water inflow and to regulate the flow to the test site, flow meters as shown in Figure 5 were installed. This enable the total volume of water supplied to the test locations to be measured. The excess surface runoff water from the test site was in turn directed to the v-notch collection drain, and measured using the flow meter at the outlet. The difference in the inflow and outflow give rate of water infiltration into the soil.

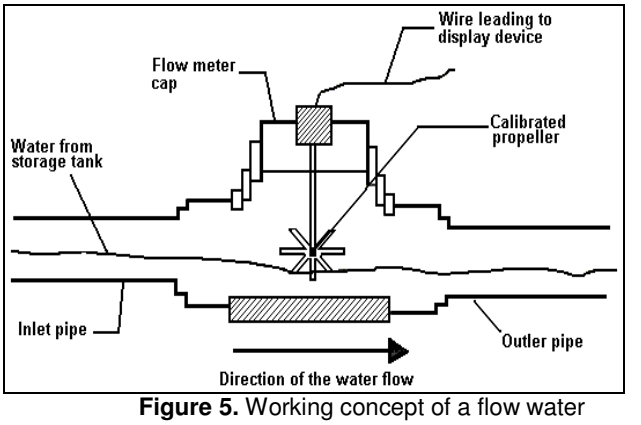

Figure 5. Working concept of a flow water

RESULT AND DISCUSSION

Field Results

The first part of the study was to examine the influence of surface cover on the infiltration rate of a cut slope in unsaturated residual soil. Six surface conditions as shown in Table 2 were studied.

Table 2. Six surface conditions of the cut slope

Case No.	Remarks
1	Test was conducted in natural condition where the slope surface was covered with the usual dense grass
2	Grass was trimmed to 1" high in order to study the effect of a well trimmed and maintained slope surface
3	Slope surface was trimmed bare, to model the condition of a fresh slope
4	Slope was covered with geosynthetic net and normal dense grass
5	Slope had both cover of geosynthetic net and grass, as in case 4, but the grass was trimmed to 1" high
6	Slope surface was stripped of its grass cover, leaving only the geosynthetic net

On berms 1 and 2, which fall roughly on soils of weathering grade V & IV, the effect of surface conditions of case 1, 2 and 3 on the water infiltration rate was studied. The results obtained are summarized in Table 3.

Table 3. Infiltration rate of berms 1 and 2

Berm	Weatheri-ng grade	Surface Condition	Infiltration rate (mm/s)	Berm	Weatheri-ng grade	Surface condition	Infiltration rate (mm/s)
1	V	1. Normal dense grass	0.40×10^{-6}	2	IV	1. Normal dense grass	0.60×10^{-6}
		2. 1" high cut grass	0.80×10^{-6}			2. 1" high cut grass	1.00×10^{-6}
		3. Bare surface	1.20×10^{-6}			3. Bare surface	2.30×10^{-6}

From the above table, it appears that the water infiltration rate into the soil increases from the fully vegetated slope to trimmed slope, and to bare surface. For a particular surface cover, berm 2, which comprised of the grade IV weathered material, has high infiltration rate indicating the more porous nature of the soil material. This is despite the fact that berm 1 is a gentler slope compared with berm 2. Steeper slope angle would enhance surface flow, and thus reduce rate of water infiltration into the slope.

The effect of surface cover on infiltration rate was studied on berm 3 and 4 for surface conditions of 3, 4, 5 & 6. The results obtained are summarized in Table 4. Both the slopes were roughly of the same angle, between 34 – 36^{o}. These berms fall roughly on soils of weathering grade IV & III.

Table 4. Infiltration rate of berms 3 and 4

Berm	Weatheri -ng grade	Surface Condition	Infiltration rate (mm/s)	Berm	Weatheri -ng grade	Surface condition	Infiltration rate (mm/s)
3	IV - III	4. Geosynthetic & normal grass	0.70×10^{-6}	4	III	4. Geosynthet ic & normal grass	0.90×10^{-6}
		5. Geosynthetic net & 1" cut grass	1.80×10^{-6}			5. Geosynthet ic net & 1" cut grass	2.00×10^{-6}
		6. Geosynthetic net only	3.61×10^{-6}			6. Geosynthet ic net only	3.01×10^{-6}
		3. Bare surface	4.61×10^{-6}			3. Bare surface	6.91×10^{-6}

From the above table, it appears that the soil infiltration rate increases from the fully vegetated slope with geosynthetic net, to cut grass slope with geosynthetic net, to geosynthetic net, and to bare surface slope only. For a particular surface cover/condition, berm 4, which was of weathered grade III soil material, had higher infiltration rate compared with berm 3, which was of weathered soil of intermediate grade of IV – III. This is also shown in Table 5 when the infiltration rate of all the four berms, i.e. of four different weathering grades, and for bare surface condition only, are compared.

Table 5. Infiltration rate of berms 1, 2, 3 and 4 for bare surface condition only

Berm 1	Weathering grade	Infiltration rate for bare surface condition ((mm/s)
1	V	1.20×10^{-6}
2	IV	2.30×10^{-6}
3	IV – III	4.61×10^{-6}
4	III	6.91×10^{-6}

Numerical Study

A comparative study was performed to compare factor of safety against slope instability obtained with conventional slope stability analysis with analysis in-cooperating unsaturated soil parameters. Computer software Seep/W was used to perform the seepage analysis coupled with the Slope/W software which was used to perform slope stability analysis using the extended Mohr Coulomb criterion to account for an increase in soil strength due to the matric suction (Fredlund & Rahardjo, 1993). Seepage analysis of the cut slope was performed incorporating the 2 ½ hours heavy rainfall at 122.4 mm/hour and the measured rates of infiltration as shown in Tables 3-5, for slopes of the various weathering grades and surface cover.

As in the field tests, the following surface covers are considered; slope surface covered with natural grass, slope surface covered with 1" high cut grass, slope surface covered with natural grass and geosynthetic, slope surface covered with 1" high cut grass and geosynthetic, slope surface covered with geosynthetic only and bare slope surface.

Table 6 summarizes the input parameters considered in the analysis, in accordance to the respective weathering grade.

Table 6. Input parameters for soils of various weathering grades

Weathering grade/Berm	Slope cover	Infiltration rate x 10^{-6} m/s	*Cohesion c'* (kPa)	*Angle of friction,* ϕ'	*Increase in shear strength due to suction,* ϕ^b	*Unit weight,* γ (kN/m^3)
V (Berm 1)	Natural grass	0.40	10	26	26	18
	1" high cut grass	0.80				
	Bare slope	1.20				
IV (Berm 2)	Natural grass	0.60	8	28	26	18
	1" high cut grass	1.00				
	Bare slope	2.30				
IV&III (Berm 3)	Natural grass & geosynthetic	0.70	4	31	24	18
	1" high cut grass & geosynthetic	1.80				
	Geosynthetic only	3.61				
	Bare slope	4.61				
III (Berm 4)	Natural grass & geosynthetic	0.90	0	33	19	18
	1" high cut grass & geosynthetic	2.00				
	Geosynthetic only	3.01				
	Bare slope	6.91				

The results obtained in term of factor of safety with respect to the various cases analyzed are given in Table 7 below.

Table 7. Summary of factor of safety

Description/ Slope cover	Berm / Weathering grade	Berm 1 V	Berm 2 IV	Berm 3 IV - III	Berm 4 III
Conventional analysis without matric suction		1.592	1.535	1.388	1.204
Analysis incorporating matric suction, prior to simulated rain		2.785	2.330	2.108	1.757
After 2 ½ hrs rain; slope surface covered with natural grass		2.696	2.201	-	-
After 2 ½ hrs rain; slope surface covered with 1" high cut grass		2.523	2.132	-	-
After 2 ½ hrs rain; bare slope surface		2.440	1.978	1.698	1.289
After 2 ½ hrs rain; slope surface covered natural grass and geosynthetic		-	-	1.988	1.574
After 2 ½ hrs rain; slope surface covered with 1" high cut grass and geosynthetic		-	-	1.857	1.458
After 2 ½ hrs rain; slope surface covered with geosynthetic only		-	-	1.731	1.406

The factor of safety obtain from analysis by incorporating matric suction is much higher than the factor of safety obtained from the conventional slope stability analysis without matric suction. The differences in factor of safety by incorporating matric suction ranges between 12% to 35% higher as compared to the conventional slope stability analysis.

There is a trend of reduction in factor of safety with rain, in particular for slopes with the lesser cover. As expected the worst condition is for case of bare slope surface.

The higher the soil infiltration rate, as in the case of soil of weathering grade IV and III, the lower are the factor of safety.

CONCLUSION

From the results of the study, the soil infiltration rate as measured from the field test shows an increase from fully vegetated slope with geosynthetic net, to cut grass slope with geosynthetic net, to geosynthetic net, and to bare surface slope only.

For a particular surface cover/condition, soil of weathering grade III had higher infiltration rate compared soils of intermediate grade (IV – III), grade IV and grade V.

The factor of safety obtain from analysis by incorporating matric suction is much higher than the factor of safety obtained from the conventional slope stability analysis without matric suction.

There is a trend of reduction in factor of safety with rain, in particular for slopes with the lesser cover and as expected the worst condition is for case of bare slope surface.

The higher the soil infiltration rate, as in the case of soil of weathering grade III, the lower is the factor of safety.

REFERENCES

Affendi. A., and Ali, F.H. (1994) Field measurement of soil suction. *Proceeding 13th International Conference on Soil Mechanic and Foundation Engineering*. New Delhi. 3: 1013-1016.

Ali, F.H. and Rahardjo, H. (2004) Unsaturated residual soil. *Tropical Residual Soils Engineering*. Huat, Gue & Ali (eds). Leiden. Balkema, 57-72.

Anderson, M.G. (1991) Hydrology, slope stability and cut slope design. IEM/PWD, Malaysia: Kuala Lumpur, May 1991.

Brand, E.W. (1984) Landslide in Southeast Asia. *Proceedings of 4th International Conference on Landslide.* State of the art report. Toronto, 1: 17-59

Fredlund, D.G. and Morgenstern, N.R. (1977) Stress state variables for unsaturated soils. *J. of the Geotechnical Engineering Divison, ASCE*, 103: 447–466.

Fredlund, D.G. and Rahardjo, H. (1987) Soil mechanics principles for highway engineering in Arid regions. *In Soil Mechanics Considerations: Arid and Semiarid areas.* Transportation research record 1137: 1–11.

Fredlund, D.G. and Rahardjo, H. (1993) *Soil mechanics for unsaturated soils*. New York: John Wiley & Sons Inc.

Komoo, I. and Mogana, S.N. (1988) Pysical characterization of weathering profiles of clastic metasediments in Peninsular Malaysia. *Proceeding. 2nd Conference on Geomech. In Tropical Soils. Singapore,*1: 37-42.

Little, A.L. (1969) The engineering classification of residual tropical soils. Proc. 7th *International Conference Soil Mechanics and Foundation engineering, Mexico*, 1: 1-10.

Othman, M.A .(1989) Highway cut slope instability problem in West Malaysia. PhD thesis. University of Bristol. Unpublished.

Seep/W, Version 3. User's guide for finite element seepage anlaysis. Geo-Slope International Ltd., Canada.

Shaw-Shong, L. (2004) Slope failures in tropical residual soil. *Tropical Residual Soils Engineering*. Huat et al (ed). Leiden. Balkema, 71-102.

Slope/W, Version 3. User's guide for slope stability analysis. Geo-Slope International Ltd. Canada.

Suhaimi, A.T. (1997) Comparative study of infiltration in residual soils. *Proceeding 4th Regional Conference in Geotechnical Engineering (Geotropika 97)*. Malaysia, 343-354.

Guide to Authors

Aims and Scope:

The Malaysian Construction Research Journal (MCRJ) is the journal dedicated to the documentation of R&D achievements and technological development relevant to the construction industry within Malaysia and elsewhere in the world. It is a collation of research papers and other academic publications produced by researchers, practitioners, industrialists, academicians, and all those involved in the construction industry. The papers cover a wide spectrum encompassing building technology, materials science, information technology, environment, quality, economics and many relevant disciplines that can contribute to the enhancement of knowledge in the construction field. The MCRJ aspire to become the premier communication media amongst knowledge professionals in the construction industry and shall hopefully, breach the knowledge gap currently prevalent between and amongst the knowledge producers and the construction practitioners.

Articles submitted will be reviewed and accepted on the understanding that they have not been published elsewhere. The authors have to fill the Declaration of the Authors form and return the form via fax to the secretariat. The length of articles should be between 3,500 and 8,000 words or approximately 8 – 15 printed pages (final version). The manuscripts should be written in English or Bahasa Melayu an abstract in English must be included. The original manuscript should be typed one sided, single-spacing, single column with font of 10 point (Times New Roman). Paper size should be of Executive (18.42 cm x 26.67 cm) with 2 cm margins on the left, right and bottom and 3 cm for the top. Authors can submit the manuscript:

- By e-mail to maria@cidb.gov.my / hazim@cidb.gov.my
- By hardcopy and softcopy in Microsoft-Word format to MCRJ Secretariat:

Malaysian Construction Research Journal (MCRJ)
Construction Research Institute of Malaysia (CREAM)
CIDB Head Office
10th Floor, Grand Season Avenue
No. 72, Jalan Pahang
53000 Kuala Lumpur, Malaysia
Tel : (6) 03-26170200
Fax : (6) 03-40456828

Type of fonts: All text, drawing, graph must be written using Times New Roman
Language: Follow the spelling of the Oxford English Dictionary.
Size/Page Setup: Executive (18.42 cm x 26.67 cm)
Paper title: Arial, 16.

CODIFICATION AND APPLICATION OF SEMI-LOOF ELEMENTS FOR COMPLEX STRUCTURES

Author's name (full name): Arial, 9pt. should follow below the title.

Jamalodin Noorzaei[1], Mohd. Saleh Jaafar, Abdul Waleed Thanoon, Wong Jern Nee

Affiliation (including post codes): Arial, 9pt. Use numbers to indicate affiliations.

[1]Department of Civil Engineering, Faculty of Engineering, Universiti Putra Malaysia, 43400 UPM, Serdang, Selangor, Malaysia

Abstract: Arial Bold, 9pt. Left and right indent 0.25 inch.

Abstract: it should be single paragraph of about 100 – 250 words.

Keywords: Times New Roman Bold, 9pt (Italic). Left and right indent 0.25 inch.

Keywords: *Cooling tower; Finite element code; Folded plate; Semiloof shell; Semiloof beam*

Body Text: Times New Roman, 11 pt. All paragraph must be differenciate by 0.25 inch tab.

Heading 1: Arial Bold + Upper Case, 11pt.
Heading 2: Arial Bold + Lower Case, 11pt.
Heading 3: Arial Italic + Lower Case, 11pt.

Units: All units and abbreviations of dimensions should conform to SI standards.

Figures: Figures should be in box with line width 0.5pt. All illustrations and photographs must be numbered consecutively as it appears in the text and accompanied with appropriate captions below them.

Figures caption: Arial Bold + Arial, 9pt. should be written below the figures.

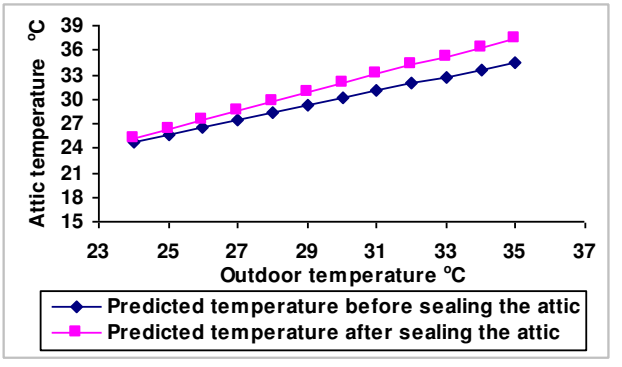

Figure 8. Computed attic temperature with sealed and ventilated attic

Tables: Arial, 8pt. Table should be incorporated in the text.

Table caption: Arial Bold + Arial, 9pt. Caption should be written above the table.

Table Line: 0.5pt.

Table 1. Recommended/Acceptable Physical water quality criteria

Parameter	Raw Water Quality	Drinking Water Quality
Total coliform (MPN/100ml)	500	0
Turbidity (NTU)	1000	5
Color (Hazen)	300	15
pH	5.5-9.0	6.5-9.0

(Source: Twort et al. 1985; MWA,1994)

Reference: Times New Roman, 11pt. Left indent 0.25inch, first line left indent – 0.25inch. Reference should be cited in the text as follows: "Berdahl and Bretz (1997) found…" or "(Bower et al. 1998)". References should be listed in alphabetical order, on separate sheets from the text. In the list of References, the titles of periodicals should be given in full, while for books should state the title, place of publication, name of publisher, and indication of edition.

Journal

Sze, K. Y. (1994) Simple Semi-Loof Element for Analyzing Folded-Plate Structures. *Journal of Engineering Mechanics*, 120(1):120-134.

Books

Skumatz, L. A. (1993) Variable rate for municipal solid waste: implementation, experience, economics and legislation. Los Angeles: Reason Foundation,157 pp.

Thesis

Wong, A. H. H. (1993) *Susceptibility to soft rot decay in copper-chrome-arsenic treated and untreated Malaysian hardwoods*. Ph.D. Thesis, University of Oxford. 341 pp.

Chapter in book

Johan, R. (1999) Fire management plan for the peat swamp forest reserve of north Selangor and Pahang. In Chin T.Y. and Havmoller, P. (eds) *Sustainable Management of Peat Swamp Forests in Peninsular Malaysia* Vol II: Impacts. Kuala Lumpur: Forestry Department Malaysia, 81-147.

Proceedings

Siti Hawa, H., Yong, C. B. and Wan Hamidon W. B. (2004) Butt joint in dry board as crack arrester. *Proceeding of 22nd Conference of ASEAN Federation of Engineering Organisation* (CAFEO 22). Myanmar, 55-64.

MCRJ Volume 3 | No. 2 | 2008

Contents

ISSN 1985-3807